Impact of *Rictor* Deletion in Adipocytes and Brain on Gene Expression in Perivascular Adipose Tissue and Blood Pressure Regulation

---

Dissertation

zur

Erlangung der naturwissenschaftlichen Doktorwürde

(Dr. sc. nat.)

vorgelegt der

Mathematisch-naturwissenschaftlichen Fakultät

der

Universität Zürich

von

Katja Drägert

aus

Deutschland

Promotionskomitee

Prof. Dr. Roland Wenger (Vorsitz)

Dr. Elvira Haas (Leitung der Dissertation)

Prof. Dr. Edouard Battegay

Prof. Dr. Michael Hall

Zürich, 2015

Table of Content

List of figures

RESULTS SECTION - PART II

APPENDIX

List of tables

Abbreviations

AMPK	AMP-activated protein kinase
ANG I	Angiotensin I
ANG II	Angiotensin II
ANP	Atrial natriuretic peptide
Atgl	Adipocyte triglyceride lipase
BAT	Brown adipose tissue
BMAL1	Brain-muscle arnt like 1
BMDM	Bone-marrow-derived macrophages
BMI	Body mass index
BNP	Brain natriuretic peptide
Ccg	Clock-controlled gene
cGMP	Cyclic guanosinmonophosphat
CK1δ	Casein kinase 1 delta
CK1ε	Casein kinase 1 epsilon
CLOCK	Circadian locomotor output cycles kaput
CNS	Central nervous system
CO	Carbonic oxide
COX	Cyclooxygenase
CRY1/2	Cryptochrome ½
CVS	Cardiovascular system
Cyp51A1	Cytochrome P450, family 51, subfamily A, polypeptide 1
DAG	Diacylglycerol
DEPTOR	DEP domain containing mTOR-interacting protein
EC	Endothelial cell
EDCF	Endothelium-derived contracting factor
EDHF	Endothelium-derived hyperpolarizing factor
EDRF	Endothelium-derived relaxing factor
eNOS	Endothelial nitric oxide
ET-1	Endothelin-1
Fdps	Farnesyl diphosphate synthetase
FDR	False discovery rate
FFA	Free fatty acids

FGF	Fibroblast growth factor
GTP	Guanosine-5'-triphosphate
H_2O_2	Hydrogen peroxide
H_2S	Hydrogen sulfide
HFD	High-fat diet
Hsl	Hormone-sensitive lipase
IGF-1	Insulin-like growth factor
iNOS	Inducible nitric oxide
IP_3	Inositol-1,4,5-trisphosphat
Irf4	Interferon regulatory factor 4
LPS	Lipopolysaccharide
M3	Muscarinic acetylcholine receptor 3
MCC	Medullary cardiovascular center
Mcpt4	Mast cell protease 4
MI	Myocardial infarction
mLst8	Mammalian lethal with sec-13 protein 8
mSin1	Mammalian stress-activated MAP kinase interacting protein 1
mTOR	Mammalian target of rapamycin
Nampt	Nicotinamide phosphoribosyltransferase
nNOS	Neuronal nitric oxide
NO	Nitric oxide
NPAS2	Neuronal PAS domain protein2
Nsdhl	NAD(P) dependent steroid dehydrogenase-like
O_2^-	Superoxide anion
ob/ob	Leptin-deficient mouse (obese mouse)
$ONOO^-$	Oxidant peroxynitrite
PDCF	PVAT-derived contracting factor
PDRF	PVAT-derived relaxing factor
PE	Phenylephrine
PER1/2	Period 1/2
PGC1α	Pparg-co-activator 1 alpha
PGC-1α	PPARg co-activator 1-α
PI3K	Phosphatidylinositol 3-kinase
PIP_2	Phosphatidylinositol-4,5-bisphosphate
PKC-α	Protein kinase C alpha

PKG	Protein kinase G
PLA_2	Phospholipase A_2
PLC	Phospholipase C
Pparα	Peroxisome proliferation activator receptor alpha
Pparγ	Peroxisome proliferation activator receptor gamma
PRAS40	Proline-rich AKT substrate 40 kDa
Protor1/2	Protein observed with RICTOR 1 and 2
PVAT	Perivascular adipose tissue
qRT-PCR	Quantitative real time PCR
RAAS	Renin-angiotensin-aldosterone-system
Raptor	Regulatory associated protein of mTOR
REV-ERBα/β	Nuclear receptor subfamily 1, group D, member 1 or 2
Rictor	Rapamycin-insensitive companion of TOR
RORα/β/γ	Retinoic-acid related orphan receptor alpha, beta or gamma
ROS	Reactive oxygen species
SCN	Suprachiasmatic nuclei
Serpine1/Pai1	Serine (or cysteine) peptidase inhibitor, clade E, member 1
Sesn2	Sestrin 2
sGC	Soluble guanylate cyclase
SGK1	Serum- and glucocorticoid-induced protein kinase 1
Sirt1	Sirtuin 1
T2DM	Type 2 diabetes mellitus
TEL2	Telomere maintenance 2 (also known as TELO2)
TMP	Transmural pressure
TP	Thromboxane receptor
TTi1	TELO2 interacting protein 1
VEGF	Vascular endothelial growth factor
VSMC	Vascular smooth muscle cell
WAT	White adipose tissue

Summary

Perivascular adipose tissue (PVAT) surrounds most systemic blood vessels and is a well-known regulator of blood vessel reactivity. In hypertension, deregulated PVAT properties contribute to the impairment of the functionality of the adjacent blood vessel. A question that remains to be addressed is which signaling pathways are involved in the deregulation of PVAT function in these pathophysiological conditions. One of the central cellular regulators is the mammalian target of rapamycin (mTOR) acting as a sensor for environmental conditions. mTOR exists in two functional distinct complexes, mTORC1 and mTORC2. The rapamycin-insensitive companion of TOR (RICTOR) is a component of mTORC2 and essential for mTORC2 activity. Focusing on the role of mTORC2 in the cardiovascular system, our laboratory discovered mTORC2 as a potential regulator of PVAT function. Using *adipocyte protein 2* (*aP2*) gene promoter-driven CRE-recombinase expressed in adipocytes, deletion of *Rictor* in mice ($Rictor^{aP2KO}$) identified mTORC2 in PVAT as a novel regulator of vascular reactivity primarily by controlling pro-inflammatory molecule expression such as inducible nitric oxide synthase (iNOS). Inhibition of iNOS restored vascular reactivity indicating a significant contribution of iNOS to the impaired vascular reactivity.

The present study aimed to assess whether mTORC2 contributes to blood pressure regulation and to identify signaling pathways involved using $Rictor^{aP2KO}$ mice.

Verification of *Rictor* deletion in $Rictor^{aP2KO}$ mice revealed reduced mRNA expression of *Rictor* in PVAT, in epididymal fat (EFAT), in adipocytes isolated from EFAT, in the brain regions suprachiasmatic nucleus (SCN) and cortex, while in the aortic tissue, the kidney, the heart, the stromal vascular fraction, monocytes and T cells the expression of *Rictor* was similar in $Rictor^{aP2KO}$ and control mice. Cross sections of thoracic PVAT uncovered a higher adipocyte cell density of $Rictor^{aP2KO}$ mice. Analysis of daily insulin fluctuations has shown an overall increase of the 24 hour insulin plasma levels in $Rictor^{aP2KO}$ mice. To investigate whether the changes in vascular reactivity and morphology of $Rictor^{aP2KO}$ mice translate into higher blood pressure, hemodynamic parameters were recorded using radiotelemetry in free moving mice. The 24 hour average of the mean (MAP; $P<0.05$) and diastolic arterial pressure (DAP; $P<0.05$) was slightly increased in $Rictor^{aP2KO}$ mice compared with controls. Separate analysis of the 12 hour light and 12 hour dark periods revealed time-of-day dependent effects of RICTOR/mTORC2 on blood pressure regulation. During the dark period the physiological decline in MAP was strongly impaired in $Rictor^{aP2KO}$ mice. Similarly, heart rate (HR; $P<0.01$) and locomotor activity parameters were elevated and remained high during the progression of the dark period in these mice. Inhibition of iNOS using subcutaneously implanted mini pumps releasing 1400W did not lower blood pressure in $Rictor^{aP2KO}$ mice. To evaluate possible hypertrophic changes, we assessed the morphology of the heart. Mean absolute heart weights in $Rictor^{aP2KO}$ mice were

higher compared with controls, while the mean relative to body heart weight was not changed. Interventricular septal and right ventricular free wall thickness (P=0.08 and P=0.09, respectively) tended to be increased and cardiomyocytes were mild hypertrophic (P<0.01) in *Rictor*^{aP2KO} mice. mRNA expression of the cardiac hypertrophic biomarkers *atrial natriuretic peptide* (*Anp*; P<0.05) and *brain NP* (*Bnp; P=0.11*) was reduced in these mice and mRNA transcriptional levels of the NP receptors *Npr2* (P<0.05) and *Npr3* (P<0.05) were decreased in adipocytes isolated from EFAT. A similar expression pattern was detected in PVAT.

To identify connections of the physiological changes observed in *Rictor*^{aP2KO} mice to the mTORC2 network, a micro array analysis of the expressed PVAT genome was performed. 68 genes were differentially expressed (P<0.05 and fold change > 1.5) in PVAT of *Rictor*^{aP2KO} mice compared with controls. Subsequent gene ontology analysis revealed the circadian rhythm regulated by clock genes as the most affected pathway. Well-designed clock gene expression controls daytime-dependent behaviors and mammalian physiology. Mutations and deletions of clock genes have been associated with changes in blood pressure and locomotor activity. In this context, it was essential to clarify the impact of *Rictor* deletion on peripheral clock gene expression in PVAT during a 24 hour cycle. mRNA expression level of *Period 1* (*Per1*), *Circadian locomotor output cycles kaput* (*Clock*), *Cryptochrom 1* (*Cry1*) and *Retinoic-acid related orphan receptor alpha* (*Rorα*) were reduced specifically during the light period, while *Period 2* (*Per 2*) exhibited a phase shift at the transition from the light to the dark period in PVAT of *Rictor*^{aP2KO} mice compared with controls. Intriguingly, we found *Rictor* mRNA expression to be time-of-day dependent in control mice with highest levels during light period. Similar, mTORC2 activity was daytime dependent as the phosphorylation of AKT at Ser473 was higher at the beginning of the light period. In addition to the reduced *Rictor* mRNA expression, we found a 17 % reduction in brain size in *Rictor*^{aP2KO} mice compared with controls. Therefore, a potential impact of *Rictor* deletion in the brain cannot be excluded, particularly in the SCN where the biological master clock is located, that might explain the observed changes in daily fluctuations of blood pressure and locomotor activity. In the SCN, 24 hour mRNA expression of core clock genes was similar between groups.

In conclusion, the data of the present study show for the first time the importance of RICTOR and/or mTORC2 in the brain and adipocytes to regulate daily fluctuating physiological processes such as blood pressure and locomotor activity. This function of RICTOR is likely located downstream or independent of the molecular clock mechanisms in the SCN, and may involve the hormones NPs and insulin. In PVAT, affected clock genes might contribute to the increased pro-inflammatory molecule expression. Future studies to elucidate these complex interactions in the adipocyte-brain axis may lead to the identification of novel strategies to develop effective treatments against hypertension.

Zusammenfassung

Perivaskuläres Fettgewebe (PVAT) umschließt die meisten systemischen Blutgefäße und reguliert ihre Reaktivität. Bei Bluthochdruck und Fettleibigkeit verändern sich die Eigenschaften des PVATs und ebenso die Reaktivität der umschlossenen Blutgefäße. Trotz intensiver Forschung sind Signalwege im PVAT unter physiologischen und pathophysiologischen Bedingungen wenig charakterisiert.

Von grundlegender Bedeutung für die Integration von Signalen auf zellulärer Ebene ist das Protein „mammalian target of rapamycin“ (mTOR). mTOR ist eine evolutionär konservierte Kinase und integriert die durch Wachstumsfaktoren und Nährstoffe generierten Signale auf zellulärer Ebene und reguliert das Zellwachstum. mTOR ist Bestandteil von zwei verschiedenen Proteinkomplexen: Komplex 1 (mTORC1) und Komplex 2 (mTORC2). Ein für die Aktivität von mTORC2 essentielles Adapterprotein ist „rapamycin-insensitive companion of TOR“ (RICTOR). Um die Rolle von mTORC2 in PVAT näher zu charakterisieren, haben wir in unserem Labor eine spezifische Mausmutante verwendet, in der das Gen *Rictor* nicht funktionsfähig exprimiert wird. Der Gen Knockout wurde unter Verwendung des *adipocyte protein 2* (*aP2*)-Promoter/CRE-Rekombinase Systems generiert.

Unter Verwendung dieses Mausmodels (*Rictor*^{aP2KO}) konnte unser Labor kürzlich zeigen, dass mTORC2 zur Regulierung von PVAT Eigenschaften unter physiologischen Bedingungen beiträgt. In *Rictor*^{aP2KO} Mäusen, ist die mTORC2 Aktivität im PVAT reduziert. Dies führt zu einer erhöhten Expression von pro-inflammatorischen Molekülen (tumor necrosis factor alpha, interleukin 6 und inducible nitric oxide synthase/iNOS). Durch spezifische Inhibierung von iNOS konnte die Reaktivität der thorakalen Aorta in *Rictor*^{aP2KO} Mäusen wieder hergestellt werden. Dies deutet auf einen signifikanten Beitrag von iNOS zur veränderten vaskulären Reaktivität der thorakalen Aorta hin.

Ziel dieser Studie war es herauszufinden, ob mTORC2 nicht nur zur vaskulären Reaktivität beiträgt, sondern auch Einfluss auf die Regulierung des Blutdrucks in Mäusen hat. Des Weiteren wurde die Genexpression in PVAT von *Rictor*^{aP2KO} im Vergleich zu Kontrollmäusen näher analysiert.

Deletion von *Rictor* in *Rictor*^{aP2KO} Mäusen führte zur Reduktion der Genexpression von *Rictor* im PVAT, epididymalem Fettgewebe (EFAT), in von EFAT isolierten Adipozyten sowie den Gehirnregionen suprachiasmatischer Nukleus (SCN) und Kortex. In der Aorta, der Niere, dem Herz, der „stromal vascular fraction“, Monozyten und T Zellen konnte keine veränderte *Rictor* Expression in *Rictor*^{aP2KO} festgestellt werden. Weiterführende histologische Untersuchungen ergaben zudem eine erhöhte Zelldichte des thorakalen PVATs in *Rictor*^{aP2KO} Mäusen. Eine Analyse der Insulin-Konzentration im Blut über einen Zeitraum von 24 Stunden, ergab einen erhöhten Insulin-Spiegel in *Rictor*^{aP2KO} Mäusen.

Morphologische Veränderungen des PVATs bzw. dessen Einfluss auf die vaskuläre Reaktivität deuten auf mögliche Veränderungen im Blutdruck hin. Um dieser Frage nachzugehen, haben wir unter Verwendung von Radiotelemetrie in sich frei bewegenden *Rictor*^{aP2KO} und Kontrollmäusen Blutdruck sowie ihre Bewegungsaktivität gemessen. Für den mittleren arteriellen Blutdruck (MAP; *P<0.05*) als auch für den diastolische Blutdruck (DAP; *P<0.05*) wurden erhöhte Durchschnittswerte über 24 Stunden in den *Rictor*^{aP2KO} Mäusen gemessen. Eine separate Analyse der 12 Stunden Tag- und 12 Stunden Nachtphase ergab einen tageszeitenabhängigen Effekt von RICTOR/mTORC2 auf die Blutdruckregulation. Im Gegensatz zu den Kontrollmäusen, konnte kaum ein physiologischer Rückgang des MAP in *Rictor*^{aP2KO} Mäusen während der 12 Stunden Nachtphase beobachtet werden. Auch die Herzrate (HR; *P<0.01*) und die Bewegungsaktivität waren erhöht und ihre physiologische Abnahme in der 12 Stunden Nachtphase stark verringert in *Rictor*^{aP2KO} Mäusen. *In vivo* Infusion von 1400W, einem iNOS spezifischen Inhibitor, durch subkutan implantierte osmotische Minipumpen konnte nicht den Blutdruck in *Rictor*^{aP2KO} Mäusen normalisieren. Morphologische Untersuchungen des Herzens ergaben leicht hypertrophe Kardiomyozyten in *Rictor*^{aP2KO} Mäusen sowie eine verringerte Expression der natriuretischen Peptide (NP) *Anp* (*P*<0.05) und *Bnp* (*P=0.11*). Des Weiteren war die Genexpression der NP Rezeptoren *Npr2* (*P*<0.05) und *Npr3* (*P*<0.05) in Adipozyten, welche vom EFAT isoliert wurden, verringert. Im PVAT fand sich ein ähnliches mRNA Expressionsmuster.

Um einen Zusammenhang zwischen Veränderungen im Blutdruck bzw. der Bewegungsaktivität in *Rictor*^{aP2KO} Mäusen mit der verringerten mTORC2 Aktivität zu untersuchen, haben wir die Genexpression im PVAT gemessen. Die Analyse ergab 68 signifikant veränderte Gene (*P*<0.05 und „fold change“ > 1.5) in *Rictor*^{aP2KO} Mäusen im Vergleich zu den Kontrollmäusen. Eine vertiefende Genontologie-Analyse ergab, dass ein Großteil dieser Gene mit dem zirkadianem Rhythmus assoziiert ist. Veränderungen dieser sogenannten Uhren-Gene mit Hilfe von Mutationen, führen zu Veränderungen im Blutdruck, die mit der Bewegungsaktivität assoziiert waren. In *Rictor*^{aP2KO} Mäusen, die Expressionsanalyse dieser Uhren-Gene auf mRNA Ebene im PVAT über 24 Stunden ergab Veränderungen in folgenden Genen: *Period 1* (*Per1*), *Circadian locomotor output cycles kaput* (*Clock*), *Cryptochrom 1* (*Cry1*) und *Retinoic-acid related orphan receptor alpha* (*Rorα*) zeigten in der 12 Stunden Tagphase eine verringerte Expression, wohingegen *Period 2* (*Per2)* eine Phasenverschiebung beim Übergang von der Tag- zur Nachtphase aufwies. Alle anderen Uhren-Gene wiesen keine Veränderung in ihrem Expressionsmuster auf. Interessanterweise war die Expression von *Rictor* im PVAT ebenfalls tageszeitenabhängig und zu Beginn der 12 Stunden Tagphase am Höchsten.

Veränderungen des tageszeitenabhängigen Rhythmus im Blutdruck und der Aktivität in den *Rictor*^{aP2KO} Mäusen hat uns dazu veranlasst, den Einfluss der Deletion von *Rictor* im Gehirn näher zu analysieren. Eine wichtige Rolle in der tagezeitenabhängigen Regulierung des Blutdrucks spielt der suprachiasmatische Nukleus (SCN). Eine Analyse der Expression der Uhren-Gene im SCN über 24

Stunden ergab keine Unterschiede zwischen *Rictor*^{aP2KO} und Kontrollmäusen. Dies deutet darauf hin, dass RICTOR/mTORC2 nicht zur Regulierung der Expression der Uhren-Gene im SCN beitragen. Interessanterweise, ähnlich dem PVAT ist auch im SCN die Expression von *Rictor* tageszeitenabhängig.

Zusammenfassend konnte in dieser Studie zum ersten Mal gezeigt werden, dass RICTOR und/oder mTORC2 in die Regulierung von Blutdruck und Bewegungsaktivität involviert sind. In *Rictor*^{aP2KO} Mäusen war nicht nur der Blutdruck erhöht, sondern auch sein physiologischer Rückgang während der 12 Stunden Nachtphase stark beeinträchtigt. Herzrate und Bewegungsaktivität zeigte einen ähnlichen tageszeitenabhängigen Verlauf. Die für die tageszeitenabhängige Regulierung von Blutdruck und Bewegungsaktivität wichtige Expression von Uhren-Genen im SCN war unverändert. Wohingegen die veränderte periphere Expression von Uhren-Genen im PVAT möglicherweise zur erhöhten Expression pro-inflammatorischer Moleküle beiträgt. Weiterführende Studien zur Untersuchung des Einflusses von RICTOR/mTORC2 auf die Gehirn-Fettgewebe-Achse könnten zu effizienteren Behandlungen von Bluthochdruck beitragen.

1. Introduction

1.1 The circulatory system

1.1.1 Organization and function of the circulatory system

The circulatory system evolved as a consequence of increased complexity and size of multicellular organisms [1]. For these organisms, simple diffusion is not adequate to supply oxygen and nutrients to the innermost cells. The circulatory system is comprised of a large number of interconnected vessels different in structure, size and function [2]. It can be divided into the lymphatic and the cardiovascular system [2]. The lymphatic system assembles of lymph, lymph nodes and vessels, microvessels and is essential for returning excess interstitial fluid to the blood [1, 2]. The primary function of the cardiovascular system is to deliver blood throughout the body. It plays an essential role in the transport of oxygen and carbon dioxide, blood cells, nutrients and metabolic waste to and from metabolic active cells [3]. In addition, secondary roles developed [1]: (1) fast distribution of circulating hormones and neurotransmitter to responding cells, (2) strengthened immune response against pathogens and (3) improved heat dissipation to the surface of a multicellular organism. A simplified overview of the cardiovascular system in humans is given in **figure 1-1-1**.

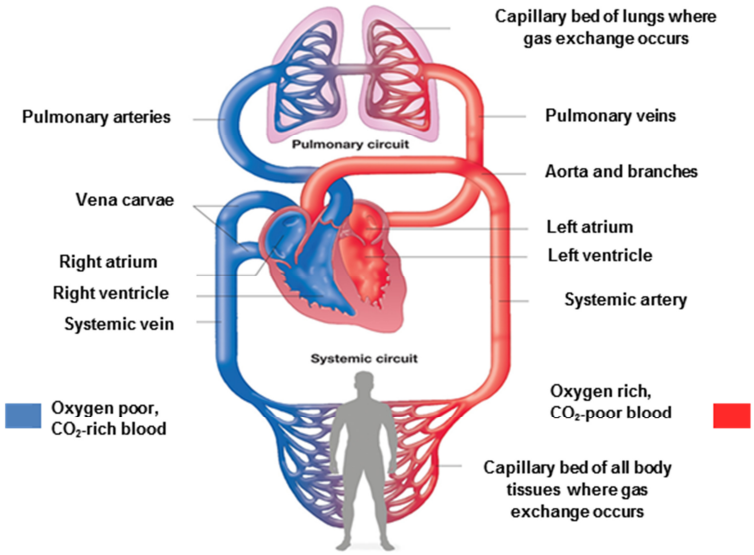

Figure 1-1-1: Overview of the cardiovascular system and circulation cycle of blood in humans. At the beginning of the circulation cycle, returning deoxygenated blood from the organs flows into the right atrium and enters the pulmonary circuit. Via the right ventricle blood is pumped into the pulmonary arteries and becomes oxygenated. Blood flows back to the left atrium of the heart and is pumped via the left ventricle and aorta into systemic arteries (systemic circuit). Capillaries provide organs with oxygen and nutrients before deoxygenated blood flows back to the right atrium of the heart and the circulation cycle starts again. Red colored blood vessels transport oxygenated blood, while blue colored vessels transport deoxygenated blood. Figure adapted from www.biology-forums.com

On the basis of its anatomy, the cardiovascular system can be subdivided into the pulmonary and systemic circuit [1]. In both circuits, the heart is the major driver pumping blood and its components through different blood vessels to the lungs and systemic organs [1]. Deoxygenated blood is pumped from the right ventricle of the heart via pulmonary arteries to the lungs were it becomes oxygenated. When oxygenated, blood returns via the pulmonary veins to the left atrium of the heart entering the systemic circuit. Oxygenated blood is pumped into the arterial system consisting of arteries, arterioles and arterial capillaries providing organs with oxygen and nutrients. Deoxygenated blood enriched in metabolic by-products flows through the venous capillaries, venoles and veins back to the right atrium of the heart entering the pulmonary circulation again [3]. This process is also called the circulation cycle **(figure 1-1-1)**.

1.1.2 Blood vessels: Types and distribution

Depending on their anatomy and function, blood vessels can be divided into three major types: (1) arteries carrying blood from the heart to the systemic organs or lungs, (2) capillaries were gases and nutrients are exchanged and (3) veins collecting capillary blood and carrying it back to the heart. Based on anatomical differences, arteries can be classified in elastic (conduit) arteries and muscular (distributing) arteries [4, 5]. Elastic arteries are located close to the heart and large in diameter [2]. They carry large volumes of blood under high-pressure away from the heart. Fluctuations in blood volumes are diminished by vessel wall properties (several layers of elastin) generating a more uniform blood flow. In humans, the largest elastic artery is the aorta (radius of ~1.13 cm) originating at the aortic root. The aorta accommodates blood ejected from the left ventricle of the heart. The aorta branches into smaller arteries and arterioles, the smallest blood vessel type in the arterial bed accounting for the vast majority of blood vessels [2]. They can be referred to as muscular arteries (~0.4 cm in diameter). Their function is to reduce blood flow and to ensure adequate blood distribution within organs and tissues. As resistance of muscular arteries is rather stable, this type of blood vessels is also referred to as resistance arteries. Before transition to the venous system, arterioles branch into capillaries with an average size of ~ 3 µm and a total surface area of 1000 m^2 in humans [1, 2]. The capillary network ensures exchange of nutrients, water and gases between blood and the surrounding tissue. This occurs mainly by simple diffusion. From the capillary network, blood flows through the venous system (venoles and veins) back to the heart. The venous system mainly functions as a collecting system for capillary blood and is characterized by low blood pressure [1]. To maintain blood flow in these conditions, veins are equipped with venous valves to avoid accumulation of blood in the lower parts of the human body.

1.1.3 Blood vessel wall: structure and function

As described already in chapter 1.1.2, the cardiovascular system is not made of non-elastic vessels similar in structure and size. Depending on the blood vessel function, wall composition, the diameter and thickness vary widely throughout the cardiovascular system. In the broadest sense, the wall of most blood vessels is anatomically formed of three distinct layers [2]: tunica intima, tunica media and tunica adventitia **(figure 1-1-2)**.

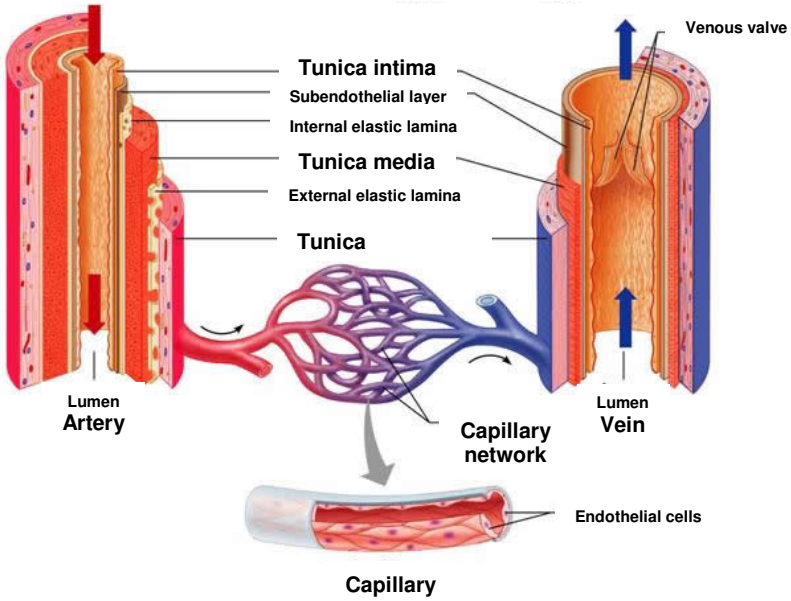

Figure 1-1-2: Blood vessel wall structure of an artery, vein and capillary. The vessel wall of most arteries and veins is anatomically formed of three distinct layers: tunica intima, tunica media and tunica adventitia. Depending on function and localization of blood vessels, composition and thickness of individual vessel wall layers can vary widely. Capillaries are mainly composed of a single endothelial layer. Arrows indicate the direction of the blood flow. Red colored blood vessels illustrate oxygenated blood, while blue colored vessels indicate deoxygenated blood. Figure adapted from www.rci.rutgers.edu

The tunica intima forms the innermost lining and consists of a single layer of endothelial cells (ECs) which directly faces the lumen of the blood vessel. In addition, an internal elastic lamina and fibro-elastic connective tissue provide stability and flexibility to the endothelial layer. No matter how distinct blood vessels are, a common characteristic is the single ECs layer [2]. The tunica media is the middle layer of a blood vessel. It is predominately made up elastic fibers and vascular smooth muscle cells (VSMCs) common to all blood vessels, but not capillaries. The third and outermost layer is the tunica adventitia and consists mainly of connective tissue [6]. Depending on blood vessel function and hierarchy, the manifestation of these three layers is more or less distinctive [1, 4]. Arteries such as the aorta are thick-walled. Multiple vascular smooth muscle cell layers and increased amounts of elastin and collagens are important for maintaining artery

function (high-pressure system) and blood flow. In addition, most systemic blood vessels are surrounded by perivascular adipose tissue (PVAT) [7], which secrets vasoactive substances regulating vascular tone and homeostasis [8, 9]. In chapter 1.3.3, PVAT composition and function will be discussed in more detail.

1.1.3.1 Function of endothelial and vascular smooth muscle cells

A single layer of ECs, the endothelium, forms the inner lining of the blood vessel. *De novo* formation of ECs into an endothelium occurs only in embryos. ECs originate from the early mesoderm involving differentiation of angioblasts and the formation of pre-blood vessels. Fibroblast growth factors (FGF) and vascular endothelial cell growth factor (VEGF) are crucial in this process. This process is called vasculogenesis [10, 11]. The expansion of existing blood vessels based on sprouting of ECs is called angiogenesis, mostly seen in wound healing processes or tumor growth [10]. Primarily, ECs provide a selective permeable barrier between the circulating blood and the blood vessel wall. In addition, other EC functions evolved including the regulation of vascular tone and homeostasis, response to inflammation and facilitation of blood flow [10]. ECs express a variety of receptors on the cell surface allowing the binding of circulating bioactive molecules. These include autacoids (e.g. acetylcholine, 5-hydroxytryptamine), hormones (e.g. insulin) and catecholamines (e.g. adrenalin, noradrenalin) [12, 13]. Receptor binding stimulates the secretion of vasoactive molecules from the endothelium (e.g. nitric oxide, prostaglandins) balancing vasodilation (relaxation) and vasoconstriction (contraction) of VSMCs in the tunica media. Various pathophysiological conditions including hypertension, obesity and diabetes can disturb physiological ECs function.

VSMCs primary function is to adapt vascular tone to physiological requirements. Through the contraction and relaxation of VSMCs, blood vessel diameter and thereby blood pressure, flow and blood distribution within organs is regulated [1]. VSMCs are differentiated [14] and express a unique combination of receptors, ion channels and contractile molecules to ensure VSMC contractile and dilatory properties. Interestingly, VSMCs maintain the ability to change their phenotype to a dedifferentiated state upon changes in environmental cues [14]. Dedifferentiated VSMCs have a distinct cell shape and function. These cells are characterized by a significant increase in migration, proliferation, and a different gene and protein expression profile. Dedifferentiation can be observed in the progression of hypertension, arteriosclerosis, and after vascular wall injury.

1.1.3.2 Mechanism of vasodilation in arteries

Vasodilation and vasoconstriction of blood vessels adjust vascular resistance adapting blood pressure and flow to the needs of an organism and environmental cues. The different layers of a blood vessel, particularly ECs and VSMCs, play a key role in these processes.

In 1980, Furchgott and Zawadzki were the first describing the important role of ECs in the regulation of blood vessel tone. They demonstrated the release of an endothelium-derived relaxation factor (EDRF) upon acetylcholine stimulus [15]. This EDRF has later been discovered to be nitric oxide (NO) [16] causing vasodilation of underlying VSMCs. Since then other circulating factors have been identified to trigger EDRFs production in ECs. These include insulin [17, 18], adiponectin [19, 20] and thyroid hormones [21]. Gaseous NO is able to diffuse freely across membranes and is the best characterized vasoactive molecule released from ECs [22, 23]. NO has multiple effects on the blood vessel wall. It inhibits adhesion of platelets and leukocytes to the endothelium, sustains vascular repair mechanisms controlling VSMCs migration and proliferation as well as stimulating EC migration. In ECs, NO is biosynthesized from the amino acid L-argenine and NADPH constitutively by the calcium (Ca^{2+})-dependent endothelial nitric oxide synthase (eNOS; also known as NOS III). Synthesis can be adjusted upon stimuli including circulating bioactive molecules. eNOS is exclusively expressed in ECs. Two other isoforms have been identified sharing up to 60 % homology in the amino acid sequence [22]. Similar to eNOS, neural NOS (nNOS; also known as NOS I) is constitutively expressed, but only in central and peripheral neuronal cells. Inducible NOS (iNOS; also known as NOS II) activity is independent of intracellular Ca^{2+} concentration. iNOS expression is mainly found in macrophages, abnormal cells states such as after myocardial infarction and other pathophysiological conditions. An overview of the NO synthesis in ECs is given in **figure 1-1-3**.

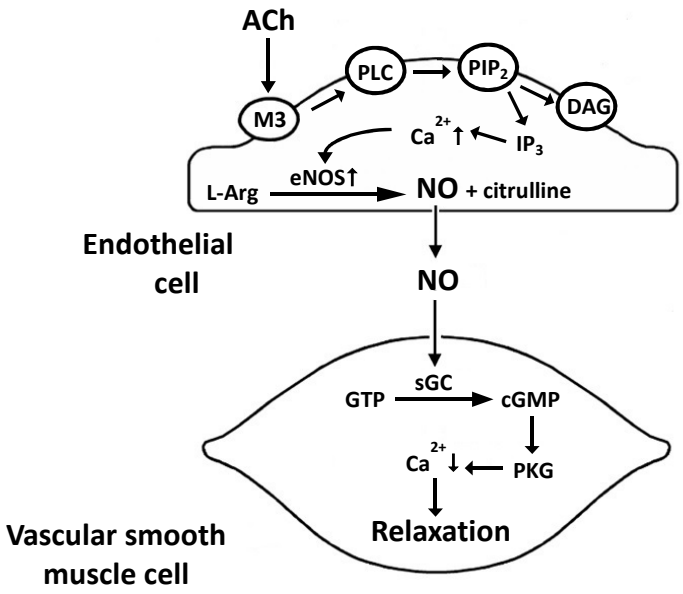

Figure 1-1-3: Production of nitric oxide in endothelial cells and relaxation of vascular smooth muscle cells. Upon binding of various vasoactive molecules and/or shear stress, nitric oxide is synthesized in endothelial cells from L-arginine by endothelial nitric oxide synthase. As a gas, nitric oxide diffuses freely to underlying vascular smooth muscle cells. Nitric oxide enhances the conversion of guanosine-5'-triphosphate into cyclic guanosine-monophosphate promoting vascular smooth muscle cell relaxation due to decreased intracellular Ca^{2+} concentration. Ach (acetylcholine), M3 (M3-muscarinic receptors), PLC (Phospholipase C), PIP_2 (phosphatidylinositol 4, 5-bisphosphate), DAG (Diacylglycerol), L-Arg (L-Arginine), eNOS (endothelial nitric oxide synthase), Ca^{2+} (Calcium), IP_3 (Inositol-1,4,5-trisphosphat), NO (nitric oxide), GTP (Guanosine-5'-triphosphate), sGC (Soluble guanylate cyclase), cGMP (Cyclic guanosinmonophosphat), PKG (Proteinkinase G). Figure adapted from [13, 23].

Upon binding of acetylcholine to its receptor on ECs membrane, phospholipase C (PLC) becomes activated leading to the conversion of phosphatidylinositol 4, 5-bisphosphate (PIP_2) to inositol 1, 4, 5- triphosphate (IP_3) and diacylglycerol (DAG). Increased intracellular IP_3 concentration facilitates Ca^{2+}-influx into ECs via Ca^{2+}-channels, which activates calmodulin. Calmodulin binds to eNOS increasing its activity promoting the synthesis of NO. NO diffuses to VSMCs leading to an intracellular increase in soluble guanylate cyclase (sGC) activity. sGC converts guanosine-5'-triphosphate (GTP) to cyclic guanosine 3`, 5`-monophosphate (cGMP). cGMP activates protein kinase G (PKG) decreasing intracellular Ca^{2+}-concentration and thus, promoting vasodilation of VSMCs. Under pathophysiological conditions including hypertension, obesity and diabetes, but also during ageing, NO bioavailability is reduced as a consequence of ECs dysfunction [13, 24]. This favors vasoconstriction of VSMCs [25].

1.1.3.3 Mechanism of vasoconstriction in arteries

In addition to its ability to release EDRFs and EDHF, the endothelium produces endothelium-derived contracting factors (EDCFs) which cause vasoconstriction of underlying VSMCs [13, 26]. Summarized in **figure 1-1-4**, the release of EDCFs can be increased upon activation of ECs by 5-hydroxytryptamine (5-HT), angiotensin II (ANG II) and chronically elevated stretch, but also other substances including adenosine diphosphate and superoxide anion (O_2^-) [27, 28].

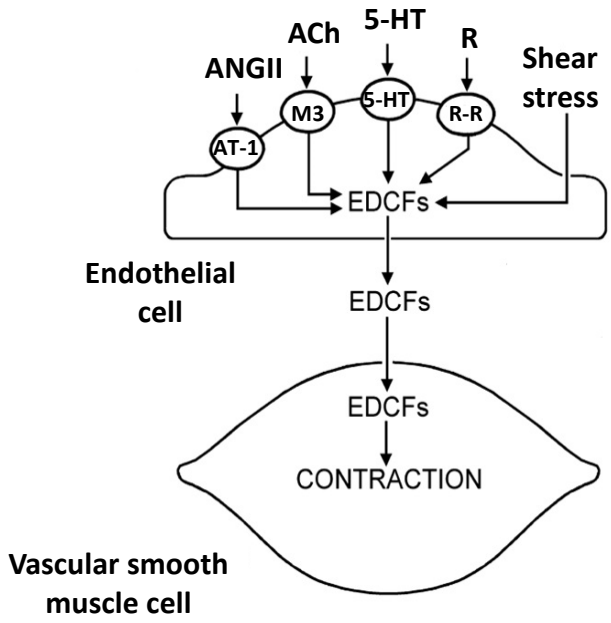

Figure 1-1-4: Endothelium-derived contracting factors. Upon binding of different vasoactive substances to corresponding receptors on endothelial cell surface, generation of endothelium-derived contracting factors is induced. The release of these factors causes the contraction of underlying vascular smooth muscle cells. ACh (acetylcholine), ANGII (angiotensin II), AT-1 (angiotensin receptor 1), EDCFs (endothelium- derived contracting factors), M3 (M3-muscarinic receptors), R (other vasoactive substances), R-R (receptor for other vasoactive substances), 5-HT (5-hydroxytryptamine). Figure adapted from [13].

Under physiological conditions, the effect of EDCFs is superimposed mainly by NO. ECs dysfunction and reduced NO bioavailability as seen in hypertension facilitate the release of EDCFs causing increased vasoconstriction of VSMCs. The vast majority of EDCFs belongs to the group of prostaglandins [28], which are synthesized from arachidonic acid through the cyclooxygenase (COX) in ECs. Prostaglandins play a key role in endothelium-dependent contractions as COX inhibition prevent nearly all endothelium-dependent contractions [27]. Upon release, EDCFs bind to their specific G-protein-coupled receptors (mostly TP receptors) on the VSMCs surface, initiating vasoconstriction.

1.1.4 Blood pressure regulation

Arterial blood pressure is a function of four different factors within the cardiovascular system: peripheral resistance, cardiac output, cardiac compliance and blood volume [1]. Determinates are subjected to a broad range of regulations. The medullary cardiovascular center (MCC) is located in the medulla oblongata and part of the short-term regulation of arterial blood pressure. The MCC coordinates rapid neuronal response to changes in baroreceptor (sensitive to transmural pressure changes of the blood vessel wall) and chemoreceptor signaling [1]. MCC output results in fast modifications of cardiac output and peripheral resistance via sympathetic and parasympathetic nerve activity [3]. Sympathetic response increases cardiac output and compliance via noradrenaline release which acts on β_1-adrenergic receptors on cardiac cells surface. Parasympathetic output decreases mainly cardiac output. Modulation of peripheral resistance is mostly achieved via sympathetic nervous activity [3]. The released neurotransmitter noradrenaline (postganglion sympathetic nerves) and adrenaline (adrenal medulla) act on adrenergic receptors expressed on VSMCs surface. Whether vasodilation or vasoconstriction is induced depends on e.g. the agonist released and the adrenergic receptor expressed [1]. In addition, a broad range of tissues and organs are known to secrete humoral and non-humoral factors which affect short-term and intermediate regulation of arterial blood pressure [1]. Insulin secreted by the pancreas increases NO bioavailability contributing to vasodilation of VSMCs [29]. It is well known that adipose tissue releases a variety of substances possessing vasoactive properties [30, 31]. Substances include adiponectin, leptin, plasminogen-activated factor 1 (PAI-1) and TNF-α. An implication in arterial blood pressure regulation is also well established for the natriuretic peptides (NPs) [32]. Atrial (ANP) and brain NP (BNP) are mainly synthesized by the atrial myocardium and ventricles of the heart, respectively. Under physiological conditions, ANP and BNP inhibit e.g. sympathetic activity to cause bradycardia and are involved in the long-term control of arterial blood pressure by regulating sodium retention in the kidney [3]. Long-term regulation of blood pressure is achieved mainly via renal fluid volume regulation and the renin-angiotensin-aldosterone system (RAAS). Major effectors are the lymphatic system modulating extracellular fluid volume (ECFV) and sodium and water resorption of the kidneys. This in turn changes total blood volume which has a profound effect on cardiac output and arterial blood pressure. Similar to short-term regulation, the sympathetic nervous system is also implicated in long-term control of arterial blood pressure [33]. Interestingly, arterial blood pressure shows time-of-days dependent variations which are influenced by the master circadian clock in the suprachiasmatic nucleus and explained in detail in chapter 1.2.

1.1.5 Dysregulation of blood pressure in hypertension

Dysregulation of arterial blood pressure can cause hypertension. It is one of the most common cardiovascular diseases in human adults [34]. It is characterized by chronically elevated blood pressure with blood pressure readings ≥ 140/90 mmHg in humans age 20 and older, and is categorized into different stages (**Table 1-1-1**). In addition, hypertension can be classified according to the (1) severity of the vascular disease (mild, moderate, serve or malignant), (2) the arterial pressure increase (diastolic, systolic or both) and (3) etiology (essential or secondary) [35]. The prevalence of hypertension in adults 35 to 64 years of age varies widely among countries in Europe and North America. Highest rates have been found in Germany (~55 %), lowest in Italy (~38 %), while rates in the United States (~30 %) and Canada (~27 %) are only half of those in Germany [36, 37]. It was shown that 90 to 95 % of patients suffer from essential hypertension (also known as primary or idiopathic) with unknown cause explaining elevations in blood pressure [38]. Only 5 to 10 % of patients suffer from secondary hypertension, which can be a consequence of kidney disease, the cardiovascular or endocrine system as well as pregnancy and medication side effects [39].

Table 1-1-1: Blood pressure categories according to the American Heart Association definition. Blood pressure can be considered to be as normal, if blood pressure readings are less than 120/80 mmHg. Table adapted from www.heart.org

Blood pressure category	Systolic (mm Hg)		Diastolic (mmHg)
Normal	< 120	and	< 80
Prehypertension	120 – 139	or	80 – 89
High blood pressure (Hypertension) Stage 1	140 – 159	or	90 – 99
High blood pressure (Hypertension) Stage 2	160 – 179	or	100 - 109
Hypertensive crisis	≥ 180	or	≥ 110

Triggers of essential hypertension are varied and can arise from the combination of different genetic and demographic circumstances [40]. In human adults age 60 to 69, the prevalence to suffer from hypertension is 69 % compared with younger people and the onset of hypertension in women is earlier than in men [41]. In addition, various environmental factors can influence the onset and severity of hypertension. These factors include bodyweight, physical activity, diet and smoking [42, 43].

Different pathophysiological factors and mechanisms are implicated in the onset of essential hypertension. In animal models of hypertension, an imbalance between the sympathetic and parasympathetic nervous system has been observed to contribute to the development of hypertension. In humans, sympathetic hyperactivity as well as increased levels of neurotransmitters adrenalin and noradrenalin has been observed in normotensive people with a

positive family history of hypertension [44, 45]. Similar, obese and diabetic patients are often found to be hypertensive combined with increased sympathetic nervous activity compared to lean controls. This might be due to increased plasma insulin (hyperinsulinemia) to compensate insulin resistance [46]. In addition, insulin resistance has been linked to endothelial dysfunction promoting the development of hypertension [47]. Long-term sympathetic hyperactivity is also associated with vascular remodeling of resistance arteries [48]. Changes in blood vessel wall structure and reactivity are well known to increase peripheral vascular resistance and thus arterial blood pressure [48]. In addition, structural changes of the blood vessel wall are often accompanied by endothelial dysfunction [49, 50]. This pathophysiological state is mainly characterized by increased oxidative stress leading to a reduction of NO and prostacyclin bioavailability. This favors vasoconstrictor production and the progression of hypertension. In addition, ANG II is a well-known contributor of oxidant production in the blood vessel wall. Pathophysiological action of ANG II on ECs up-regulates the formation of oxidant peroxynitrite ($ONOO^-$) reducing NO action on VSMCs. Elevated levels of ANG II often correlate with changes in kidney function and RAAS.

If untreated, hypertension can cause a variety of health consequences referred to as end-organ damage such as different heart and coronary arteries diseases, stroke, kidney damage and peripheral vascular diseases.

1.2 Impact of the mammalian circadian clock on the cardiovascular system

1.2.1 The mammalian circadian clock: definition and anatomical organization

Organisms are subjected to rhythmic changes of the environment. Most important are recurring day and night cycles based on earth rotation as well as seasonal cycles caused by the earth orbiting the sun. Organisms have adapted their physiology and behavior according to these changes. As a consequence, biological clocks evolved generating endogenous rhythms. Depending on the length of the period, rhythms can be infradian (< 24 hours), ultradian (> 24 hours) or circadian (~ 24 hours). A fundamental feature of circadian rhythms is their entrainment to exogenous timing signals (term: Zeitgeber) and its persistence also in the absence of such signals (free-running) [51]. It is important to distinguish between circadian and daily rhythms. The latter have a period of ~ 24 hours and are driven by recurring environmental cues, but do not persist under constant conditions (e.g. complete darkness). In mammals, the primary exogenous timing signal is light, which is translated via ocular photoreception into an endogenous timing system governed by the circadian clock [51]. The mammalian circadian clock is organized in a hierarchy of oscillators **(figure 1-2-1)** [52].

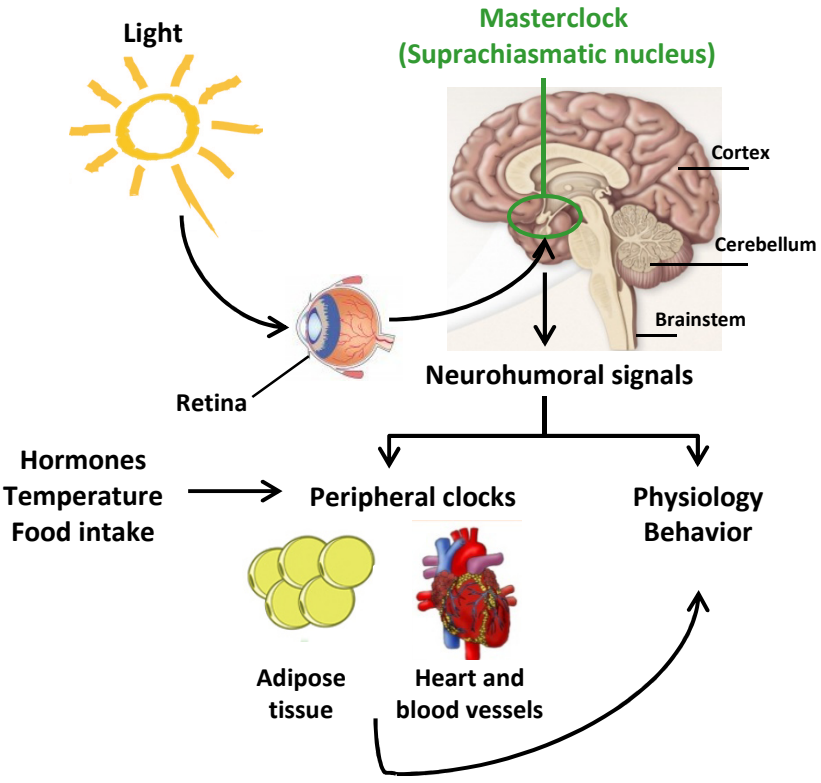

Figure 1-2-1: Hierarchical organization of the mammalian circadian clock. The master circadian clock is located at the suprachiasmatic nucleus (SCN) translating exogenous light signals into an endogenous timing system. Via neurohumoral signals, the SCN affects physiology/behavior directly or synchronizes peripheral clocks affecting tissue-specific metabolism. Peripheral clocks can be entrained to other environmental cues such as temperature and feeding behaviors.

The master circadian clock is located in the suprachiasmatic nucleus (SCN). The SCN is located at the anterior hypothalamus dorsal to the optic chiasm and bilateral to the third ventricle [53, 54]. The SCN is mainly entrained to light stimuli. In humans, the SCN is composed of ~ 50000 neurons (mice ~ 20000). To ensure stable master circadian clock oscillation and output, SCN neurons are synchronized with each other through unique processes [55]. Three different mechanisms are believed to play a fundamental role in the "coupling of SCN-neurons". These include neuropeptidergic signaling, electrical synapses and synaptic potentials [56-61]. In general, the SCN can be considered as a master synchronizer. It coordinates through neurohumoral factors independent "slave" peripheral circadian clocks in various tissues to achieve an interconnected circadian rhythm on whole body level [52]. Peripheral circadian clocks autonomously control tissue specific circadian metabolism. Although similar on the molecular basis (see chapter 1.2.2), master and peripheral clocks exhibit some profound differences. First, cells in peripheral tissues lack the ability of coupling and thus network properties [62]. Unlike SCN explants, which can be caped for weeks in culture without any changes in gene expression oscillation, in peripheral tissues oscillating gene expression patterns dampen quickly after a few days *ex vivo*. However, disruption of SCN neuron coupling leads to arrhythmic gene expression patterns [55]. The second major difference is the ability of peripheral clocks to respond not only to SCN-derived signals, but also to other stimuli such as temperature, feeding cues (e.g. nutrient availability) and hormones [63-65]. In contrast, the SCN primarily respond to light stimuli. SCN neurons are blind to their own signals [52] and can't be entrained to "peripheral zeitgeber" as long as coupled with each other.
To achieve the accuracy and reliability needed for interconnected circadian rhythms in different tissues, the molecular mechanism behind must be well-designed. Dysfunctional circadian clocks can cause serious health problems in mice which manifest in disturbed function of adipose tissue [66-68], pancreas [69] and the cardiovascular system [70, 71]. The main molecular drivers of the mammalian circadian clock will be discussed in the following section.

1.2.2 Molecular components of the mammalian circadian clock

The molecular basis of the circadian clock is similar in the SCN and peripheral tissues [72] and is illustrated in **figure 1-2-2**. It consists of interconnected and auto-regulated transcriptional-translational feedback loops driving approximately 24 hour expression patterns of different core clock genes.

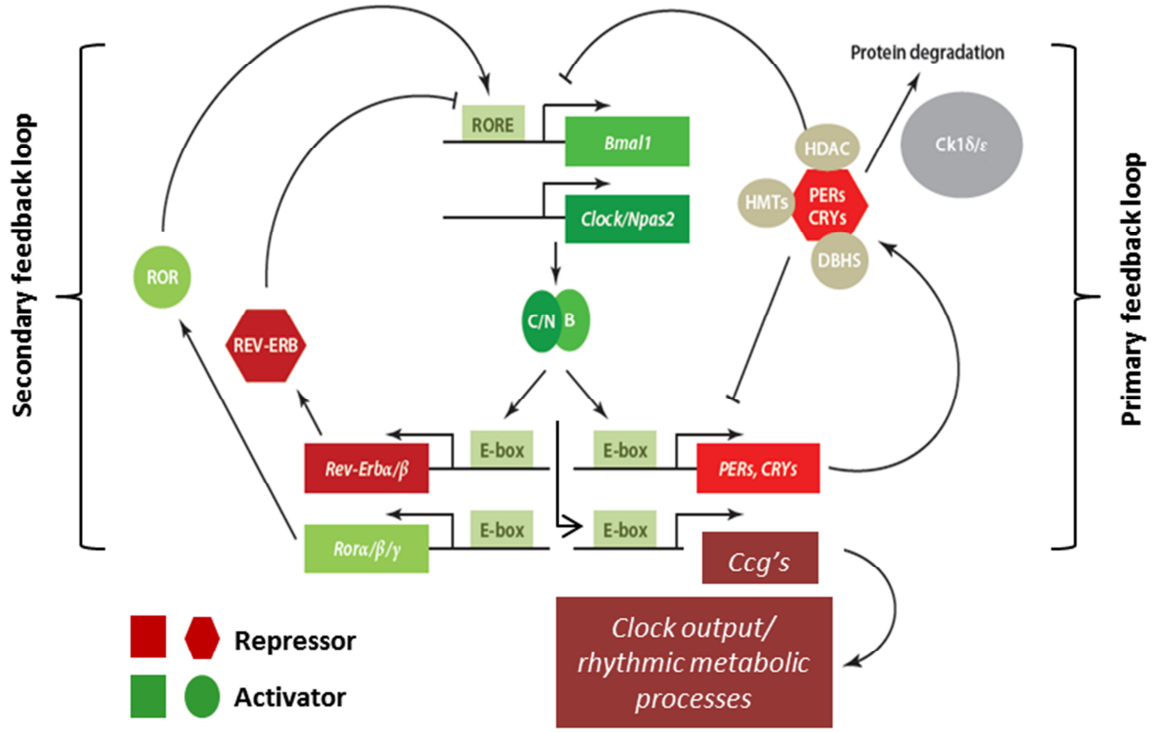

Figure 1-2-2: Molecular components of the mammalian circadian clock. 24 hour rhythms in physiology and behavior are achieved through interconnected transcriptional-translational feedback loops. These loops are composed of a set of transcriptional activators (green), which induce expression of its own repressors (red). To drive rhythmicity of biological processes, activators induce transcription of clock-controlled genes (Ccg's). *Bmal1* (*Brain-muscle arnt like 1*), *Clock* (*Circadian locomotor output cycles kaput*), *Npas2* (*Neuronal PAS domain protein 2*), C/N (CLOCK/NPAS2), C/B (CLOCK/BMAL1), *Rev-Erb-α/β* (*nuclear receptor subfamily 1, group D, member 1* and *2*), *Rorα/β/γ* (*retinoic acid-related orphan receptor alpha* and *beta*), PERs (PERIOD proteins), CRYs (CRYPTOCHROME proteins), HDAC (histone deacetylase), HMTs (histone methyltransferase), DBHS (members of the Drosophila behavior human splicing family), CK1δ/ε (Casein kinases 1δ and 1ε). Figure adapted from [52].

In the primary feedback loop, the positive limp consists of the genes *Brain-muscle arnt like 1* (*Bmal1*), *Circadian locomotor output cycles kaput* (*Clock*) and *Neuronal PAS domain protein 2* (*Npas2*) encoding basic helix loop helix; Period-Arnt-Single minded (bHLH-PAS) proteins. Heterodimers of BMAL1/CLOCK or BMAL1/NPAS2 initiate transcription of target genes with E-box element-containing promoters [51]. Genes include those of *Period* (*Per1, Per2, Per3*) and *Cryptochrome* (*Cry1, Cry2*). PER and CRY proteins are part of the negative limb of the primary feedback loop. PER and CRY dimerize, translocate to the nucleus and repress the transcriptional activity of BMAL1/CLOCK and BMAL1/NPAS2 [72]. Stability and nuclear translocation of PER/CRY is regulated by post-translational modifications (e.g. phosphorylation, ubiquitination) involving e.g. Casein kinases 1δ and 1ε (CK1δ; CK1ε) and Histone methyltransferases (HMTs) [73-75]. This is necessary to reset the transcriptional cycle. In addition, BMAL1/CLOCK and BMAL1/NPAS2 induce a second feedback loop interconnected to the feedback loop already described. Expressed

retinoic acid-related orphan receptor proteins REV-ERB's (REV-ERB α and β) and ROR's (RORα, β and γ), compete for ROR-response elements (RORE) within the promoter region of *Bmal1* [76]. REV-ERB's have been found to repress, while ROR's activate *Bmal1* transcription [76-78]. Both transcription regulating elements are necessary to ensure normal period regulation and precision of the mammalian circadian clock. Clock output manifests in adapted oscillating gene expression of clock-controlled genes (ccg's) regulating a variety of metabolic processes and organ function. Ccg´s include *transcription factors such as D site albumin promoter binding protein* (*Dbp*), *nuclear factors interleukin 3, regulated* (*Nfil3*) or *peroxisome proliferator activated receptor alpha/beta* (*Pparα/β*).

1.2.3 Mammalian circadian clock and metabolism

Circadian clocks might have evolved to balance energy intake, storage and utilization. Thus, it is not surprising that in humans and rodents, many aspects of the physiology and metabolism display circadian rhythmicity [79, 80]. These include body temperature, activity, lipid metabolism, hormone secretion, blood pressure and heart rate regulation. To achieve rhythmicity, metabolism and circadian clock are molecularly interconnected with each other [80]. 5 to 10 % of all genes expressed in a cell oscillate in a day-time dependent manner [81-84]. In peripheral tissues, this is achieved through master circadian clock-output, but also feedback loops set-up between molecular components of peripheral circadian clocks and different nutrient sensors [75, 80, 85]. Nutrient sensors include nicotinamide phosphoribosyltransferase (NAMPT), sirtuin1 (SIRT1), protein kinase, AMP-activated, alpha 1 catalytic subunit (Prkaa1; also known as AMPK) and various transcription factors (e.g. DBP, NFIL3, PPAR's, ROR's, PGC-1α, SIRT1). These proteins transmit information about the cellular nutrient state to coordinate metabolic processes. In addition, input from nutrient sensors has been found to reset the phase of peripheral circadian clocks [52]. Thus, peripheral circadian clocks not only relay on input from the master circadian clock in the SCN. This has been underpinned by a study in experimentally SCN-lesioned mice as peripheral clocks retain their ability to maintain individual synchronal expression of clock genes, but showed phase misalignment between individual tissues clocks [86]. Thus, it is unsurprising, that disruption of the circadian rhythm and its molecular basis impacts many physiological processes. In our modern society, shift work, jet lag and over-nutrition are assumed to induce circadian clock and metabolic misalignment [87, 88]. Progression of pathophysiological conditions including cardiovascular diseases, obesity and diabetes are assumed to be a consequence of this misalignment. In the following paragraph, peripheral circadian clocks in the cardiovascular system and adipose tissue will be discussed in more details.

1.2.4 Circadian clock and the cardiovascular system

Various cardiovascular processes including blood pressure, vascular function and heart rate exhibit day-of-time dependent variations [89-92]. These changes arise through various endogenous and exogenous signals. Although mechanistically incompletely understood, these signals are aligned to the circadian rhythm and orchestrate cardiovascular functions [71, 93, 94]. The SCN is thought to play an important role in this process communicating integrated exogenous signals via the endocrine and autonomic nervous system [95, 96]. This might affect different hypothalamic regions associated with blood pressure regulation, RAA system, endothelial regulation of vascular tone and circulating vasoactive peptides [71]. Epidemiological studies indicate an association of circadian misalignment and the onset of cardiovascular diseases underscoring the importance of the circadian clock in this regard [87, 88, 97, 98]. In shift workers, the risk of cardiovascular diseases is increased relative to daytime workers [98]. Acute myocardial infarctions, stroke and ventricular tachycardia have been reported to manifest mainly in the morning hours [99-101]. Growing evidence has been accumulating for a direct role of the molecular components of the circadian clock regulating cardiovascular functions [71]. Targeted deletions of core clock genes in mice further strengthened this association. Deletion of *Per2* decreases endothelial NO production impairing vasorelaxation of VSMCs [102]. *Cry1/2* double knockout mice were shown to have increased circulating aldosterone level resulting in salt-sensitive hypertension [103]. VSMC-specific deletion of *Pparg* inhibits *Bmal1* expression leading to elevated mean arterial pressure and heart rate [104]. This further strengthened the association of metabolic dysfunction, circadian misalignment and cardiovascular diseases. Studies in patients diagnosed with type 2 diabetes mellitus (T2DM) uncovered elevated blood pressure and heart rate associated with defects in 24 hour blood pressure rhythmicity [105]. Mouse models of T2DM showed a similar phenotype complemented with changes in circulating vasoactive hormones, vascular and sympathetic tone [106-109]. Interestingly, rhythmic food intake is abolished in T2DM mouse models and mice fed with high-fat diet, that can be restored with a strict feeding regime [110, 111]. This suggests a profound relationship of the circadian clock and the metabolism in blood pressure regulation. In addition, adipose tissue, particularly relevant to metabolic homeostasis, is essential for the control of cardiovascular functions [9, 30, 112]. Circadian misalignment in adipose tissue might negatively affect the activity of the cardiovascular system [68].

1.3 Adipose tissue

1.3.1 Adipose tissue function

The classical roles of adipose tissue are to store free fatty acids (FFA) and to release them during periods of fasting to ensure sufficient energy availability [113]. Additional functions such as non-shivering thermogenesis, protection of organs against mechanical damage and thermal insulation evolved [113]. However, over the last 20 years, adipose tissue has been recognized as a complex endocrine organ [114, 115]. Adipose tissue communicates with and plays a critical role in the regulation of function of nearly all other organs. This is achieved through endocrine and paracrine interactions. Analysis of adipose tissue secretory profile revealed a variety of hormones (termed adipokines), cytokines and other bioactive molecules secreted [114, 116]. Most prominent adipokines are leptin and adiponectin as well as cytokines including interleukins and TNF-α. Secreted factors have been implicated in the physiological responses including appetite control, hormone secretion, inflammatory processes and vascular reactivity [113].

On the other hand, adipose tissue function is controlled through a variety of hormonal, neuronal and local factors (autocrine interaction) [113, 117]. Most prominent hormones are insulin and glucagon; both are secreted from pancreatic cells, balancing FFA storage and release. Adipose tissue is highly innervated by nerve endings from the parasympathetic and sympathetic nervous system to control tissue function [118]. CNS output has been implicated in lipolysis [119] and leptin secretion [120]. In addition, the parasympathetic nervous system plays a critical role in regulating adipose tissue insulin sensitivity [121].

1.3.2 Structural heterogeneity of adipose tissue

Adipose tissue mainly consists of adipocytes [122]. In addition, other cell types including preadipocytes, macrophages, fibroblasts and endothelial cells have been found and termed as stromal vascular fraction (SVF). The SVF accounts for a variety of factors secreted from adipose tissue and is indispensable for adipose tissue function [123]. Depending on adipocyte morphology and function, at least two distinct adipose tissue types are known: brown and white adipocytes (**Figure 1-3-1**) [124, 125].

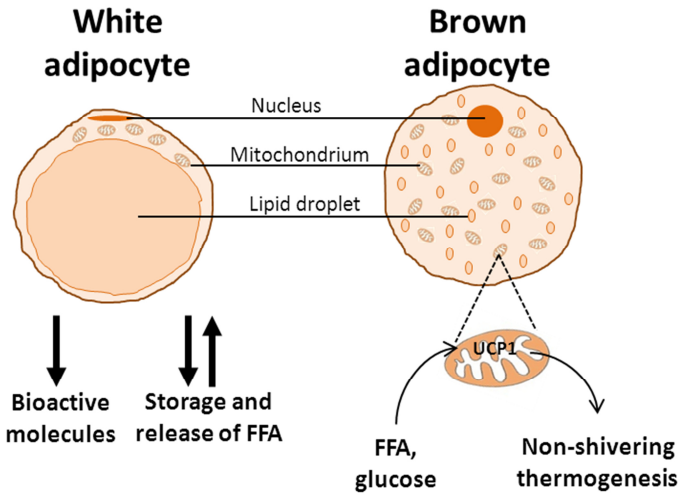

Figure 1-3-1: Morphology and function of white and brown adipocytes. A white adipocyte contains one large unilocular lipid droplet. Cytoplasm area is limited containing a few mitochondria and a squeezed nucleus. In contrast, a typical brown adipocyte comprises multilocular lipid droplets and densely packed mitochondria. For non-shivering thermogenesis, brown adipocyte mitochondria are uniquely equipped with uncoupling protein 1 (UCP1). FFA (free fatty acids).

White adipose tissue (WAT) is characterized by adipocytes large in diameter (25 - 200 µm) containing unilocular lipid droplets [126]. WAT is the most abundant adipose tissue type in humans and mice. It is best known for body's largest energy store and the release of multiple adipokines (adiponectin, leptin) and cytokines (TNF-α, IL-6). In contrast, brown adipose tissue (BAT) is less abundant and composed of small multilocular adipocytes (< 60 µm) enriched in mitochondria [117, 127]. BAT mainly contributes to heat production through non-shivering thermogenesis. For this purpose, brown adipocytes uniquely express uncoupling protein 1 (UCP1) necessary for mitochondrial uncoupling of oxidative phosphorylation [128] and heat production instead of ATP. Other BAT specific markers are cell death-inducing DNA fragmentation factor, alpha subunit-like effector A (CIDEA), PR domain containing 16 (PRDM16) and PPARgamma co-activator 1 alpha (PGC1α) [117, 124]. Many years, BAT has been thought to play a role only in rodents and human infants. This assumption has completely changed as distinct BAT deports in the neck and trunk region has been reported by Nedergaard and Cannon in human adults in 2007 [129]. Additional studies confirmed these findings [130, 131]. In addition, both adipose tissue types are found in different anatomical areas of the body in both humans and mice (**Figure 1-3-2**) [132]. Depending on the anatomical area, adipose tissue depots are different in structure, cell composition and biological function. One of these adipose tissue depots is perivascular adipose tissue.

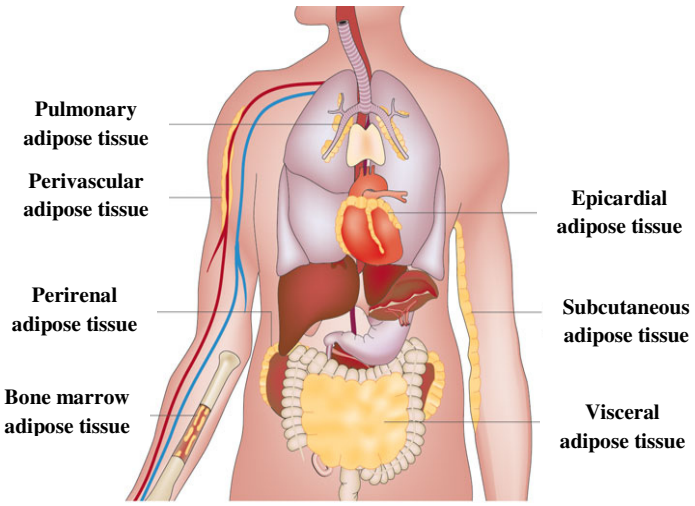

Figure 1-3-2: Anatomical localization of different adipose tissue depots throughout the human body. Most abundant are visceral and subcutaneous adipose tissue depots. Other depots are located around the kidney, heart, bone marrow, pulmonary and systemic arteries. Figure adapted from [133].

1.3.3 Perivascular adipose tissue

1.3.3.1 Structure and function

Perivascular adipose tissue (PVAT) surrounds most systemic blood vessels. It lies directly on the adventitia without any separating structure. Although initially thought to play only a role in structural support of underlying blood vessel, PVAT has been recognized to regulate blood vessel tone and homeostasis [9, 134, 135].

Referring to the different types of adipose tissue, PVAT can be classified as either white or brown-like adipose tissue. In mice, Fitzgibbons *et al.* identified PVAT surrounding the thoracic aorta as brown-like [7]. In this study, perivascular adipocytes express a nearly identical BAT gene profile including *Ucp-1*, *Cidea* and *Prdm16*. Furthermore, perivascular and brown adipocyte morphology resembles in multilocular lipid droplets and abundant mitochondria. In contrast, PVAT surrounding the abdominal aorta [136], mesenteric [137] and coronary arteries [138] can be referred to as white. The heterogeneity of regional PVAT depots localized in different vascular beds further translates to distinct secretory profiles [137].

In accordance to its specific function in the regulation of blood vessel reactivity, PVAT properties differ from other adipose tissue depots [138]. PVAT has distinct gene expression and secretory profiles, but also perivascular adipocytes with a distinct developmental stage [138]. PVAT consist of adipocytes and SVF. Similar to other adipose tissue depots, SVF is crucial for PVAT function and secretes bioactive molecules [139]. This becomes clearly evident under pathophysiological conditions such as hypertension and obesity [140-142] and will be reviewed in chapters 1.3.3.3 and 1.3.3.4.

1.3.3.2 Paracrine effects of PVAT on blood vessel reactivity

In 1991, Soltis and Cassis were the first describing the importance of PVAT on blood vessel reactivity [8]. Performing *ex vivo* organ chamber experiments, they demonstrated reduced vasoconstriction to noradrenalin of aortic rings with PVAT compared to aortic rings without PVAT isolated from rats. Almost a decade later, these findings were rediscovered [143, 144]. Today, PVAT is widely accepted as an endocrine organ regulating vascular tone and homeostasis.

Similar to other adipose tissues, PVAT secretes a variety of substances mediating PVAT vasoactive properties. Substances can induce vasodilation, vasoconstriction or both of underlying VSMCs. Under physiological conditions, PVAT exerts vasodilating properties as secretion of vasoconstrictors is low and superimposed by vasodilators. Adiponectin [145], visfatin [146] and methyl palmitate [147] have been discovered as PVAT-derived relaxing factors (PDRFs) promoting vasodilation. Leptin [148], hydrogen peroxide (H_2O_2) as well as TNF-α and IL-6 contribute to blood vessel tone by their vasodilatory and vasocontractile properties. Although still under investigation, mechanisms mediating PVAT vasodilating properties are diverse. They can be endothelium-dependent or independent and involve the action of various vasorelaxing metabolites [149-152]. Mechanisms independent of the endothelium involve activation of VSMC potassium channels (mainly K_{ATP}; K_V; K_{BKa}) [153-156]. Interestingly, effects of some PVAT-derived vasoactive substances such as TNF-α and H_2O_2 highly depend on the vascular bed, species and their concentrations [31, 157]. The role of nerve endings in PVAT is poorly understood and controversial. Dukrovska *et al.* reported that the release of vasoactive substances from PVAT does not involve nerve endings [154], other hypothesized that nerve endings are important for normal PVAT function [158].

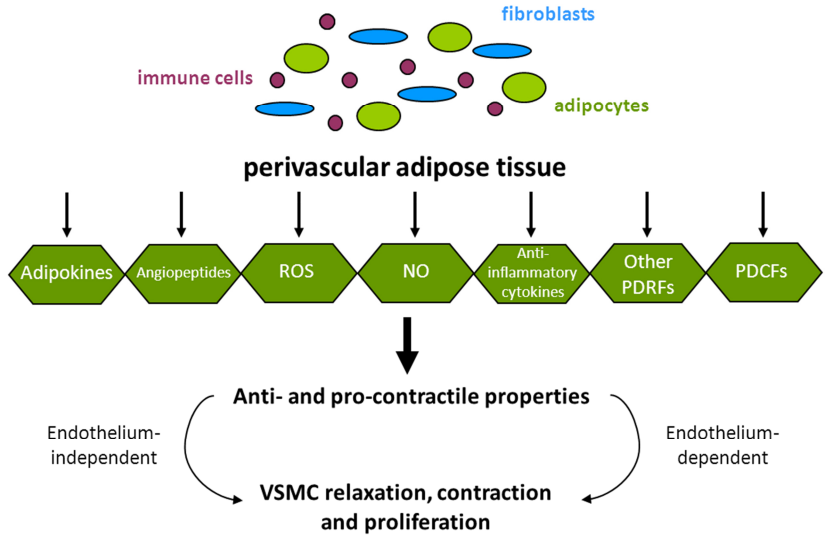

Figure 1-3-3: PVAT-derived vasoactive substances implicated in the regulation of vascular reactivity. PVAT vasoactive properties are mediated through a variety of substances secreted from different cells types which reside within PVAT. Anti- and pro-contractile properties can be dependent and independent of the endothelium mediating VSMC relaxation and contraction as well as proliferation. Figure adapted from [159].

Interestingly, some studies ruled out the release of PVAT-derived vasocontracting factors (PDCFs). These include not only H_2O_2, leptin, TNF-α and IL-6, but also different angiopeptides, resistin and reactive oxygen species (ROS) [159, 160]. PDCFs have been implicated in mediating vasoconstriction of underlying VSMCs, an observation which has already been made by Soltis and Cassis [8]. Mechanisms might be Ca^{2+}-dependent and independent [31, 161]. Intriguingly, the release of PDCFs has been reported to be increased under pathophysiological conditions [9]. Angiotensin II (ANGII) promotes the conversion of NO into oxygen free radicals impairing vasodilation of VSMCs [162]. Elevated ANGII levels have been further connected to the increased secretion of pro-inflammatory and adhesion-promoting molecules. This enhances adhesion and migration of monocytes through the blood vessels promoting vascular dysfunction.

1.3.3.3 Role of PVAT in hypertension

As already described in chapter 1.1.5, hypertension is a multifactorial disorder and characterized by an increase in blood pressure. In the vasculature, ECs dysfunction and VSMC remodeling are two widely accepted states contributing to the progression of hypertension. The role of PVAT is less well understood. Data from a few rodent studies pointed out that reduction in PVAT mass contributes to the loss of PVAT anti-contractile properties [147, 163-165]. This has been associated with increased vasoconstriction in different vascular beds. The mechanism how PVAT's anti-contractile properties get lost in hypertension is still a question of ongoing research. It is conceivable, that different mechanisms have to be taken into consideration.

Secretome analysis performed by Ruan *et al.* in hypertensive DOCA-salt rats, identified complement 3 as the most abundant molecule secreted from thoracic PVAT [165]. Complement 3 has been implicated in vascular remodeling, a common process in hypertension. However, dysregulation of VSMC vasodilatory response to PVAT-derived anti-contractile signals has also been shown [166]. Several independent studies revealed a reduction in PDRFs secretion from PVAT. This includes methyl palmitate, leptin and adiponectin, which could be linked to elevations in VSMC constriction [147, 156]. Loss of PVAT anti-contractile properties could be in part mediated through an increase in pro-contractile molecules released from PVAT and macrophages such as TNF-α and superoxide anions [167]. Elevated TNF-α levels further promote the secretion of other pro-inflammatory cytokines (e.g. IL-6) from PVAT triggering vessel wall inflammation. Vascular inflammation negatively impacts vessel wall properties and is a common characteristic of hypertension [135].

PVAT infiltrating cells might further contribute to PVAT dysfunction in hypertension. Withers *et al.* demonstrated that deletion of monocytes protects mice against experimentally induced hypertension [139]. Macrophages are a well-known source of TNF-α [168]. In PVAT, increased TNF-α levels have been reported to reduce adiponectin secretion diminishing NO bioavailability to VSMC [169-172]. Thus, it is likely, that infiltrating macrophages and vessel wall inflammation contribute to loss of PVAT anti-contractile properties during hypertension.

1.3.3.4 Role in obesity

In situations with balanced energy intake and expenditure, PVAT exerts protective and beneficial properties on the vasculature. Properties are directly related to PVAT mass. There is growing evidence that obesity contributes to PVAT dysfunction. Mechanisms are still incompletely understood. Studies in humans and rodents emphasize that changes in PVAT secretory profile as well as infiltrating immune cells are integral parts in this process. In obese humans, PVAT mass is increased and anti-contractile properties are diminished [173]. This has been linked to alterations in the secretome of PVAT and increased PDCFs and pro-inflammatory molecules secretion. Studies in mouse models of obesity pointed into the same direction. Genetically or HFD-induced obesity promotes PVAT dysfunction [138, 174, 175]. In line with other adipose tissue depots, secretion of vasoactive substances is changed. For instance, the release of adiponectin from perivascular adipocytes is reduced [176], while leptin secretion is enhanced [138, 177]. Both contribute to endothelial dysfunction diminishing NO bioavailability and promote vasoconstriction of VSMC. Interestingly, in obese mice, hypertrophic perivascular adipocytes promote the generation of a hypoxic, pro-inflammatory and oxidative environment within the vasculature [173]. This might be in part triggered through changes in PVAT secretory profile and manifests in increased

macrophage infiltration, ROS production as well as eNOS dysfunction [175, 177]. Interestingly, insulin mediated vasodilation of VSMC can be modulated by adipokines [178] and changes in adipokine abundance might impair insulin signaling.

1.3.4 Circadian clock, diurnal rhythm and adipose tissue function

There is growing evidence that the circadian clock controls adipose tissue development and endocrine function [66, 67, 179]. Interplay between adipose tissue and the circadian clock has been demonstrated by the discovery of core clock gene expression in various adipose tissue depots [84, 180]. Clock-output manifests in rhythmic lipolytic activity and adipokine secretion [181, 182]. Mutations and gene polymorphism of core clock genes and ccg´s can disrupt physiological adipose tissue function and development. Mice lacking *Bmal1* or *Per2* show impaired adipogenesis, fatty acid oxidation and lipogenesis [67, 179]. Deletion of *Clock* leads to hyperlipidemia and hyperleptinemia, but also impairs pancreatic β-islet proliferation and insulin secretion [183] increasing the risk of T2DM. Epidemiological studies in humans further strengthened these findings. In obese humans, circulating leptin and adiponectin do not follow physiological 24 hour rhythms [184]. Genetic polymorphisms of different core clock genes have been linked to an increased risk of obesity and its comorbidities such as cardiovascular diseases and T2DM [185, 186]. In this context, time of food intake and time restricted feeding has been found to influence circadian clock-output. Intake of high-caloric food in the evening and drop of breakfast has been associated with increased weight gain [187]. Shift workers develop an increased risk of obesity and associated comorbidities [87, 188]. Studies in mouse models of obesity confirm these findings [189]. In adipose tissue, irregular feeding/fasting cycles result in changed expression patterns of lipolytic enzymes and adipokine secretion [190]. In contrast to time-restricted feeding, excessive or restricted caloric intake seems to affect both, the master circadian clock in the SCN and peripheral circadian clocks.

In mouse models of obesity, clock gene expression is altered in the central nervous system (CNS) [191]. This probably affects the communication between the master circadian clock and adipose tissue. Nutrient sensors are attributed to play a fundamental role and might provide a mechanistically link between the nutritional state and the circadian clock. Studies in e.g. staggerer mice ($Ror\alpha^{sg/sg}$), a natural loss-of-function mutant strain of the clock gene *Rorα,* revealed that these mice are resistant to HFD-induces obesity [192, 193].

1.4 Impact of the mTOR complex 2 on the cardiovascular system

1.4.1 The mammalian target of rapamycin: an overview

The mammalian target of rapamycin (mTOR) is an evolutionarily conserved atypical serine/threonine kinase integrating both intra- and extracellular signals [194]. Intensive research over the last two decades discovered that mTOR signaling pathways are associated with central cellular processes involved in energy storage and expenditure, cell growth and proliferation as well as cytoskeletal organization (**figure 1-4-1**). As the name implicates, the natural bacterial product rapamycin is a potent inhibitor of the mTOR kinase activity [195]. mTOR assembles in two functionally distinct multiprotein complexes, mTOR complex 1 (mTORC1) and complex 2 (mTORC2) (**figure 1-4-1**). Common to both complexes are the catalytic subunit mTOR, mammalian lethal with sec-13 protein 8 (mLST8) [196, 197], DEP domain containing mTOR-interacting protein (DEPTOR) [198] and the TTi1/TEL2 complex (TELO2 interacting protein 1/ Telomere maintenance 2) [199]. In contrast, the regulatory associated protein of mTOR (RAPTOR) [196] and proline-rich AKT substrate 40 kDa (PRAS40) [55, 69] are specific to mTORC1. mTORC2 contains the additional proteins rapamycin insensitive companion of TOR (RICTOR) [200], mammalian stress-activated map kinase interacting protein 1 (mSIN1) [201] and protein observed with RICTOR 1 and 2 (PROTOR1/2) [202].

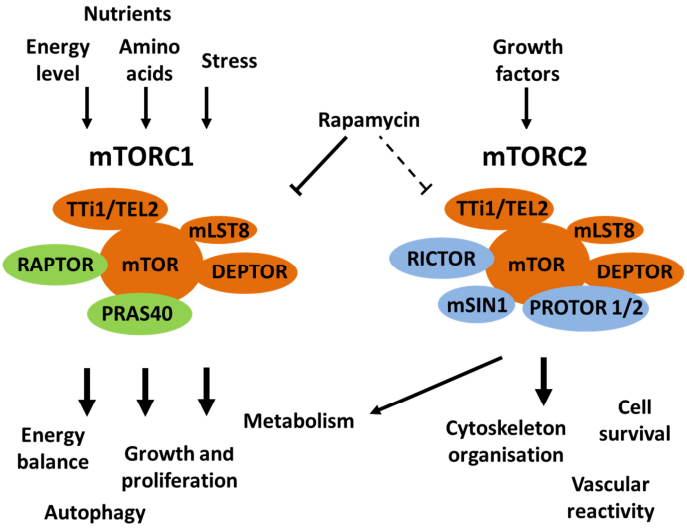

Figure 1-4-1: Structural composition, activators and cellular functions are different for mTORC1 and mTORC2. mTORC1 can be activated by a brought range of intra- and extracellular signals. Activation of mTORC2 is restricted to growth factors. Proteins RAPTOR and PRAS40 are specific to mTORC1. mTORC2 is characterized by its essential proteins RICTOR, mSIN1 and PROTOR1/2. Acute rapamaycin treatment can inhibit mTORC1 activity, while mTORC2 signaling is only inhibited upon prolonged treatment with rapamycin. mTOR (mammalian target of rapamycin), TTi1/TEL2 (TELO2 interacting protein 1/ Telomere maintenance 2), mLST8 (mammalian lethal with sec-13 protein 8), DEPTOR (DEP domain containing mTOR-interacting protein), RAPTOR (regulatory associated protein of mTOR), PRAS40 (proline-rich AKT substrate 40 kDa), RICTOR (rapamycin insensitive companion of TOR), mSIN1 (mammalian stress-activated map kinase interacting protein 1), PROTOR 1/2 (protein observed with RICTOR 1 and 2). Figure adapted from [203].

In addition, both mTOR complexes have distinct substrate specificity and cellular functions [194], but are also functionally interconnected with each other [204]. Rapamycin inhibits mTORC1 activity, while mTORC2 is relatively insensitive. However, prolonged treatment with rapamycin has been shown to disrupt mTORC2 function [205].
In the following section, function and signaling pathways of mTORC2 will be discussed in more detail.

1.4.2 The mammalian target of rapamycin complex 2

In contrast to mTORC1, which upstream regulators and downstream effectors are well characterized, less are known about how mTORC2 kinase activity is regulated and controls processes on the cellular and whole-body level [206, 207]. The absence of specific mTORC2 inhibitors has complicated the studies of this protein complex.
The usage of various genetic approaches uncovered that mTORC2 plays a key role in different cellular processes, including cell survival and proliferation as well as actin cytoskeleton organization [208]. mTORC2 signaling seems to be insensitive to nutrients, but is affected by growth factors such as insulin and insulin-like growth factor 1 (IGF-1). Mechanisms behind are not fully understood, but require phosphatidylinositol 3-kinase (PI3K) [209]. Several independent studies revealed phosphorylation of various members of the cAMP-dependent, cGMP dependent, protein kinase C (AGC kinase) family by mTORC2. These members include thymoma viral proto-oncogene 1 (AKT1) [210], serum- and glucocorticoid-induced protein kinase 1 (SGK1) [211] and protein kinase C alpha (PKC-α) [200].
RICTOR is essential for mTORC2 kinase function, acting as a scaffold recruiting different substrates to the complex [200]. Deletion of *Rictor* in cells has been shown to strongly impair mTORC2 kinase activity [206, 208]. Mouse models lacking *Rictor* in specific tissues such as pancreas, brain and adipose tissue additionally allowed the understanding of the mTORC2 signaling network and its contribution to tissue specific and overall body functions. Mice lacking *Rictor* in pancreatic β-cells exhibit moderate hyperglycemia and glucose intolerance [212]. These defects might be due to reduced β-cell mass, pancreatic insulin production and glucose-stimulated insulin secretion suggesting an active role of mTORC2 in maintaining β-cell proliferation in response to proliferative stimuli. In brain, *Rictor* deletion in the whole CNS results in reduction of brain mass, changed neuron morphology and function. As a possible consequence, motor activity is impaired in these mice [213]. Interestingly, Siuta *et al.* investigated the role of *Rictor* in the CNS using a slightly different mouse model and observed schizophrenia-associated behavior as well as changed neurotransmitter content in brain [214]. Cybulski *et al.* showed that mice lacking *Rictor* in adipocytes display increased lean mass, are slightly insulin-resistant, but exhibit no alterations in

adipogenesis and fat mass [215]. This phenotype is possible due to an increase in IGF-1 and insulin production. Interestingly, these knockout mice accumulate less overall fat mass upon HFD feeding compared with control mice fed with the same diet. Taken together, these studies strongly implicate an active role of RICTOR and/or mTORC2 in regulating adipose tissue function.

1.4.3 Implication of mTOR in the cardiovascular system

Although mTORC2 is a regulator of cellular and metabolic processes, its role in the cardiovascular system is poorly understood.

Both, RICTOR and mTOR are necessary for cardiovascular development during mouse embryogenesis. Embryos with full body knockout of *Rictor* exhibit impaired vascular system formation and die at embryonic day E10.5 [216, 217]. Interestingly, deletion of *Rictor* in heart (*Rictor*$^{\alpha Mhc\text{-}Cre}$) has no effect on postnatal heart functions, while its deletion in embryonic heart tissue (*Rictor*$^{Mesp1\text{-}Cre}$) causes heart failure and embryonic lethality [218]. Constitutive deletion of *mTor* in cardiomyocytes (c-*mTOR*$^{\alpha\text{-}MhcKO}$) causes embryonic lethality at embryonic day E13.5 [219]. In these embryos, the cardiomyocyte number is significantly reduced resulting in cardiac dilation and dysfunction. Similar to c-*mTOR*$^{\alpha\text{-}MhcKO}$ mice, tamoxifen-induced cardiomyocyte-specific deletion of *mTor* in adult mice promotes cardiac dilation and heart failure [220]. Mice suffer from mitochondrial dysfunction of cardiomyocytes, which are subjected to increased fibrosis and apoptosis. Mice die after a couple of weeks after tamoxifen injections. Thus, data indicate that mTOR is not only necessary for normal cardiac development during embryogenesis, but also maintain cardiac function and metabolism in adult mice.

Studies published accomplishing the role of mTORC2 on cardiac and vascular function in stressed and unstressed situations are sparse. Yano *et al.* uncovered a cardioprotective role of mTORC2 in ischemic preconditioned mouse hearts [221] as inhibition of both mTOR complexes, but not mTORC1 alone, attenuated mTORC2 protective effects.

In mice with experimentally induced myocardial infarction (MI), selective inhibition of mTORC2 by *Rictor* knockdown enhances ischemic damage [222]. Increased cardiomyocyte fibrosis and cell death in these mice indicate a beneficial role of mTORC2 in cardiomyocyte survival and adaptive stress response after MI. Interestingly, in the same study, evidence was provided that balanced mTORC1 and mTORC2 signaling is crucial for cardiomyocyte stress response after MI. Cardiac overexpression of PRAS40, an essential component of mTORC1, inhibits mTORC1 signaling, while protective mTORC2-mediated AKT phosphorylation at Ser473 (pAKT^{Ser473}) was enhanced, improving cardiac function after MI.

A study performed in our laboratory from Bhattacharya *et al.* demonstrated that mTORC2 in PVAT is a novel regulator of the reactivity of the thoracic aorta in mice [223]. Analysis of thoracic aortas

with and without PVAT revealed increased vasoconstriction and impaired vasodilation in response to phenylephrine. We demonstrated an up-regulation of pro-inflammatory molecule expression in thoracic PVAT including IL-6, TNF-α and iNOS without changed macrophage content. Thus, impaired mTORC2 function in PVAT diminishes PVAT vasodilatory properties affecting vascular reactivity of the thoracic aorta.

Collectively, although only limited information is available on cardiac and vascular mTORC2 function, previous reports suggest a beneficial role of mTORC2 in unstressed and stressed conditions. To better understand the role of mTORC2 in the cardiovascular system, knockout or transgenic animal models targeting specifically cells of the vascular wall are required.

1.5 Aim of the study

Intensive research over the last 10 years has increased our knowledge on perivascular adipose tissue (PVAT) function and its interaction with the underlying blood vessel. Complex mechanisms regulate PVAT properties. If deregulated, PVAT properties contribute to the impairment of adjacent blood vessel reactivity as observed in hypertension and obesity. Despite of all efforts, a question that remains to be addressed is which signaling pathways contribute to changes in PVAT function in hypertension and other pathophysiological conditions. Recently, we identified mTORC2 as a novel regulator of vascular reactivity as vasoconstriction was increased and vasodilation impaired using mice lacking *Rictor* in adipocytes generated by crossing *Rictor*$^{fl/fl}$ mice with *aP2*-CRE transgenic mice (*Rictor*^{aP2KO}). Thoracic PVAT properties changed to a more pro-inflammatory state as showed by increased pro-inflammatory molecules expression. Inhibition of iNOS normalized vascular function. However, nothing is known about the mTORC2 signaling network in PVAT and how impaired mTORC2 functions contribute to altered PVAT properties.

Three main objectives of the study presented here were:

(1) To investigate daily blood pressure and locomotor activity regulation in *Rictor*^{aP2KO} and control mice by recording hemodynamic parameters using a radiotelemetric approach.

(2) To identify and characterize RICTOR-associated signaling pathways in PVAT involved in functionality of PVAT using a micro array. This approach allows analyzing mRNA expression of the whole genome.

(3) To investigate the impact of iNOS inhibition on blood pressure using subcutaneously implanted mini pumps emitting the iNOS-specific inhibitor 1400W or saline as solvent control.

2. Results

2.1 Part I

DELETION OF RICTOR IN BRAIN AND FAT ALTERS PERIPHERAL CLOCK GENE EXPRESSION AND INCREASES BLOOD PRESSURE

Contributions:

Katja Drägert[1,2], Indranil Bhattacharya[1,2], Giovanni Pellegrini[3], Petra Seebeck[4], Abdelhalim Azzi[5], Steven A. Brown[5], Stavroula Georgiopoulou[1,2], Ulrike Held[6], Przemyslaw Blyszczuk [7], Margarete Arras[8], Rok Humar[1,2], Michael N. Hall[9], Edouard Battegay[1,2,10], Elvira Haas[1,2]

[1]Research Unit, Department of Internal Medicine, University Hospital Zurich

[2]Center of Competence Multimorbidity and University Research Priority Program "Dynamics of Healthy Aging", University of Zurich

[3]Institute of Veterinary Pathology, Vetsuisse Faculty, University of Zurich

[4]Zurich Integrative Rodent Physiology, University of Zurich

[5]Institute of Pharmacology and Toxicology, University of Zurich

[6]Horten Center for Patient-Oriented Research and Knowledge Transfer, University of Zurich

[7] Cardioimmunology, Center of Molecular Cardiology, University of Zurich

[8]Division of Surgical Research, University Hospital Zurich, Switzerland

[9]Biozentrum, University of Basel

[10]Zurich Center for Integrative Human Physiology, University of Zurich

All Switzerland

Short Title: MTORC2 regulates blood pressure and peripheral clock gene expression

Correspondence to: Elvira Haas, Research Unit, Department of Internal Medicine

University Hospital Zurich, Wagistrasse 12, 8952 Schlieren, Switzerland

Email: Elvira.haas@usz.ch, Phone: +41 44 5563234, Fax: +41 44 5563232

Key words: mTOR complex 2, RICTOR mouse, adipose tissue, arterial pressure, circadian clocks, locomotor activity

2.1.1 Abstract

The mammalian target of rapamycin complex 2 (mTORC2) contains the essential protein RICTOR and is activated by growth factors. mTORC2 in adipose tissue contributes to the regulation of glucose and lipid metabolism. In the perivascular adipose tissue mTORC2 ensures normal vascular reactivity by controlling expression of inflammatory molecules.

To assess whether RICTOR/mTORC2 contributes to blood pressure regulation, we applied a radiotelemetry approach in control and *Rictor* knockout (*Rictor*^{aP2KO}) mice generated by using *adipocyte protein-2* gene promoter-driven CRE recombinase expression to delete *Rictor*. 24 hour mean arterial pressure was increased in *Rictor*^{aP2KO} mice, and the physiologic decline in mean arterial pressure during the dark period was impaired. In parallel, heart rate and locomotor activity were elevated during the dark period with a pattern similar to blood pressure changes. This phenotype was associated with mild cardiomyocyte hypertrophy, decreased cardiac natriuretic peptides and their receptor expression in adipocytes. Moreover, clock gene expression was reduced or phase-shifted in PVAT. No differences in clock gene expression were observed in the master clock suprachiasmatic nucleus, though *Rictor* gene expression was also lower in brain of *Rictor*^{aP2KO} mice.

Thus, the present study highlights the importance of RICTOR/mTORC2 for interactions between vasculature, adipocytes and brain to tune physiological outcomes such as blood pressure and locomotor activity.

2.1.2 Introduction

The serine/ threonine kinase mammalian target of rapamycin (mTOR) is ubiquitously expressed and exists in 2 multi-protein complexes, mTOR complex 1 (mTORC1) and complex 2 (mTORC2) [1,2]. The rapamycin-insensitive companion of mTOR (RICTOR) is essential for the role of mTORC2 in propagating phosphoinositid-3-kinase elicited signals originating from hormones and growth factors [2, 3]. mTORC2 phosphorylates and activates members of the AGC kinase family such as AKT [4]. Adipocyte-specific ablation of *Rictor* results in higher lean mass due to increased levels of insulin and insulin-like growth factor (IGF-1), enhanced glucose metabolism and insulin resistance in mice [5, 6]. Using this mouse model we have recently shown that vascular reactivity of the thoracic aorta with perivascular adipose tissue (PVAT) is altered and levels of inflammatory molecules in the PVAT are elevated [7]. However, the specificity of *adipocyte protein-2* (*aP2*) gene promoter-driven CRE recombinase expression for adipose tissue, an approach which was used for all above mentioned studies, may vary and affect other tissues [8]. Consequently, target gene expression data from different organs should be considered for interpretation. In the present study we refer to these mice as $Rictor^{aP2KO}$ mice.

In a healthy condition, PVAT releases vasoactive molecules conferring anti-contractile properties to PVAT [9]. In obesity, PVAT's secretory profile changes to favor a pro-inflammatory state compromising PVAT's anti-contractile properties [10]. Impaired PVAT function contributes to alterations in vascular reactivity which manifests itself in blood pressure changes as observed previously in a rat model of hypertension [11]. Intriguingly, inflammation is present in the vasculature in animal models of hypertension [12, 13], which supports the idea that inflammation of PVAT might play a significant role in the development of hypertension. The key characteristics of essential hypertension are hyperactivation of the renin-angiotensin aldosterone system and the sympathetic nervous system [14]. These 2 systems are also under the control of the circadian clock [15], which is not surprising considering the diurnal fluctuations in blood pressure. Clock genes are part of a hierarchically organized circadian clock system in which the suprachiasmatic nucleus (SCN) in the hypothalamus serves as a master clock [16]. The SCN is entrained by the light/dark cycle and transmits humoral and neural signals to synchronize peripheral clocks located in most tissues, including the heart, adipose tissue and blood vessels [15].

In the present study, we examined whether the increase in aortic contractility due to impaired PVAT function, which we reported previously, translates into elevated blood pressure.

2.1.3 Results

2.1.3.1 Mean arterial pressure is increased and its physiological decline nearly absent in Rictor^{aP2KO} mice

To investigate whether the increased aortic contractility which we observed previously in *Rictor*^{aP2KO} mice [7] translates into higher blood pressure, hemodynamic parameters were recorded using radiotelemetry. The 24 hour average of mean arterial pressure (MAP, Figure 1B, left panel and table S1) and diastolic arterial pressure (DAP, Table S1) were increased in *Rictor*^{aP2KO} mice (+5.4mmHg and +4.4mmHg, respectively; $P<0.05$), while systolic arterial pressure (SAP) displayed an upward trend ($P=0.08$, Table S1) compared with control mice. Pulse pressure was similar between groups (Table S1). To determine diurnal patterns of MAP in *Rictor*^{aP2KO} and control mice, we analyzed data obtained from a telemetric measurement over 7 days. Both groups displayed diurnal rhythmicity of MAP (Figure 1A, left panel). A detailed analysis for day five is shown in Figure 1A (right panel). However, the physiological decline of MAP in *Rictor*^{aP2KO} mice during the second half of the dark period appeared to be nearly absent (Figure 1A). Therefore, we analyzed MAP during the first and second half of the dark period separately. MAP was not significantly different during the first half of the dark period (Figure 1B, grey shaded area). While decreasing significantly during the second half only in controls ($P<0.05$), MAP remained high in *Rictor*^{aP2KO} mice (Figure 1B, grey shaded area). The Pearson correlation coefficient between time and MAP values during the second half of the dark period for control and *Rictor*^{aP2KO} mice had median values of -0.3 and 0, respectively (Figure 1C). This suggests that the decline in MAP during the second half of the dark period is nearly absent in *Rictor*^{aP2KO} mice. In the first half of the light period, MAP values were different between groups ($P<0.05$), while MAP levels were similar in the second half, showing a steady increase with highest values at the transition to the dark period (ZT12/ 7pm; Figure 1B). A detailed analysis of the DAP, SAP, and heart rate (HR) for day five revealed that these blood pressure parameters followed similar patterns as MAP (Figure 1D).

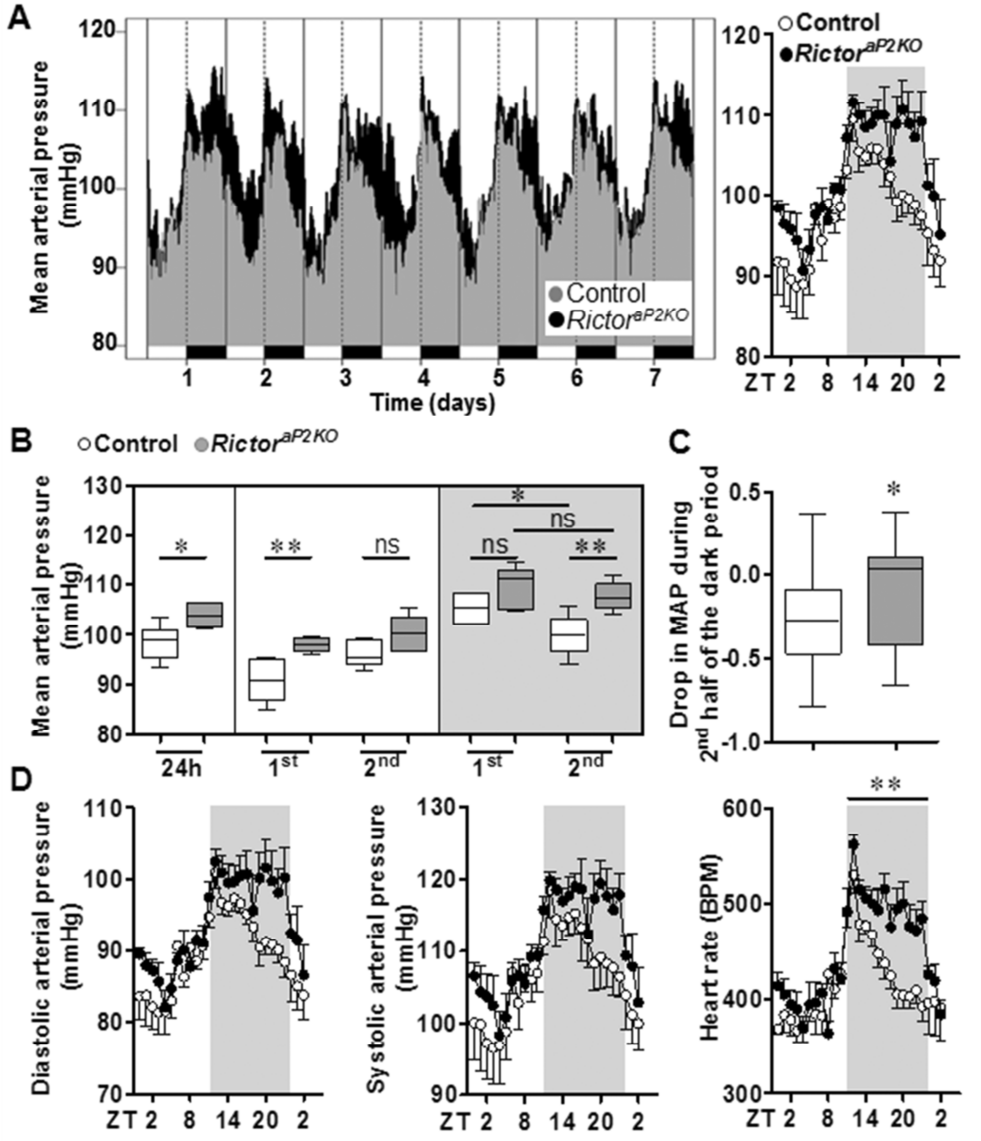

Figure 1: Mean arterial pressure is increased and its physiological decline is strongly impaired in *Rictor*^{aP2KO} mice. (A, left panel) Diurnal fluctuations of MAP are represented as 1 hour running median in *Rictor*^{aP2KO} and control mice. The 12:12 hour light/dark cycle is schematically depicted as white and black bars, respectively (light was switched on at Zeitgeber time (ZT) 0: 7 am; light off: 7 pm/ ZT12). (**A, right panel)** MAP values are represented as hourly means ± SEM for day five. The grey shaded area denotes the dark period. **(B)** MAP measurements were analyzed during 24 hours, for the first and second half of the light and dark periods, separately. The median is indicated as a horizontal line**.** (**C**) MAP drops in control, but not in *Rictor*^{aP2KO} mice during the 2nd half relative to the 1st half of the dark period. (**D**) Diastolic and systolic arterial pressure and heart rate were analyzed in the conditions outlined in A. n=5/6. **P*<0.05, ***P*<0.01 vs control. ns indicates nonsignificant.

2.1.3.2 Impaired decline of locomotor activity during the dark period and overall hyperactivity in Rictor^{aP2KO} mice

Locomotor activity is an important parameter that could account for the observed changes in blood pressure regulation [17]. In both mouse groups, the intensity of locomotor activity followed a diurnal pattern (Figure 2A). In control mice, locomotor activity peaked at the beginning of the dark period and gradually decreased as the dark period progressed. During the light period, only low activity was observed (Figure 2A, upper panel) in these mice. Interestingly, in the second half of the dark period, *Rictor*^{aP2KO} mice had a tendency to maintain high locomotor activity (Figure 2A, lower panel, red shaded areas: 1:00 to 7:00 am), which appeared to continue intermittently as indicated by the spikes during the light period (Figure 2A, lower panel). A detailed analysis for day 5 is shown in Figure 2B. Next, we quantified overall activity data collected during the telemetric measurements. During the light and dark periods, *Rictor*^{aP2KO} mice displayed a strong trend towards higher intensity of activity (light, P=0.082; dark, P=0.18, Table S2). Interestingly, the percentage of time during which mice show activity [17], an alternative measure for locomotor activity, was increased in *Rictor*^{aP2KO} mice compared with controls during a 24 hour cycle (Figure 2D, Table S2). Analyzing the light and the dark periods separately, we observed a significant increase in the time during which *Rictor*^{aP2KO} mice show activity compared with controls (Table S2). During the dark period this increase was remarkably more pronounced.

Differences in HR during the dark period amounted to +50 and +19 BMP per minute during light period in *Rictor*^{aP2KO} mice compared with controls (Table S1, P<0.05). Similarly to MAP, HR remained high during the progression of the dark period (Figure S1). To visualize the similar patterns of MAP, HR and locomotor activity during the dark period, these parameters were plotted in a single diagram displaying intensity of activity and MAP or HR, using two different y-axes (Supplemental Figure S2A and B). The curves for the intensity of activity were highly similar to those for MAP and HR within the groups.

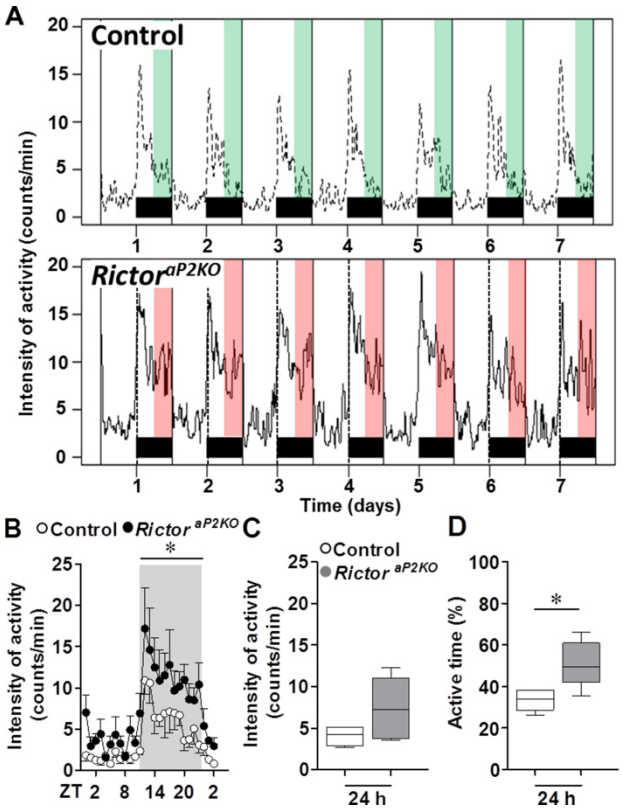

Figure 2: Intensity of activity and active time are increased in *Rictor*^{aP2KO} mice. (A) Values plotted represent the 1 hour running median of the intensity of activity for control and *Rictor*^{aP2KO} mice. The black bars at the bottom indicate the 12 hour dark period and the red and green shaded areas correspond to the second half of the dark period in *Rictor*^{aP2KO} (lower panel) and control (uppe panel), respectively. (**B**) Measurements were analyzed during 24 hour on day five. The grey shaded area indicates the dark period. Values are means ± SEM. **(C)** Intensity of activity and **(D)** active time during a 24 hour cycle are represented. The median for each group is indicated as a horizontal line. n=5/6. **P*<0.05 vs control.

2.1.3.3 aP2 promoter-driven CRE expression ablates Rictor in adipocytes and brain

To confirm deletion of *Rictor* in adipocytes in our current set of *Rictor*^{aP2KO} mice, we measured mRNA expression levels in PVAT using quantitative real time-PCR. Steady state mRNA expression levels of *Rictor* were reduced by 59% in PVAT, while they were similar in the aortic tissue between mouse groups (Figure 3A). As adipose tissue consists not only of adipocytes, but also other cells referred to as stromal vascular fraction (SVF), we separated adipocytes from SVF. In adipocytes from epididymal adipose tissue (EFAT) of *Rictor*^{aP2KO} mice, *Rictor* expression was decreased by 58%, while similar levels were measured in control and knockout SVFs (Figure 3A). Further analysis of *Rictor* mRNA expression levels revealed no differences in the heart, kidney, liver, monocytes and T cells between groups (Figure 3A). Interestingly, *Rictor* mRNA levels were decreased in the brain (SCN by 76%; cortex by 66%, Figure 3A). Collectively, these data suggest that *Rictor* is specifically ablated in the adipocytes and brain, while SVF and aortic tissue were not affected.

We further characterized the impact of *Rictor* deletion in PVAT and brain. Histological examination of cross sections of thoracic aortas with PVAT revealed higher perivascular cell density in *Rictor*^{aP2KO} mice compared with controls (Figure 3B, right panel). Consistently, the number of nuclei was 57% higher in PVAT from *Rictor*^{aP2KO} mice (P<0.01, Figure 3B). Brains of *Rictor*^{aP2KO} mice appeared smaller (Figure 3C, left panel) and absolute brain weight was decreased by 17% compared with controls (Figure 3C, right panel).

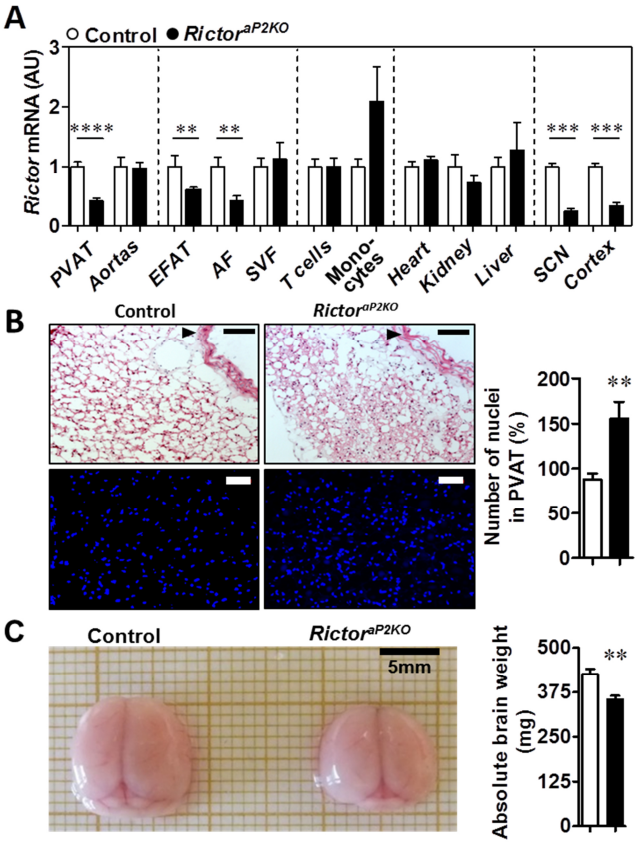

Figure 3: *aP2*/CRE-driven deletion of *Rictor* decreases expression of *Rictor* in adipocytes and brain. **(A)** Steady state mRNA expression levels of *Rictor* were determined using qRT-PCR in *Rictor*^{aP2KO} and control mice. Values are expressed in arbitrary units (AU). PVAT: n=8, aortas: n=7/8, EFAT: n=8/9, adipocyte fraction (AF): n=7/11, stromal vascular fraction (SVF): n=4, T cells and monocytes: n=2/4, heart and kidney: n=7/8, liver: n=3, SCN (suprachiasmatic nucleus): n=3/5 and cortex: n=3/5. **(B)** Cross sections of thoracic aortas with PVAT from control and *Rictor*^{aP2KO} mice stained with haematoxylin/eosin (upper panel; black bar: 100 µm), and Hoechst (lower panel; white bar: 50 µm). Arrowheads indicate the thoracic aorta. Cell density of the perivascular tissue was determined by counting Hoechst-stained nuclei (n=5). **(C)** Representative photographs of brains and quantification of absolute brain weight from each genotype (n=7/8). Values are means ± SEM. ***P*<0.01, ****P*<0.005, and *****P*<0.001 vs control.

2.1.3.4 Evidence of mild cardiomyocyte hypertrophy in Rictor^{aP2KO} mice

Next, we carried out morphological assessment of the heart to evaluate the presence of possible hypertrophic changes. Mean absolute heart weights were higher in *Rictor^{aP2KO}* mice (Figure 4A), while mean relative to body heart weights were not changed compared with controls (Figure 4A). Right ventricular free wall and interventricular septal thickness was increased in *Rictor^{aP2KO}* mice (*P*=0.09 and *P*=0.08, respectively, Figure 4A). The hearts of *Rictor^{aP2KO}* mice exhibited histological changes consistent with mild cardiomyocyte hypertrophy, as indicated by a 25% increase in the cardiomyocyte cross-sectional area (Figure 4B, *P*<0.01). Staining with Masson's trichrome revealed no evidence of fibrosis in the myocardium (data not shown). As it has been shown that *Rictor^{aP2KO}* mice exhibit increased organ size [5], we suspect that increased absolute heart weights and mild enlargement of the cardiomyofibres are most likely due to the overall phenotype, rather than to a compensatory change secondary to the only mild increase in blood pressure. In addition, there were no findings consistent with vascular remodeling secondary to hypertension [18], such as narrowing of the lumen, medial hypertrophy or increased adventitial fibrosis in the aorta or in the renal and pulmonary small and large arteries of *Rictor^{aP2KO}* mice (Supplemental Figure S3 and data not shown). Representative cross sections of heart, kidney and aortic arch are shown in supplemental figure S3. Interestingly, gene expression levels of cardiac hypertrophy biomarkers were decreased in the heart of *Rictor^{aP2KO}* mice: *Atrial natriuretic peptide* (*Anp*) was decreased by 52% (*P*<0.05), while *brain NP* (*Bnp*) and *β-myosin heavy chain* (*β-Mhc*) showed a strong downwards trend (Figure 4C, left panel). The natriuretic peptides (NPs) bind to the transmembrane high affinity NP receptors NPR1, NPR2 and NPR3 [19]. These receptors are expressed in adipocytes to regulate adipose tissue metabolism including lipolysis and adipokine secretion [19]. *Npr2* and *Npr3* mRNA expression levels were decreased in adipocytes isolated from EFAT by 51% and 45%, respectively (Figure 4C, middle panel). A similar expression pattern of NP receptors was measured in PVAT (Figure 4C, right panel). In contrast, the *Anp* gene expression was nearly absent in PVAT.

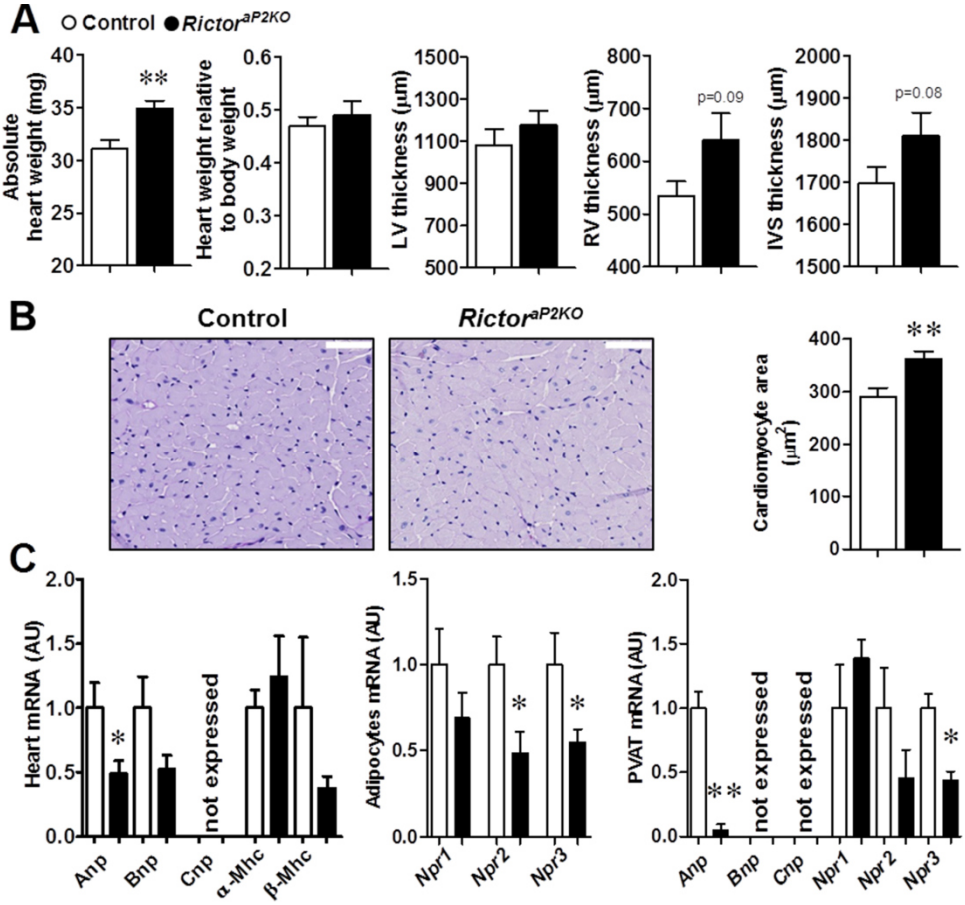

Figure 4: Mild cardiomyocyte hypertrophy and decreased gene expression of natriuretic peptides and their receptors in *Rictor*^{aP2KO} mice. (**A**) Quantification of total heart weight, heart weight relative to body weight, LV, RV and IVS thickness. n=7/8. (**B**) Representative images of heart tissue stained with Periodic acid-Schiff reaction (white bar: 50 µm) and quantification of cardiomyocyte area. (**C**) Steady-state mRNA expression levels of indicated genes were determined in heart (left panel, n=7/8), in adipocytes from EFAT (middle panel, n=6/7), and in PVAT (right panel, n=3) using qRT-PCR. Values are expressed in arbitrary units (AU). **P*<0.05 and ***P*<0.01 vs control. IVS (interventricular septum), LV (left ventricle), RV (right ventricle). *Anp* indicates *atrial natriuretic peptide*; *Bnp*, *brain natriuretic peptide*; *Cnp*, *C-type natriuretic peptide; Mhc*, *myosin heavy chain*; and *Npr*, *natriuretic peptide receptor*.

2.1.3.5 Higher insulin levels and variations in Rictor^{aP2KO} mice

In previous studies using *aP2* gene promoter-driven CRE-recombinase to knockout *Rictor* in mice [5, 6], diurnal fluctuations of insulin were not investigated. Therefore, we measured insulin levels every 4 hours during a 24 hour cycle (Figure S4A). Insulin levels were higher at the beginning of the light period at ZT2 (9am), and a trend towards higher insulin levels could also be observed during the dark period at ZT14 (9pm) and ZT18 (1am) (Figure S4A). Overall, levels of insulin varied 7.6-fold during a 24 hour cycle while in controls only a 1.6-fold variation was quantified (Figure S4A). Glucose levels in plasma were significantly higher at the end of the light period (ZT10; 5pm)

followed by a sharp decline at ZT14 in *Rictor*^{aP2KO} mice, indicating that higher insulin levels might lead to decreased glucose plasma levels at the beginning of the dark period. (Figure S4B).

2.1.3.6 Identification of differentially expressed genes in PVAT of Rictor^{aP2KO} *mice*

Data from blood pressure and locomotor activity analyses revealed a complex phenotype in the *Rictor*^{aP2KO} mice which could not be explained solely by the induction of pro-inflammatory molecule expression in PVAT. To identify differentially expressed genes in PVAT of *Rictor*^{aP2KO} mice, we performed a micro array analysis. Gene Ontology analysis of differentially expressed genes (Table S4) revealed the circadian rhythm as the most affected pathway in PVAT (Table S3). The data have been deposited in GEO database (Accession Number: GSE67077).

2.1.3.7 Divergent clock gene expression in perivascular adipose tissue, but not in the suprachiasmatic nucleus, in Rictor^{aP2KO} *mice*

To further examine the impact of *Rictor* deletion on clock genes, we analyzed mRNA expression levels of core clock genes *Bmal1, Clock, Npas2, Cry1/2, Per1/2*, *Rev-Erb-alpha* (*Rev-Erb-α*) and *Rorα* over a 24 hour cycle in PVAT and in aortic tissue (Figure 5 and supplemental figure S5, respectively). In aortic tissue, mRNA expression levels were mostly comparable between mouse groups and followed similar diurnal patterns (Figure S5). In PVAT, expression of *Clock*, *Cry1*, *Per1*, and *Rorα* was lower only during the light period in *Rictor*^{aP2KO} mice compared with controls (Figure 5). For *Per2*, a phase-shift at the transition from the light to the dark periods was observed. Collectively, these data suggest that ablation of *Rictor* in adipocytes strongly impacts clock gene expression in PVAT, but has only minimal effects on these genes in the aortic tissue.

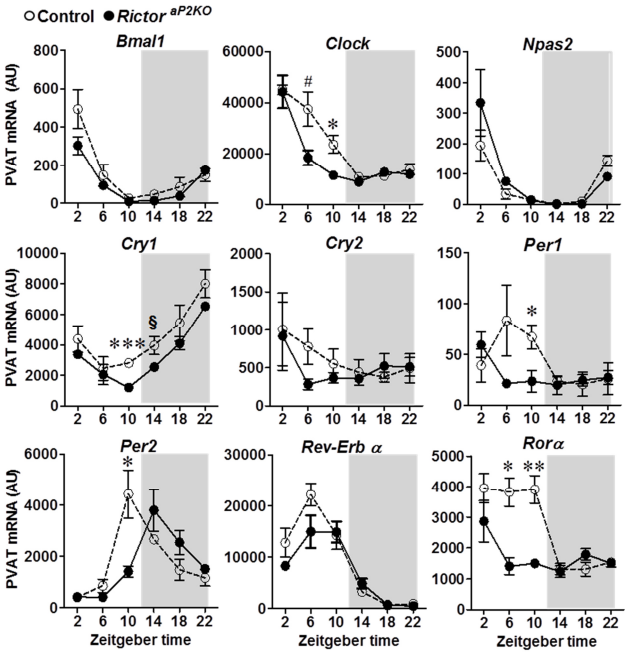

Figure 5: Steady state mRNA expression levels of core clock genes are different in perivascular adipose tissue (PVAT) of *Rictor* knockout (*Rictor*^{aP2KO}) mice during the light period. mRNA expression levels of core clock genes in PVAT were determined using qRT-PCR. Grey shaded areas represent the 12 hour dark period. Values are expressed in arbitrary units (AU). n=3 per group and time point**.** **P*<0.05, ***P*<0.01, ****P*<0.005, #*P*=0.06 and §*P*=0.08 vs control.

We found that the circadian rhythm of blood pressure (Figure 1) and locomotor activity (Figure 2) is altered in *Rictor*^{aP2KO} mice. Thus, we quantified clock gene expression in the SCN during a 24 hour cycle. No differences in the mRNA expression levels of *Bmal1*, *Npas2*, *Clock*, *Cry1/2*, *Per1/2*, *Rev-Erb-α* and *Rorα* were detected between mouse groups (Figure 6). Collectively, these findings indicate that decreased *Rictor* expression in the SCN does not affect core clock gene expression, while expressional changes of *Clock*, *Rorα*, *Per1/2*, and *Cry1* in PVAT are likely to contribute to increased blood pressure observed in *Rictor*^{aP2KO} mice.

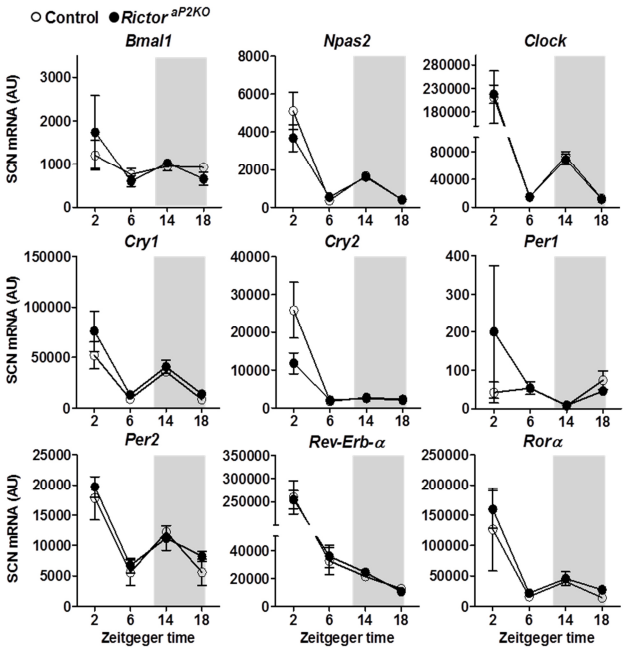

Figure 6: Deletion of *Rictor* does not affect core clock gene expression in the suprachiasmatic nucleus. mRNA expression levels of core clock genes in the suprachiasmatic nucleus (SCN) of *Rictor*^{aP2KO} and control mice were analyzed using qRT-PCR. Grey shaded areas represent the 12 hour dark period. Values are expressed in arbitrary units (AU). n=3/5 per group and time point.

2.1.4 Discussion

This is the first study to show that RICTOR/mTORC2 acts as a regulator for coordinated diurnal expression of clock genes in PVAT, but not in the SCN. At the whole body level, RICTOR/mTORC2 in adipose and brain tissue contributes to the diurnal regulation of blood pressure and locomotor activity. The presented data demonstrate the importance of the mTORC2 signaling pathway in the brain to adipocyte axis for daily fluctuations of physiological processes.

We and others have recently shown that mTORC2 activity controls inflammatory molecule expression using tissue-specific *Rictor* knockout mouse models [7, 20]. We showed that vascular contractility in *Rictor*^{aP2KO} mice is increased due to enhanced secretion of pro-inflammatory cytokines in PVAT [7]. Ablation of *Rictor* strongly reduced AKT^{Ser473} phosphorylation, resulting in impaired mTORC2 signaling [5-7]. Consequently, we assign the observed changes in *Rictor*^{aP2KO} mice to the impaired mTORC2 downstream signaling.

In the present study, we explored these findings further by studying blood pressure regulation in *Rictor*^{aP2KO} mice. In line with our hypothesis, *Rictor*^{aP2KO} mice showed increased MAP and alterations of its diurnal patterns. The increase in blood pressure parameters was too small to be considered as hypertension. In fact, our observations rather point towards a phenotype in *Rictor*^{aP2KO} mice which is termed pre-hypertension in patients [21]. The term pre-hypertension is defined as blood pressure levels of 120-139 mmHg for systolic and 80-89 mmHg for diastolic blood pressure, respectively [21]. Applying this definition to mice, we established a pre-hypertensive phenotype in the *Rictor*^{aP2KO} mice. At the tissue level, we found that cell density of thoracic PVAT, shown to be highly similar to brown adipose tissue (BAT) [22], is increased in *Rictor*^{aP2KO} mice. Intriguingly, it has been demonstrated that perivascular cell density is increased in an animal model of hypertension [11], and that adipocytes in BAT lacking *Rictor* are smaller [23]. This led us to speculate that elevated blood pressure is at least partially linked to the higher cell density in PVAT of *Rictor*^{aP2KO} mice.

NPs are hormonal regulators of vasodilation and natriuresis lowering blood pressure [24]. We report that *Anp* and *Bnp* mRNA expression levels are reduced in hearts of *Rictor*^{aP2KO} mice. Our results obtained in mice are in agreement with the findings in a study with patients showing that a pre-hypertensive state is associated with a deficiency of circulating BNP levels [25]. Interestingly, low plasma levels of NPs have been identified as a common predisposition for metabolic and cardiovascular diseases [19]. In line with data from hyperinsulinemic rats displaying a hypertensive phenotype [26], we showed that in *Rictor*^{aP2KO} mice hyperinsulinemia is associated with increased heart rate and blood pressure. Thus, high levels of insulin and its strong variability during the

course of the day might disable appropriate diurnal blood pressure regulation and/or reduce expression of *Anp* and *Bnp* in *Rictor*^{aP2KO} mice. Studying other pathophysiological mechanisms of hypertension [27], such as the activation of the renin-angiotensin-aldosterone system and the sympathetic nervous system, and changes in salt sensitivity was beyond the scope of the present study. Particularly, the possible impact of angiotensin II (ANG II) on the regulation of insulin-dependent AKT activation warrants further investigation as ANG II plays a major role in the pathogenesis of insulin resistance and in the diurnal regulation of blood pressure [28]. We focused on locomotor activity, another important factor that can influence heart rate and blood pressure [17]. Locomotor activity was sustained and high in *Rictor*^{aP2KO} mice during the dark period, which could explain in part the strong impairment of the physiological decline of MAP in *Rictor*^{aP2KO} mice.

We also investigated the deletion of *Rictor* in different organs in more detail, based on the fact that the tissue-specificity of the *aP2* gene promoter employed to produce the conditional knockout may not be restricted to adipocytes [8, 29]. Interestingly, activity of the *aP2* promoter-driven CRE recombinase in the brain was established [8, 29] and confirmed by our data. Using the brain-specific nestin promoter to drive CRE expression in floxed *Rictor* mice, Thomanetz et al. demonstrated that brain size was reduced by about 40% compared with controls [30]. We found a 17% reduction in brain size in *Rictor*^{aP2KO} mice, indicating that different approaches to target *Rictor* in the brain may result in brain size reduction of variable magnitude [30]. The current approach to knockout *Rictor* resulted in a 50-75% reduction of *Rictor* gene expression in adipose tissues and brain. Therefore, we considered a potential impact of *Rictor* deletion in the brain, particularly in the SCN where the biological master clock is located, to alternatively explain the observed changes in daily rhythmicity of blood pressure and locomotor activity in *Rictor*^{aP2KO} mice. Tightly regulated clock genes control daytime-dependent behaviors and mammalian physiology [31]. Mutations and deletions of clock genes in mice have been associated with changes in blood pressure and/or its diurnal patterns [32]. In the SCN, diurnal expression of core clock genes remained unaltered during the 24 hour cycle. These results imply that changes in blood pressure and locomotor activity observed in *Rictor*^{aP2KO} mice are regulated downstream or independently of the molecular clock mechanism in the SCN. Thus, the present data underpins the importance of the exact tuning of *Rictor* expression in the brain-adipose axis to ensure daily oscillation of physiological processes. The impact of *Rictor* deletion in other brain regions possibly influencing the observed phenotype of *Rictor*^{aP2KO} mice needs further investigation.

In contrast, genome wide mRNA expression analysis revealed a significant impact of *Rictor* deletion on peripheral clock gene expression in PVAT. Further analysis over a 24 hour cycle revealed significantly reduced expression of clock genes *Rorα*, *Per1*, *Cry1* and *Clock* and *Per2*

phase-shift in PVAT of *Rictor*^{aP2KO} mice. Interestingly, *Rorα* and *Per1/Per2* have been shown to contribute to the regulation of inflammatory processes in the cardiovascular system [33] and in the adipose tissue [34]. Decreased expression of *Per1*/2, *Cry1* and *Clock* was shown in inflamed EFAT of genetically obese *ob/ob* mice [34]. Thus, reduced *Rorα*, *Per1*, *Cry1* and *Clock* gene expression might facilitate the pro-inflammatory molecule expression in *Rictor*^{aP2KO} mice which we observed previously [7] and increase in blood pressure.

2.1.5 Perspectives

In summary, the present study establishes the importance of RICTOR/mTORC2 in the regulation of the interactions between vasculature, adipocytes and brain to tune oscillatory physiological outcomes such as blood pressure and locomotion. These interactions are likely to be mediated by hormones such as insulin and natriuretic peptides. Further experiments are needed to elucidate these complex relationships which might give hints for effective strategies to combat pre-hypertensive conditions in patients.

2.1.6 Acknowledgements

Special thanks go to Dr. Jelena Kühn-Georgijevic and Dr. Hubert Rehrauer from Functional Genomic Center Zurich for their support with micro array and data analysis. We would like to thank Nadine Naegele from the Institute of Physiology (University of Zurich) for performing glucose analysis in blood plasma. The authors are grateful to all members of research unit, Internal Medicine, University Hospital Zurich for stimulating discussions and, in addition, to Ana Perez-Dominguez for her excellent technical assistance.

2.1.7 Sources of Funding

This work was supported by funding from University of Zurich, University Hospital of Zurich, Hartmann Müller Stiftung, Forschungskredit of the University of Zurich (Grant-No. FK-13-026), the Swiss National Science Fundation (Grant No. 118349), Stiftung Baugarten, and Jubiläumsstiftung der Schweizerischen Lebensversicherungs- und Rentenanstalt für Volksgesundheit und medizinische Forschung (Swiss Life).

Conflict of interests. None.

2.1.8 References

1. Laplante M, Sabatini DM. Mtor signaling in growth control and disease. *Cell*. 2012;149:274-293.
2. Wullschleger S, Loewith R, Hall MN. Tor signaling in growth and metabolism. *Cell*. 2006;124:471-484.
3. Laplante M, Sabatini DM. An emerging role of mtor in lipid biosynthesis. *Curr Biol*. 2009;19:R1046-1052.
4. Oh WJ, Jacinto E. Mtor complex 2 signaling and functions. *Cell Cycle*. 2011;10:2305-2316.
5. Cybulski N, Polak P, Auwerx J, Ruegg MA, Hall MN. Mtor complex 2 in adipose tissue negatively controls whole-body growth. *Proc Natl Acad Sci U S A*. 2009;106:9902-9907.
6. Kumar A, Lawrence JC, Jr., Jung DY, Ko HJ, Keller SR, Kim JK, Magnuson MA, Harris TE. Fat cell-specific ablation of rictor in mice impairs insulin-regulated fat cell and whole-body glucose and lipid metabolism. *Diabetes*. 2010;59:1397-1406.
7. Bhattacharya I, Dragert K, Albert V, Contassot E, Damjanovic M, Hagiwara A, Zimmerli L, Humar R, Hall MN, Battegay EJ, Haas E. Rictor in perivascular adipose tissue controls vascular function by regulating inflammatory molecule expression. *Arterioscler Thromb Vasc Biol*. 2013;33:2105-2111.
8. Lee KY, Russell SJ, Ussar S, Boucher J, Vernochet C, Mori MA, Smyth G, Rourk M, Cederquist C, Rosen ED, Kahn BB, Kahn CR. Lessons on conditional gene targeting in mouse adipose tissue. *Diabetes*. 2013;62:864-874.
9. Brown NK, Zhou Z, Zhang J, Zeng R, Wu J, Eitzman DT, Chen YE, Chang L. Perivascular adipose tissue in vascular function and disease: A review of current research and animal models. *Arterioscler Thromb Vasc Biol*. 2014. doi: 10.1161/ATVBAHA.114.303029.
10. Van de Voorde J, Boydens C, Pauwels B, Decaluwe K. Perivascular adipose tissue, inflammation and vascular dysfunction in obesity. *Current vascular pharmacology*. 2014;12:403-411.
11. Li R, Andersen I, Aleke J, Golubinskaya V, Gustafsson H, Nilsson H. Reduced anti-contractile effect of perivascular adipose tissue on mesenteric small arteries from spontaneously hypertensive rats: Role of kv7 channels. *Eur J Pharmacol*. 2013;698:310-315.
12. Savoia C, Schiffrin EL. Inflammation in hypertension. *Current opinion in nephrology and hypertension*. 2006;15:152-158.
13. Harrison DG, Guzik TJ, Lob HE, Madhur MS, Marvar PJ, Thabet SR, Vinh A, Weyand CM. Inflammation, immunity, and hypertension. *Hypertension*. 2011;57:132-140.
14. Takahashi H, Yoshika M, Komiyama Y, Nishimura M. The central mechanism underlying hypertension: A review of the roles of sodium ions, epithelial sodium channels, the renin-angiotensin-aldosterone system, oxidative stress and endogenous digitalis in the brain. *Hypertension research.* 2011;34:1147-1160.
15. Dibner C, Schibler U, Albrecht U. The mammalian circadian timing system: Organization and coordination of central and peripheral clocks. *Annual review of physiology*. 2010;72:517-549.
16. Kohsaka A, Waki H, Cui H, Gouraud SS, Maeda M. Integration of metabolic and cardiovascular diurnal rhythms by circadian clock. *Endocrine journal*. 2012;59:447-456.
17. Van Vliet BN, McGuire J, Chafe L, Leonard A, Joshi A, Montani JP. Phenotyping the level of blood pressure by telemetry in mice. *Clinical and experimental pharmacology & physiology*. 2006;33:1007-1015.
18. Intengan HD, Schiffrin EL. Vascular remodeling in hypertension: Roles of apoptosis, inflammation, and fibrosis. *Hypertension*. 2001;38:581-587.
19. Gruden G, Landi A, Bruno G. Natriuretic peptides, heart, and adipose tissue: New findings and future developments for diabetes research. *Diabetes care*. 2014;37:2899-2908.

20. Festuccia WT, Pouliot P, Bakan I, Sabatini DM, Laplante M. Myeloid-specific rictor deletion induces m1 macrophage polarization and potentiates in vivo pro-inflammatory response to lipopolysaccharide. *PLoS One*. 2014;9:e95432.

21. Chobanian AV, Bakris GL, Black HR, Cushman WC, Green LA, Izzo JL, Jr., Jones DW, Materson BJ, Oparil S, Wright JT, Jr., Roccella EJ, National Heart L, Blood Institute Joint National Committee on Prevention DE, Treatment of High Blood P, National High Blood Pressure Education Program Coordinating C. The seventh report of the joint national committee on prevention, detection, evaluation, and treatment of high blood pressure: The jnc 7 report. *Jama*. 2003;289:2560-2572.

22. Fitzgibbons TP, Kogan S, Aouadi M, Hendricks GM, Straubhaar J, Czech MP. Similarity of mouse perivascular and brown adipose tissues and their resistance to diet-induced inflammation. *Am J Physiol Heart Circ Physiol*. 2011;301:H1425-1437.

23. Hung CM, Calejman CM, Sanchez-Gurmaches J, Li H, Clish CB, Hettmer S, Wagers AJ, Guertin DA. Rictor/mtorc2 loss in the myf5 lineage reprograms brown fat metabolism and protects mice against obesity and metabolic disease. *Cell reports*. 2014;8:256-271.

24. Gardner DG, Chen S, Glenn DJ, Grigsby CL. Molecular biology of the natriuretic peptide system: Implications for physiology and hypertension. *Hypertension*. 2007;49:419-426.

25. Macheret F, Heublein D, Costello-Boerrigter LC, Boerrigter G, McKie P, Bellavia D, Mangiafico S, Ikeda Y, Bailey K, Scott CG, Sandberg S, Chen HH, Malatino L, Redfield MM, Rodeheffer R, Burnett J, Jr., Cataliotti A. Human hypertension is characterized by a lack of activation of the antihypertensive cardiac hormones anp and bnp. *J Am Coll Cardiol*. 2012;60:1558-1565. doi: 10.1016/j.jacc.2012.05.049.

26. Kuo JJ, Jones OB, Hall JE. Chronic cardiovascular and renal actions of leptin during hyperinsulinemia. *Am J Physiol Regul Integr Comp Physiol*. 2003;284:R1037-1042.

27. Oparil S, Zaman MA, Calhoun DA. Pathogenesis of hypertension. *Annals of internal medicine*. 2003;139:761-776.

28. Sueta D, Koibuchi N, Hasegawa Y, Toyama K, Uekawa K, Katayama T, Ma M, Nakagawa T, Waki H, Maeda M, Ogawa H, Kim-Mitsuyama S. Blood pressure variability, impaired autonomic function and vascular senescence in aged spontaneously hypertensive rats are ameliorated by angiotensin blockade. *Atherosclerosis*. 2014;236:101-107.

29. Martens K, Bottelbergs A, Baes M. Ectopic recombination in the central and peripheral nervous system by ap2/fabp4-cre mice: Implications for metabolism research. *FEBS Lett*. 2010;584:1054-1058.

30. Thomanetz V, Angliker N, Cloetta D, Lustenberger RM, Schweighauser M, Oliveri F, Suzuki N, Ruegg MA. Ablation of the mtorc2 component rictor in brain or purkinje cells affects size and neuron morphology. *J Cell Biol*. 2013;201:293-308.

31. Brown SA, Azzi A. Peripheral circadian oscillators in mammals. *Handbook of experimental pharmacology*. 2013:45-66.

32. Rudic RD, Fulton DJ. Pressed for time: The circadian clock and hypertension. *Journal of applied physiology*. 2009;107:1328-1338.

33. Duez H, Staels B. The nuclear receptors rev-erbs and rors integrate circadian rhythms and metabolism. *Diabetes & vascular disease research : official journal of the International Society of Diabetes and Vascular Disease*. 2008;5:82-88.

34. Yamaoka M, Maeda N, Takayama Y, Sekimoto R, Tsushima Y, Matsuda K, Mori T, Inoue K, Nishizawa H, Tominaga M, Funahashi T, Shimomura I. Adipose hypothermia in obesity and its association with period homolog 1, insulin sensitivity, and inflammation in fat. *PLoS One*. 2014;9:e112813.

Novelty and Significance

What is New?

- RICTOR in adipose tissue and brain contributes to the regulation of blood pressure and locomotion.
- RICTOR stabilizes diurnal fluctuations of clock gene expression and impacts cell density in PVAT, but has no impact on clock genes in the suprachiasmatic nucleus.
- Gene expression of natriuretic peptides and their receptors is reduced in the heart and adipocytes of *Rictor*^{aP2KO} mice.

What is relevant?

- Reduced *Rictor* expression may be a key event during pre-hypertension in patients facilitating progression of the disease by increasing PVAT inflammation and by dampening of the protective signaling of natriuretic peptides.
- RICTOR in the brain-adipocyte axis contributes to the regulation of fluctuating physiological functions such as blood pressure and locomotion.

Summary

At the tissue level, *aP2* gene promoter driven CRE recombinase expression to ablate *Rictor* gene expression, results in a higher cell density and impaired daily fluctuations of core clock genes in PVAT.

At the whole body level, RICTOR/mTORC2 in adipose tissue and brain modulates diurnal fluctuations in blood pressure and locomotion and results in a smaller brain. The underlying mechanism possibly involves impaired PVAT function, induction of hyperinsulinemia and reduced natriuretic peptide signaling.

2.1.9 Supplementary data

Table S1: Summary of the hemodynamic parameters recorded in control and *Rictor*^{aP2KO} mice during the 12 hour light period, 12 hour dark period and the 12:12 hour light/dark cycle. Values represent arithmetic means ± SEM derived from 7 days of continuous measurement. n=5/6. **P*<0.05 and ***P*<0.01 versus control.

	Control			*Rictor*^{aP2KO}		
	light	**dark**	**24 hour**	**Light**	**dark**	**24 hour**
MAP, mmHg	94.4 ± 1.5	102.6 ± 1.3	98.5 ± 1.4	99.1 ± 1.0	108.7 ± 1.5*	103.9 ± 1.1*
DAP, mmHg	86.5 ± 0.5	94.0 ± 0.7	90.2 ± 0.6	89.9 ± 1.0*	99.4 ± 2.0*	94.6 ± 1.4*
SAP, mmHg	102.6 ± 2.7	111.4 ± 2.5	107.0 ± 2.6	107.4 ± 1.9	117.2 ± 1.7	112.3 ± 1.7
PP, mmHg	16.1 ± 2.7	17.3 ± 2.9	16.7 ± 2.8	17.5 ± 2.2	17.8 ± 2.2	17.7 ± 2.2
HR, BPM	400.3 ± 4.4	445.7 ± 5.0	423.0 ± 4.5	418.8 ± 11.9	495.8 ± 11.9**	457.3 ± 10.4*

Table S2: Summary of intensity of activity and percentage of active time in control and *Rictor*^{aP2KO} mice during the 12 hour light period, 12 hour dark period and 12:12 hour light/dark cycle. Values represent arithmetic means ± SEM derived from 7 days of a continuous measurement. n=5/6. **P*<0.05, ***P*<0.01 versus control.

	Control			*Rictor*^{aP2KO}		
	light	**dark**	**24 hour**	**light**	**dark**	**24 hour**
Intensity of activity, counts/min	2.0 ± 0.2	6.2 ± 0.7	4.1 ± 0.5	4.2 ± 1.1	10.5 ± 2.4	7.4 ± 1.7
Active time, %	19.6 ± 2.3	47.1 ± 2.3	33.4 ± 2.2	33.5 ± 5.6*	68.7 ± 4.7**	51.1 ± 5.0*

Table S3: Gene ontology analysis of micro array data revealed a significant impact of *Rictor* deletion in adipocytes on clock gene expression in PVAT from *Rictor*$^{\alpha P2KO}$ mice.

Process	GeneGO analysis – Pathways Maps	Total-No. of genes	Genes changed in *Rictor*$^{\alpha P2KO}$	*P*-Value
1	Neurophysiological process – Circadian rhythm	47	*Bmal1, Dec1, Cry1, Rev-Erbα, Npas2*	2.051E-07
2	Cholesterol Biosynthesis	88	*Nsdhl, Cyp51A1, Fdps*	2.103E-03
3	Regulation of lipid metabolism - Regulation of lipid metabolism via LXR, NF-Y and SREBP	38	*Cyp51A1, Ldlr*	5.492E-03
4	Protein folding and maturation - Angiotensin system maturation / Rodent version	48	*Mc-cpa, Mcpt4*	8.655E-03
5	Development - TGF-beta receptor signaling	50	*Pai1, Gadd45 beta*	9.366E-03
6	Cytoskeleton remodeling - Cytoskeleton remodeling	102	*Melc, Pai1*	3.588E-02

Gene ontology analysis of 68 differentially expressed genes ($P<0.05$; fold change > 1.5) was performed using GeneGo analysis program (www.genego.com). Most genes were assigned to networks involved in circadian rhythm, lipid synthesis/metabolism and cytoskeletal remodeling.

Table S4: Micro Array analysis revealed 68 genes to be differentially expressed in PVAT from *Rictor*^{aP2KO} mice compared to controls.

Probe Name	Accession	Gene Symbol	Gene Name	Log2 ratio	ratio	*P*-Value
10404389	NM_013674	*Irf4*	interferon regulatory factor 4	1.469	2.768	0.02768
10362420	NM_029726	*Trdn*	Triadin	1.257	2.39	1.12E-05
10345675	NM_008719	*Npas2*	neuronal PAS domain protein 2	1.233	2.35	0.003811
10410388	AK149411	*E430024C06Rik*	RIKEN cDNA E430024C06 gene	1.07	2.099	0.0008981
10362428	NM_029726	*Trdn*	Triadin	1.037	2.052	0.00779
10420247	NM_010779	*Mcpt4*	mast cell protease 4	0.9781	1.97	0.009402
10474972	NM_026929	*Chac1*	ChaC, cation transport regulator-like 1 (E. coli)	0.9555	1.939	0.03205
10371400	NM_007771	*Cry1*	cryptochrome 1 (photolyase-like)	0.9347	1.911	0.02016
10409278	NM_017373	*Nfil3*	nuclear factor, interleukin 3, regulated	0.8999	1.866	0.01812
10417371	NM_001024712 NM_100042149	*Gm3696;* *Gm2897*	predicted gene 3696 predicted gene 2897	0.7937	1.734	0.002434
10497451	NM_007753	*Cpa3*	carboxypeptidase A3, mast cell	0.733	1.662	0.02231
10516932	NM_144907	*Sesn2*	sestrin 2	0.7301	1.659	0.01513
10458555	NM_011898	*Spry4*	sprouty homolog 4 (Drosophila)	0.6833	1.606	0.004955
10419156	NM_053112 NM_007895 NM_007894 NM_001012766.1 NM_017388.1	*Ear10* *Ear2* *Ear1* *Ear12* *Ear3*	eosinophil-associated, ribonuclease A family, member 10 eosinophil-associated, ribonuclease A family, member 2 eosinophil-associated, ribonuclease A family, member 1 eosinophil-associated, ribonuclease A family, member 12 eosinophil-associated, ribonuclease A family, member 3	0.6264	1.544	0.03445
10556463	NM_007489	*Arntl*	aryl hydrocarbon receptor nuclear translocator-like	0.6218	1.539	0.0007209
10542885	NM_026054	*2810474O19Rik*	RIKEN cDNA 2810474O19 gene	0.6178	1.535	0.01522
10552143	NM_017394 NM_001024707	*Slc7a10* *Lrp3*	solute carrier family 7 (cationic amino acid transporter, y+ system), member 10; low density lipoprotein receptor-related protein 3	0.6174	1.534	0.02518
10436890	ENSMUST00000114029	*Gm10785*	predicted gene 10785	0.6097	1.526	0.0004848
10466304	NM_172442	*Dtx4*	deltex 4 homolog (Drosophila)	0.6033	1.519	0.002598
10461614	NM_028595	*Ms4a6c*	membrane-spanning 4-domains, subfamily A, member 6C	0.6029	1.519	0.004982
10399666	ENSMUST00000101538	*9030624G23Ri*	RIKEN cDNA 9030624G23 gene; similar to development and differentiation enhancing factor 2	0.5981	1.514	0.0001629
10407124	ENSMUST00000099179	*AI452195*	expressed sequence AI452195	0.5882	1.503	0.02528
10450784	NM_008205	*H2-M9*	histocompatibility 2, M region locus 9	0.585	1.5	0.02428

Continued table S4:

Probe Name	Accession	Gene Symbol	Gene Name	Log2 ratio	ratio	*P*-Value
10349694	NM_178079	*Pm20d1*	peptidase M20 domain containing 1	-0.5872	0.6656	0.01873
10588691	NM_008317 NM_019750.3	*Hyal1* *Nat6*	hyaluronoglucosaminidase 1 N-acetyltransferase 6	-0.5907	0.664	0.03446
10527920	NM_020010	*Cyp51*	cytochrome P450, family 51	-0.5943	0.6624	0.006773
10499483	NM_134469	*Fdps*	farnesyl diphosphate synthetase	-0.597	0.6611	0.0005444
10488762	NM_009228	*Snta1*	syntrophin, acidic 1	-0.6033	0.6582	0.0006908
10399588	AJ005350	*Zfp125*	zinc finger protein 125	-0.6039	0.658	0.004791
10441774	NM_013667	*Slc22a2*	solute carrier family 22 (organic cation transporter), member 2	-0.6118	0.6544	0.02106
10480725		*BC029214*	cDNA sequence BC029214	-0.6134	0.6537	0.01623
10347224	NR_004414	*Rnu2-10*	Mus musculus U2 small nuclear RNA 10 (Rnu2), small nuclear RNA	-0.631	0.6457	0.003555
10379650	AF099974	*Slfn3*	schlafen 3	-0.631	0.6457	0.003555
10373400	NM_172259	*Myl6b*	myosin, light polypeptide 6B	-0.6414	0.6411	0.04055
10347222	NR_004414	*Rnu2-10*	Mus musculus U2 small nuclear RNA 10 (Rnu2), small nuclear RNA	-0.6423	0.6407	0.004084
10600082	NM_010941	*Nsdhl*	NAD(P) dependent steroid dehydrogenase-like	-0.6434	0.6402	0.01017
10467319	NM_011255	*Rbp4*	retinol binding protein 4, plasma	-0.6646	0.6309	0.03843
10532828	NM_029956	*Mmab*	methylmalonic aciduria (cobalamin deficiency) type B homolog (human)	-0.6656	0.6304	0.03463
10603736	NR_004414	*Rnu2*	U2 small nuclear RNA	-0.6677	0.6295	0.007948
10553354	NM_175272	*Nav2*	neuron navigator 2	-0.6863	0.6214	0.008013
10578688	NR_004414	*Rnu2*	U2 small nuclear RNA	-0.7014	0.615	0.007011
10373000	NM_026858	*Xrcc6bp1*	XRCC6 binding protein 1	-0.7098	0.6114	0.00352
10477649	NM_019811	*Acss2*	acyl-CoA synthetase short-chain family member 2	-0.7105	0.6111	0.008286
10469151	NM_172471	*Itih5*	inter-alpha (globulin) inhibitor H5	-0.7122	0.6104	0.03679
10551966	NM_001012401	*Hspb6*	heat shock protein, alpha-crystallin-related, B6	-0.717	0.6084	0.005251
10583732	NM_010700	*Ldlr*	low density lipoprotein receptor	-0.7182	0.6079	0.004846
10540472	NM_011498	*Bhlhe40*	basic helix-loop-helix family, member e40	-0.7384	0.5994	0.04434
10553092	NM_016974 NM_203280	*Dbp* *Sphk2*	D site albumin promoter binding protein sphingosine kinase 2	-0.7553	0.5924	0.0003359
10585398	NM_177350	*Gldn*	gliomedin	-0.7827	0.5813	0.04205
10381460	NR_004414	*Rnu2*	U2 small nuclear RNA	-0.7874	0.5794	0.003409
10381470	NR_004414	*Rnu2*	U2 small nuclear RNA	-0.7874	0.5794	0.003409
10381472	NR_004414	*Rnu2*	U2 small nuclear RNA	-0.7874	0.5794	0.003409
10391488	NR_004414	*Rnu2*	U2 small nuclear RNA	-0.7874	0.5794	0.003409
10381458	NR_004414	*Rnu2*	U2 small nuclear RNA	-0.8027	0.5733	0.003953
10579165	NM_007789	*Ncan*	neurocan	-0.8833	0.5421	0.02653
10417734	NM_011584	*Nr1d2*	nuclear receptor subfamily 1, group D, member 2	-0.9939	0.5021	0.001567
10364149	NM_009115	*S100b*	S100 protein, beta polypeptide, neural	-1	0.4999	0.01672
10502949	ENSMUST00000083804	*snoRNA*	snoRNA	-1.067	0.4773	0.0002746

10534667	NM_008871	*Serpine1*	serine (or cysteine) peptidase inhibitor, clade E, member 1	-1.108	0.4639	0.006309
10560481	NM_008036	*Fosb*	FBJ osteosarcoma oncogene B	-1.126	0.4582	0.001421
10390691	NM_145434 NM_178060	*Nr1d1* *Thra*	nuclear receptor subfamily 1, group D thyroid hormone receptor alpha	-1.255	0.419	0.0217
10364950	NM_008655	*Gadd45b*	growth arrest and DNA-damage-inducible 45 beta	-1.36	0.3897	0.009499

Micro array was performed using cDNA transcribed from RNA of PVAT from *Rictor*^{aP2KO} mice and controls and *Affymetrix Mouse Gene 1.1 ST array Strips.* Expression data were analyzed with Affymetrix Power Tools v1.10.2 (Affymetrix, Santa Clara, CA) using the RMA algorithm. Differentially expressed genes were ranked in accordance to the fold change (P<0.05) in descending order. [1] = also known as *Rev-Erbα*; [2] = also known as *Rev-Erbβ.*

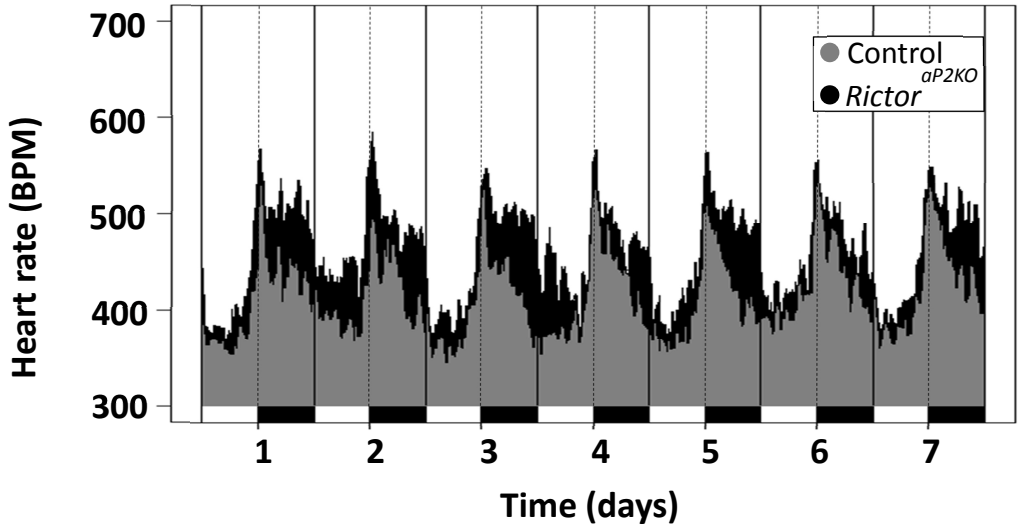

Figure S1: Heart rate is increased and its physiological decline during the dark period nearly absent in *Rictor*^{aP2KO} mice. Heart rate (HR) was recorded over a period of 7 consecutive days in *Rictor*^{aP2KO} and control mice (n=5/6) kept in a constant 12:12 hour light/ dark cycle (light on: 7 am/ ZT 0; light off: 7 pm/ ZT 12). Diurnal fluctuations of HR are represented as one hour running median. Black bars at the bottom denote the 12 hour dark period.

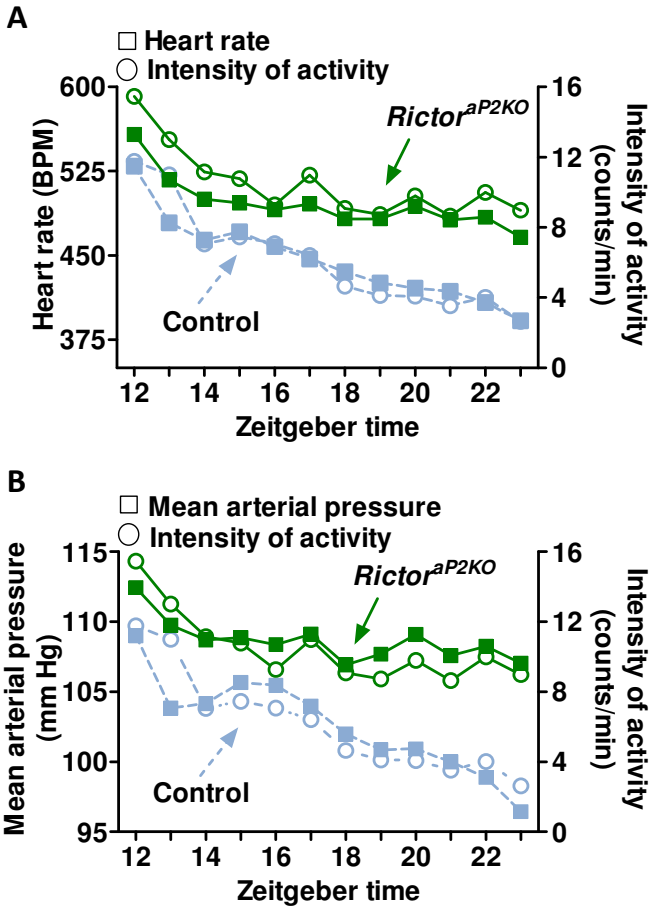

Figure S2: Time courses of mean arterial pressure, heart rate and locomotor activity display similar patterns and are less steep in *Rictor*^{aP2KO} mice during the dark period. Intensity of activity, mean arterial pressure (MAP) and heart rate (HR) were recorded over a period of 7 consecutive days in *Rictor*^{aP2KO} and control mice (n=5/6) kept in constant 12:12 hour light/ dark cycles. Hourly means of the measured parameters at the indicated time points are represented.

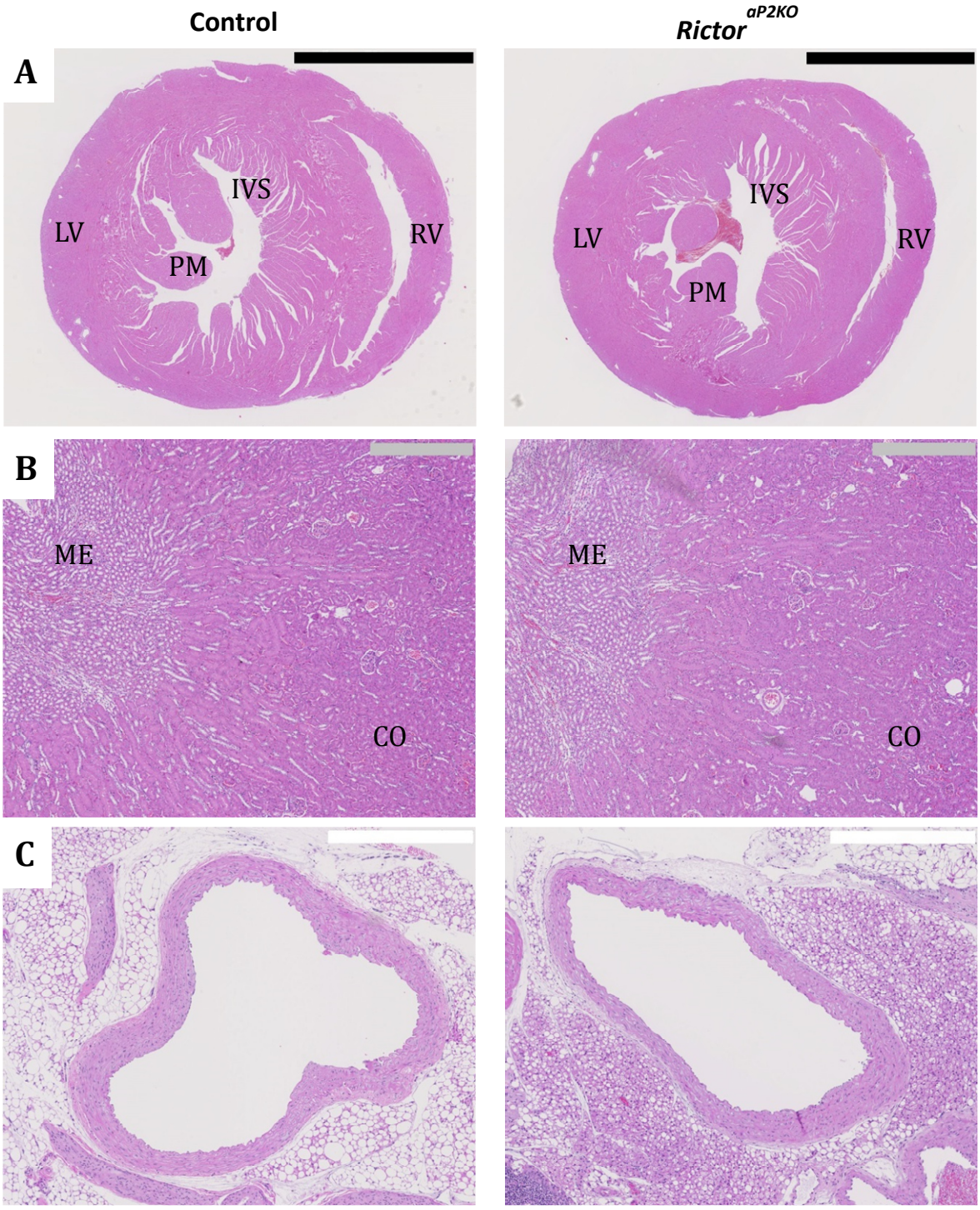

Figure S3: *aP2*/CRE-driven deletion of *Rictor* affects cell density of aortic PVAT, while no differences in the heart and kidney are noted. Representative cross-sections stained with haematoxylin/eosin of **(A)** the heart, **(B)** the kidney, and **(C)** the aortic arch with PVAT are shown. Heart sections in A were performed at the level of the papillary muscles. Black bar: 2.5 mm. Grey bar: 500 µm. White bar: 500 µm. CO (cortex), ME (medulla), IVS (interventricular septum), LV (left ventricle), PM (papillary muscles), RV (right ventricle).

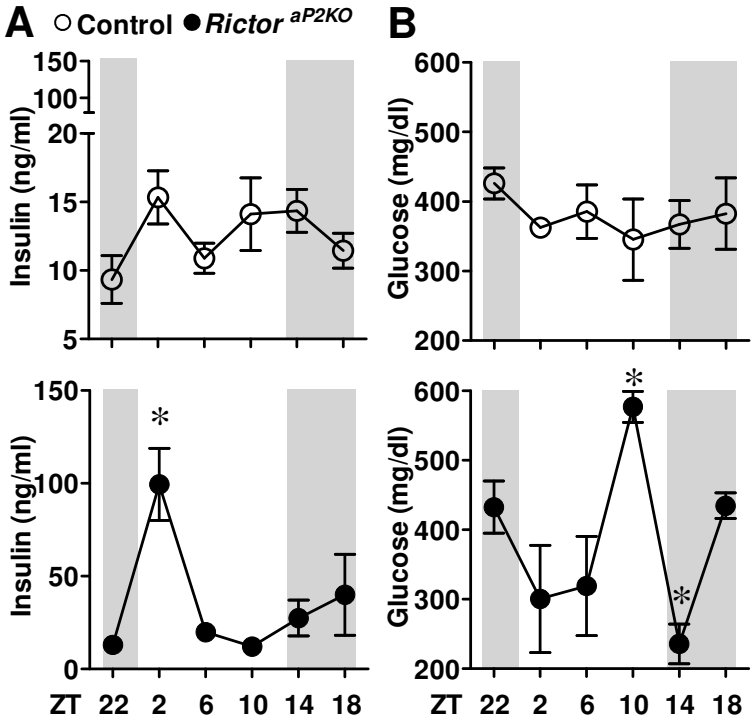

Figure S4: Strong variations in glucose and insulin plasma levels during a 24 hour cycle in *Rictor*^{aP2KO} mice. (A) Insulin and **(B)** glucose concentrations were determined in blood plasma every 4 hour using BioPlex assay and UniCel DxC 800 System, respectively. Grey shaded areas represent the 12 hour dark period. ZT (Zeitgeber time). Values represent mean ± SEM. n=3. **P*<0.05 versus control.

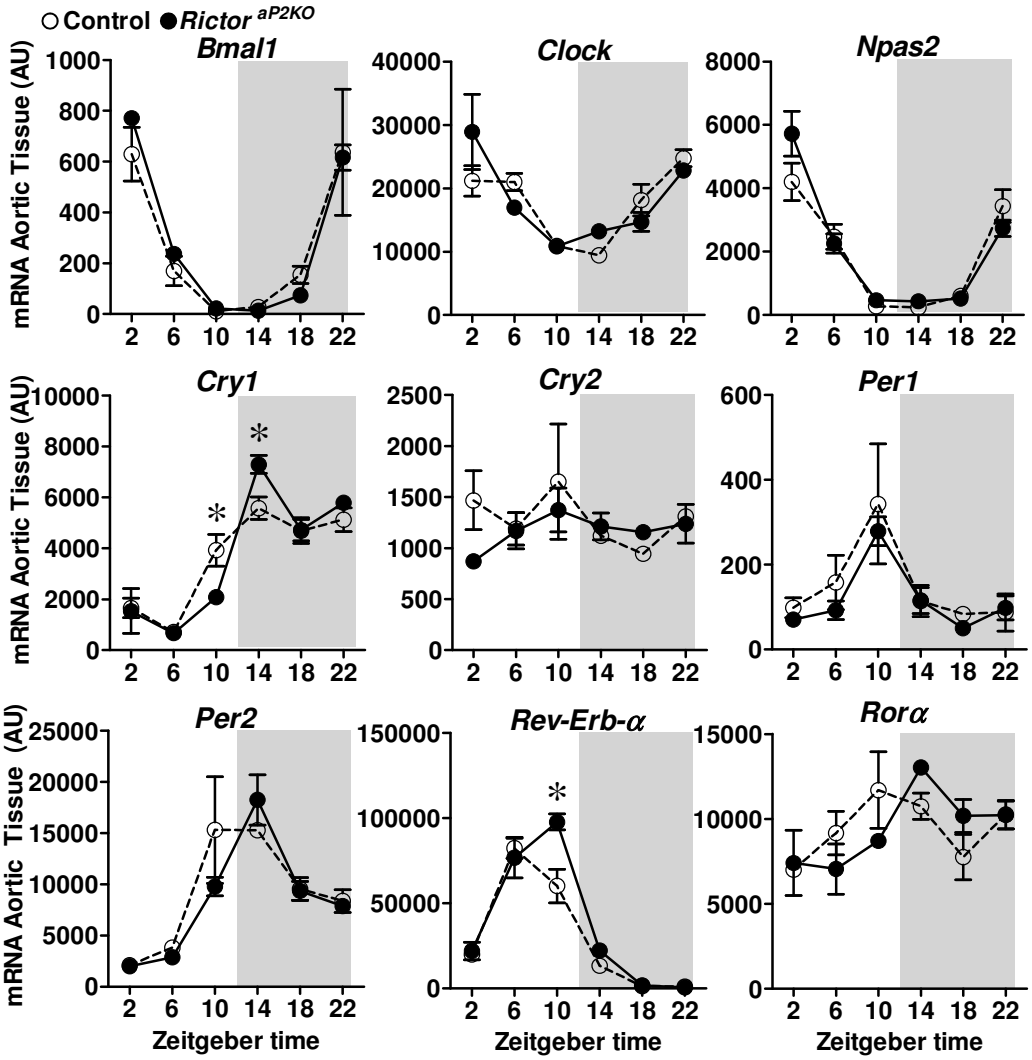

Figure S5: Steady state mRNA expression levels of core clock genes are similar in aortic tissue from control and *Rictor*^{aP2KO} mice. mRNA expression levels of core clock genes in aortic tissue were determined using qRT-PCR. Grey shaded areas represent the dark period. Values are expressed in arbitrary units (AU). n=3 per group and time point. **P*<0.05 versus control.

2.1.10 Material and Methods

Mice and tissue collection

Mice used in the present study were described in detail before [1]. Briefly, mice with deletion of *Rictor* (*Rictor*^{aP2KO}) were generated by crossing *Rictor*$^{fl/fl}$ mice with C57BL/6J mice expressing CRE recombinase under the control of the *adipocyte protein 2* (*aP2,* also known as fatty acid binding protein 4*)* gene promoter (purchased from JAX Laboratories, Bar Harbor, Maine, USA). In all experiments, male mice (18-23 weeks old) were used and as control group, littermates without the *Cre* transgene (*Rictor*$^{fl/fl}$, termed henceforth control).

Mice were kept in the institutional animal facilities (University of Zurich and University Hospital of Zurich, Switzerland) at 22 °C with a 12:12 hour light/dark cycle. Light onset was at 7 am [zeitgeber time (ZT) 0] and light offset was at 7 pm (ZT 12). Animals had access to standard chow (4.5 % calories from fat; Kliba Nafag, Kaiseraugust, Switzerland) and water *ad libitum*. All mice used were genotyped for *Rictor* (standard PCR) and *Cre* recombinase (quantitative RT-PCR) using specific mouse primers (Table S5) and standard protocols (JAX Laboratories, Bar Harbor, Maine, USA). Before sacrifice, mice were weighed and anesthetized by intraperetoneal (i.p.) injection (xylazine: 20; ketamine: 100; and acepromazine: 3.0; in mg/kg body weight) and exsanguinated via cardiac puncture. Mice used for confirmation of the *Rictor* knockout in PVAT and aortas (aortic tissue) and for the genome expression study were starved overnight and sacrificed at 9 am.

All mouse experiments described here were approved by the Kantonales Veterinaeramt of Zurich, Switzerland (License numbers ZH44/2011 and ZH184/2014). Therewith, the investigation conforms to the Guide for the Care and Use of Laboratory Animals published by the US National Institutes of Health (8th Edition, 2011).

Isolation of T cells and monocytes using fluorescence activated cell sorting

Freshly isolated spleens were passed through 70µm and 40µm cell strainers in order to obtain single cell suspension. Erythrocytes were depleted by 2 minute incubation in ACK buffer. Cells were incubated with the appropriate combination of fluorochrome-conjugated antibodies: anti-CD4 (clone RM4-4), anti-CD11c (N418, both eBioscience), anti-I-A/I-E (2G9, BD Bioscience), anti-CD11b (M1/70), anti-CD3 (17A2), anti-Ly6C (HK1.4, all Biolegend). $CD3^+CD4^+$ splenocytes were identified as $CD4^+$ T lymphocytes cells and $CD11b^+CD11c^-$MHC-II^-Ly-$6C^{hi}$ splenocytes as inflammatory monocytes. Propidium iodide (PI, eBioscience) was used to exclude dead cells. Cells were sorted with FACSAria III (BD Bioscience).

Tissue collection and histological analysis

For analysis of tissues during a 24 hour period, 3 mice from each group were sacrificed every 4 hours and different tissues from control and *Rictor*^{aP2KO} mice were collected. The first mouse groups were sacrificed at 9 am (ZT 2), 2 hours after light onset. For tissue collection during the dark period, mice were euthanized under red light to ensure no disruption of the 12:12 hour light/dark cycle. Mice were not starved before sacrifice.

After euthanasia, body weights were collected at necropsy to allow calculation of organ to body weight ratios. A complete necropsy, including a thorough external and internal gross post mortem examination was performed on each mouse. Heart and brain from each mouse were excised, dried on filter paper and weighed. Mouse heart weights were normalized to body weights (HW/BoW). Representative samples of all organs and tissues were harvested and fixed in 10 % neutral buffered formalin.

PVAT was dissected from the thoracic aorta and aortic arch and tissues were immediately placed in RNA*later*™ (Qiagen, Hilden, Germany) or directly snap-frozen. Blood collected during exsanguination was centrifuged at 8000 x g for 15 min at 4 °C, plasma in the supernatant snap-frozen and kept with all the other collected tissues at -80 °C until further analysis.

After routine paraffin wax embedding, sections (3-5 µm) were prepared and stained with haematoxylin and eosin (HE). Histological analysis was performed on the heart, aortic arch, lungs and kidneys. Three cross sections were obtained from each heart at standard distances from the apex, to visualize the left and right ventricles. The Masson's Trichrome stain was applied for the visualization of collagen fibers in the heart and lungs [2]. All slides were scanned using digital slide scanner NanoZoomer-XR C12000 (Hamamatsu, Japan) and images were taken using NDP.view2 viewing software (Hamamatsu, Japan). Cross sectional lengths of the septal wall and right and left ventricular free walls were measured.

Cardiomyocyte cross-sectional area was employed as index of cardiac hypertrophy. Periodic acid-Schiff (PAS) staining on 3-5 µm heart sections was applied to better outline the cardiomyocyte boundaries and quantify cardiomyocyte cross-sectional area. Scanned slide images were taken as mentioned above. In all mice, measurements were taken from the outline of 50 randomly selected cardiomyocytes exhibiting a clear cross-cut nucleus. Measurements were done using ImageJ 1.48 software (http://imagej.nih.gov/ij/index.html).

Recording of blood pressure and locomotor activity in mice using radiofrequency transmitters

Control and *Rictor*^{aP2KO} mice (n=5-6 per group) were implanted with a telemetry sender (TA11PA-C10, Data Sciences International, St. Paul, MN, USA) via the left carotid artery to monitor simultaneously mean (MAP), diastolic (DAP) and systolic arterial pressure (SAP), pulse pressure, heart rate (HR), and locomotor activity. Operation and post-operative care procedures were described previously [3]. Briefly, mice were anesthetized with isoflurane, and the telemetry sender implanted in the left carotid artery. The transmitter, connected with the telemetry sender via a small catheter, was positioned under the skin between the right front and hind limb. Mice were kept warm on a heating pad and monitored until fully recovered from anesthesia. After surgery, mice were single caged in a warming cabinet at 30 °C in a 12:12 hour light/dark cycle with access to food and water *ad libitum*. Recovery from surgery was allowed for 7 days before measurements were started. During measurement, mice were housed individually and the temperature in the warming cabinet was adjusted to 25 °C. Blood pressure and locomotor activity data were determined from day 8 after surgery during the following week up to three weeks post telemetry sender implantation. Data from each telemetry sender were transmitted to a receiver plate (RPC-1, Data Sciences International, St. Paul, USA) positioned below each cage and thereafter collected using the Dataquest A.R.T. system, version 4.2 (Data Sciences International, St. Paul, USA). Blood pressure was measured for 30 seconds every 5 minutes. Locomotor activity was recorded continuously by the frequency of movement of each animal across the cage in counts/min (intensity of activity). For analysis of locomotor activity, less than 0.6 counts per minute were considered as inactive and set to 0 for further calculations.

RNA isolation, reverse transcription and quantitative real-time PCR

RNA from PVAT, EFAT and adipocytes was extracted using RNeasy® lipid tissue kit, from thoracic aortas, and heart using RNeasy® fibrous tissue kit, from kidney, liver and stromal vascular fraction using RNeasy® mini kit, and T cells and monocytes using RNeasy® plus mini kit according to the protocol of the manufacturer (Qiagen, Hombrechtikon, Switzerland) respectively, including an on-column DNase digestion (RNase-free DNase, Qiagen). Before reverse transcription, RNA quantity and quality was determined using Nanodrop 2000 Spectrophotometer and Agilent 2100 Bioanalyzer. Reverse transcription of 50 ng RNA from PVAT, stromal vascular fraction and thoracic aortas was performed using WT (Whole Transcript)-Ovation® Pico RNA Amplification System (Nugen, Bemmel, Netherlands) and from EFAT, adipocytes, heart, kidney, liver, T cells and monocytes using iScript™ Reverse Transcription Supermix according manufactures recommendations (BioRad, Hercules, CA, USA). For quantitative RT-PCR, final cDNA concentration was adjusted to 10 ng in a 15 µl reaction volume. Each reaction was performed in duplicates using

Bio-Rad CFX96 Real-Time System and iQ™ SYBR® Green Supermix (BioRad, Hercules, CA, USA) and specific mouse primers. Gene expression in PVAT, thoracic aortas, EFAT and adipocytes was normalized to the reference gene *acidic ribosomal phosphoprotein* (*Arbp*), in heart, kidney and liver to the reference gene *cyclophelin B* and in the stromal vascular fraction to the reference gene *TATA box binding protein* (*Tbp*) using the comparative C(T) method [4]. If not otherwise noted, mouse primer pairs for selected genes were designed using Primer Blast (NCBI, USA) [5] and are listed in supplementary method **Table S4**.

Isolation of RNA from suprachiasmatic nucleus and brain cortex

The brain was dissected, placed in artificial cerebrospinal fluid (ACSF; NaCl - 120 mM; KCl - 2.5 mM; $MgCl_2$ x 6*H_2O - 1 mM; NaH_2PO_4 x 2*H_2O; - 1.25 mM; $NaHCO_3$ - 26 mM; HEPES - 5 mM; $CaCl_2$ - 2 mM; glucose - 16 mM; pH 7.35) and 250 to 300 µm brain slices were cut using a vibratom (Leica VT 1200, Leica Biosystems, Switzerland). Brain regions containing the SCN and cortex were identified under a binocular (Olympus SZ61, Volketswil, Switzerland), cut out, and stored at - 80°C until further analysis. SCN and cortex were homogenized in 300 µl RLT-buffer with β-mercaptoethanol by vortexing the samples 3 x 10 sec at room temperature. RNA was extracted using RNeasy® micro kit according the recommendations of the manufacturer (Qiagen, Hombrechtikon, Switzerland). 5 µl eluat from the isolation columns were reversed transcribed to cDNA using WT (Whole Transcript)-Ovation Pico RNA Amplification System (Nugen, Bemmel, Netherlands). cDNA transcription and quantitative RT-PCR were performed as described above and relative gene expression levels were normalized to *glyceraldehyde-3-phosphate dehydrogenase* (*Gapdh*).

Bioplex Analysis

Bioplex assay was performed using blood plasma collected from control and *Rictor*^{aP2KO} mice at ZT 2 (9 am) and ZT 14 (9 pm). Concentrations of insulin were measured using corresponding components of BioPlex™ Pro Mouse Diabetes assay according to the manufactures protocol in a Bioplex™ 100 machine (BioRad, Hercules CA, USA). Data were analyzed using BioPlex™ Manager 4.1.1 software and quantified based on the Logistic-5PL regression standard curve.

Blood glucose levels

Blood glucose levels were determined at ZT 2 (9 am) and ZT 14 (9 pm) in *Rictor*^{aP2KO} and control mice using UniCel DxC 800 System and specific reagent, calibration and control kits for glucose measurement (Beckman Coulter, Galway, Ireland) according manufactures recommendations.

Histology of thoracic aorta and PVAT

10 µm cross sections from thoracic aortas with PVAT were cut as described previously [6]. Prior to staining, slides were dried for 20 min at room temperature, fixed in 4 % PFA in PBS (pH 7.4) for 10 minutes and washed twice for 5 min in aqua-dest. Haematoxylin staining was performed using Mayer's haematoxylin (Dako, Baar, Switzerland) for 3-5 min followed by a 5 min washing step under slowly running tap water. For differentiation, slides were dunk twice in acidic alcohol (0.3 % HCl in 70 % EtOH) and washed immediately in aqua dest. For eosin staining, slides were incubated 30 sec in 0.1 % Eosin (Sigma, Buchs, Switzerland) washed immediately in deionized water and differentiated in 70 % Ethanol for 3 sec. Slides were washed twice for 2 min in deionized water and air dried. Coverslips were mounted with Eukit quick-hardening mounting medium (Sigma, Buchs, Switzerland) onto slides.

Staining of the nuclei using Hoechst: Fixed cross-sections were incubated for 60 min with blocking buffer (5 % goat serum in PBS / 0.1 % TWEEN). Slides were washed twice for 5 min with PBS (pH 7.4) and nuclei were stained with Hoechst (2 µg/µL in PBS, pH 7.4, Life Technologies) for 5 min. Slides were washed 3 x 5 min with PBS (pH 7.4) and mounted with fluorescent mounting medium (Dako, Baar, Switzerland).

Slides were dried at least 1 day before imaging. Images were acquired using CLSM Leica SP5 microscope and LAS-AF 2.6.3.8173 software (Leica, Heerbrugg, Switzerland). Nuclei were counted using image J 1.48 for Windows (NIH, USA) in a 475 x 340 µm area.

Genome Expression Study

Total RNA was isolated from PVAT surrounding the thoracic part of the arterial tree from control and *Rictor*^{aP2KO} mice. Total RNA was extracted using the RNeasy® lipid tissue kit according manufactures recommendation (Qiagen, Hombrechtikon, Switzerland). DNase digestion of isolated total RNA was performed in solution (RNase-free DNase, Qiagen), followed by an additional purification step of total RNA using RNeasy® mini kit according manufactures protocol (Qiagen, Hombrechtikon, Switzerland). Before further analysis, RNA quality and quantity was determined using Nanodrop 2000 Spectrophotometer and Agilent 2100 Bioanalyzer. Only total RNA with an RNA integrity number (RIN) > 8 were considered for further analysis.

Total RNA was reverse transcribed and cDNA amplified using Ambion® WT Expression kit (Affymetrix, United Kingdom) following manufacturer's protocols. Biotinylated cDNA was prepared using Encore Biotine Module (Nugen, Netherlands) according to manufacturer's recommendations and hybridized to Affymetrix Mouse Gene® 1.0 ST array strips (Affymetrix, Santa Clara, CA). Gene Chips were scanned using the Hewlett-Packard GeneArray Scanner G2500A

(Hewlett-Packard, Böblingen, Germany) and expression data analysed with Affymetrix Power Tools v1.10.2 (Affymetrix, Santa Clara, CA) using the RMA algorithm. The data discussed in this publication have been deposited in NCBI's Gene Expression Omnibus [7] and are accessible through GEO Series accession number GSE67077 (http://www.ncbi.nlm.nih.gov/geo/query/acc.cgi?&acc=GSE67077).

For further data analysis, genes were considered to be differentially expressed in *Rictor*^{aP2KO} mice if $P<0.05$ and fold change > 1.5. A gene ontology analysis was performed with genes identified using GeneGo Analysis program (www.genego.com).

Statistical Analysis

Data are expressed as means ± standard error of the mean (SEM) or as box blots in which the median is represented by a horizontal line. To this end, data from each mouse were compiled to one data point (mean) and are represented in box blots according to the mouse groups. Comparisons between groups for other experiments were analyzed by two-tailed Student's t-test. For displaying MAP, levels of locomotor activity and heart rate over time, we used running medians to smooth data. Differences were considered statistically significant at values of $P<0.05$. Statistical analyses were performed using GraphPad Prism 5.04 program for Windows (GraphPad software, SanDiego, CA, USA) and R for Windows (R Core Team 2014). R: A language and environment for statistical computing (R Foundation for Statistical Computing, Vienna, Austria. URL http://www.R-project.org/).

Table S5: Primer pairs used for standard and quantitative real-time PCR. Primer pairs were designed using «primer blast» program (NCBI, USA) [4] and are specific to mouse cDNA. Sequences for primer pairs specific for *Anp, Npra, Nprc, α-Mhc* and *β-Mhc* were already described [8,9]

Gene name	Forward Primer (5'-3')	Reverse Primer (5'-3')
Anp	CAC AGA TCT GAT GGA TTT CAA GA	CCT CAT CTT CTA CCG GCA TC
Arbp	AGCTGAAGCAAAGGAAGAGTCGGA	ACTTGGTTGCTTTGGCGGGATTAG
Bhlhe40	ACG TTG AAG CAC GTG AAA GC	CTT CCC GAC AAA TCA CCA GC
Bmal1	ACT ACA GTG GCC CTT TG CAT	GCC CAA ATT CCC ACA TCT GAA G
Bnp1	GTC TGG CCG GAC ACT CAG	TGC ACT GGT GTC TTC AAC AAC
Clock	TTA GAT CAC AGG GCA CCA CC	AGT GCT CGT GAC ATT TTG CC
Cnp	GAC ACC ACC GAA GGT CCC G	CCT GGA GTC TTG TCA CCC TTT T
Cre	GCG GTC TGG CAG TAA AAA CTA TC	ACC CGG CTG CTC TTA CTT CT
Cry 1	ATG TCC CGA GTT GTA GCA GC	TGA GAG CAA TTT CCA CCG CT
Cry 2	AGC TGA TGT GTT CCC AAG GCT	CAT AAT GGC TGC ATC CCG TT
Cyclophelin B	GGT GGA GAG CAC CAA GAC AGA	GCC GGA GTC GAC AAT GAT G
Dbp	GGA ACT GAA GCC TCA ACC AAT C	CTC CGG CTC CAG TAC TTC TCA
Gapdh	AAA TGG TGA AGG TCG GTG TG	GTT GAA TTT GCC GTG AGT GG
Nfil3	GAG CAG AAC CAC GAT AAC CCA T	TAC AGA CCG GAT GGA GGA GAC
Npas2	AGA GGC AGC TTG AAC CCA AA	GAG GGG CTA GGC ACA TTG TT
Npra	CGA AGA CAA GTG CAT CCT GAG	TGG AGA CAC AGT CAA CAC AGC
Nprb	ACC GGT CAC TTC AAG GGA AA	GGC TCC GAT GAA GCG AGT AA
Nprc	AGC TGG CTA CAG CAA GAA GG	CGG CGA TAC CTT CAA ATG TC
Per1	CCA GAT TGG TGG AGG TTA CTG AGT	GCG AGA GTC TTC TTG GAG CAG TAG
Per2	AGA ACG CGG ATA TGT TTG CTG	ATC TAA GCC GCT GCA CAC ACT
Rev-Erb-α	TGT CTA GAG ATG CTG TGC GTT T	AGG CTG CTC AGT TGG TTG TT
Rictor (PCR)	TTA TTA ACT GTG TGT GGG TTG	CGT CTT AGT GTT GCT GTC TAG
Rictor (qRT-PCR)	TGC GAT ATT GGC CAT AGT GA	ACC CGG CTG CTC TTA CTT CT
Rorα	GCT TCT AAA AGC AGG CTC GC	GGG ACT TGA AGA CAT CGG GG
Tbp	GAG TTG CTT GCT CTG TGC TG	CTG GCT TGT GTG GGA AAG AT
α-Mhc	CGC ATC AAG GAG CTC ACC	CCT GCA GCC GCA TTA AGT
β-Actin	CGT GCG TGA CAT CAA AGA GA	CCC AAG AAG GAA GGC TGG A
β-Mhc	CGC ATC AAG GAG CTC ACC	CTG CAG CCG CAG TAG GTT

References

1. Cybulski N, Polak P, Auwerx J, Ruegg MA, Hall MN. Mtor complex 2 in adipose tissue negatively controls whole-body growth. *Proc Natl Acad Sci U S A*. 2009;106:9902-9907

2. Luna L. Manual of histologic staining methods of the armed forces institute of pathology. *McGraw-Hill, NY*. 1968;3rd edition:94-95

3. Schuler B, Rettich A, Vogel J, Gassmann M, Arras M. Optimized surgical techniques and postoperative care improve survival rates and permit accurate telemetric recording in exercising mice. *BMC veterinary research*. 2009;5:28

4. Schmittgen TD, Livak KJ. Analyzing real-time pcr data by the comparative c(t) method. *Nat Protoc*. 2008;3:1101-1108

5. Ye J, Coulouris G, Zaretskaya I, Cutcutache I, Rozen S, Madden TL. Primer-blast: A tool to design target-specific primers for polymerase chain reaction. *BMC bioinformatics*. 2012;13:134

6. Bhattacharya I, Dragert K, Albert V, Contassot E, Damjanovic M, Hagiwara A, Zimmerli L, Humar R, Hall MN, Battegay EJ, Haas E. Rictor in perivascular adipose tissue controls vascular function by regulating inflammatory molecule expression. *Arterioscler Thromb Vasc Biol*. 2013;33:2105-2111

7. Edgar R, Domrachev M, Lash AE. Gene Expression Omnibus: NCBI gene expression and hybridization array data repository. Nucleic Acids Res. 2002; 30:207-210.

8. Kreusser MM, Lehmann LH, Keranov S, Hoting MO, Oehl U, Kohlhaas M, Reil JC, Neumann K, Schneider MD, Hill JA, Dobrev D, Maack C, Maier LS, Grone HJ, Katus HA, Olson EN, Backs J. Cardiac cam kinase ii genes delta and gamma contribute to adverse remodeling but redundantly inhibit calcineurin-induced myocardial hypertrophy. *Circulation*. 2014;130:1262-1273

9. Bordicchia M, Liu D, Amri EZ, Ailhaud G, Dessi-Fulgheri P, Zhang C, Takahashi N, Sarzani R, Collins S. Cardiac natriuretic peptides act via p38 mapk to induce the brown fat thermogenic program in mouse and human adipocytes. *J Clin Invest*. 2012;122:1022-1036

2.2. Part II

2.2.1 Blood pressure and locomotor activity recordings in *Rictor*^{aP2KO} and control mice

2.2.1.1 Frequency of activity in Rictor^{aP2KO} *and control mice*

In addition to the intensity of activity and active time, the frequency of activity during the 12 hour light and 12 hour dark period was analyzed of *Rictor*^{aP2KO} and control mice. The frequency of activity was calculated based on the time period where mice were active. During both, the light and the dark period, the frequency of activity (15 to 40 min) showed an upward trend in *Rictor*^{aP2KO} mice compared with controls (**Figure 2-2-1**). During the dark period (active period of mice), *Rictor*^{aP2KO} and control mice displayed an overall increase in the frequency of activity compared to the light period (**Figure 2-2-1 B**).

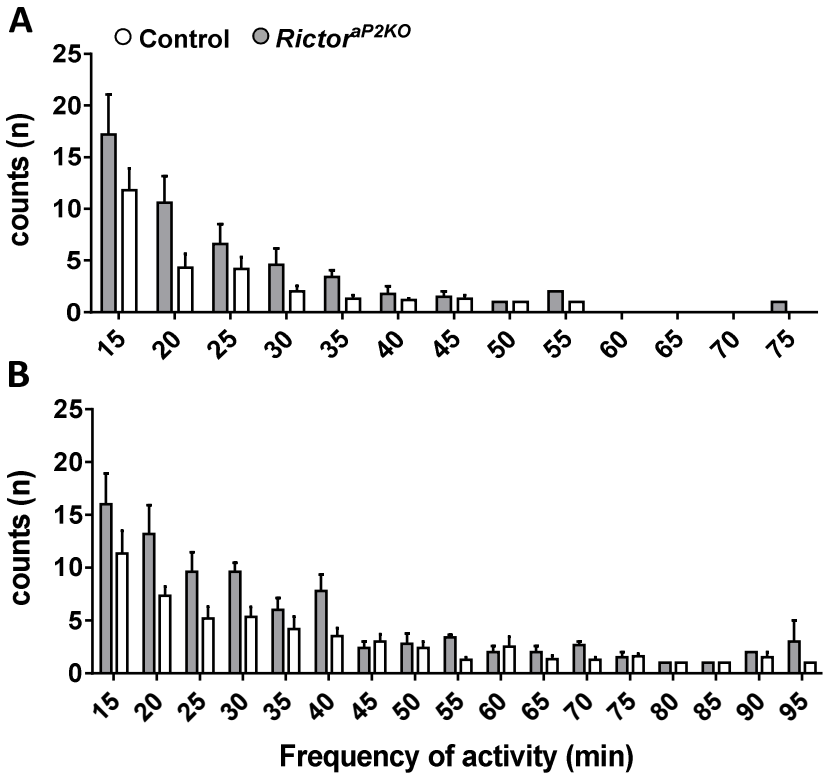

Figure 2-2-1: Frequency of activity is increased in *Rictor*^{aP2KO} mice. Frequency of activity was calculated from locomotor activity recordings over 7 consecutive days and consecutive minute's mice spent active during the **(A)** 12 hour light and **(B)** 12 hour dark period. Less than 0.6 counts per minute (15 min) were considered as inactivity. n = 5/6

2.2.2.2 Infusion of 1400W using mini pumps in Rictor^{aP2KO} and control mice

We have previously proposed that upregulated expression of the inducible nitric oxide synthase (iNOS) impaired PVAT properties to control vascular reactivity in *Rictor^{aP2KO}* mice [223]. It is well known that immune responses including the release of pro-inflammatory cytokines contribute to increased blood pressure [224]. To investigate whether the increased iNOS expression in PVAT might directly augment blood pressure, we infused the specific iNOS inhibitor 1400W (10 mg/kg per day) or saline as solvent control subcutaneously in *Rictor^{aP2KO}* mice. To this end, in addition to the telemetry device, Alzet™ mini pumps either releasing 1400W or saline were implanted after completion of blood pressure baseline measurements (ten days after telemetry device implantation). After mini pump implantation, 1400W-infused *Rictor^{aP2KO}* mice needed five days to recover as evidenced by the normalization of the heart rate after surgery to baseline levels **(Figure 2-2-2 A)**. However, in saline-infused *Rictor^{aP2KO}* mice the heart rate did not reach baseline levels ten days after mini pump implantation and was significantly higher during the dark period (**Figure 2-2-2 A**). As indicator for a possible blood pressure lowering effect of 1400W, the mean arterial pressure (MAP) was continuously monitored parallel to heart rate measurements (**Figure 2-2-2 B**) and the areas under the MAP curve (AUC) of the 1400W- and saline-infused mouse groups were calculated (**Figure 2-2-2 C**). Both, saline and 1400W infusion had no effect on MAP in *Rictor^{aP2KO}* mice (**Figure 2-2-2 C**).

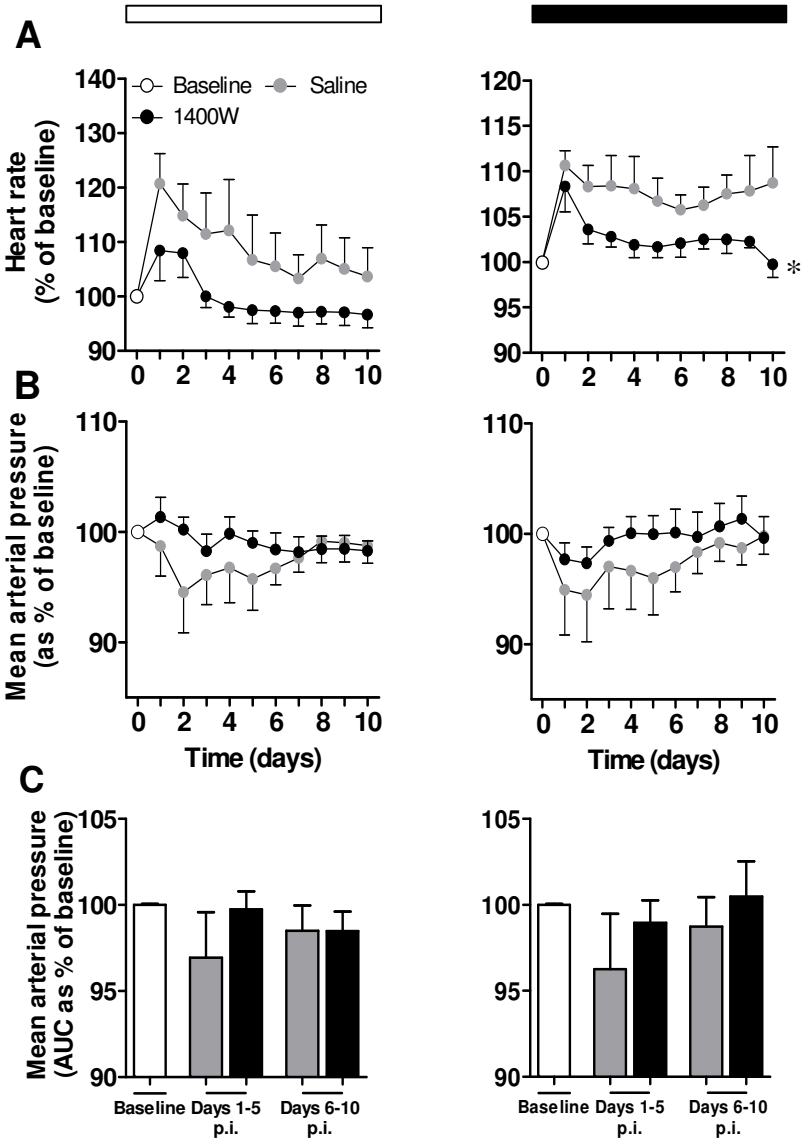

Figure 2-2-2: Inhibition of iNOS does not normalize mean arterial pressure in *Rictor*$^{\alpha P2KO}$ mice. (A) Heart rate and **(B)** mean arterial pressure (MAP) were constantly followed for 10 days post mini pump implantation (p.i.; filled with 1400W or saline) during the light (left panel) and dark period (right panel). Baseline measurements were set to 100 %. After mini pump implantation, MAP and heart rate were calculated as percentage of baseline. **(C)** 1400W treatment does not lower MAP in *Rictor*$^{\alpha P2KO}$ mice to levels recorded in controls. Areas under the curves (AUC) were calculated using daily means of MAP recordings from day 1 to 5 and 6 to 10 in *Rictor*$^{\alpha P2KO}$ mice during the light (left) and dark period (right panel). n=15 (baseline), n=7/8 (saline or 1400W treatment). The bars at the top indicate the 12 hour light (white) and 12 hour dark (black) period.

2.2.2 *Cre*-recombinase expression in *Rictor*^{aP2KO} mice

In the present study, mice with deletion of Rictor (*Rictor*^{aP2KO}) were generated crossing *Rictor*$^{fl/fl}$ mice with C57BL/6J mice expressing *Cre* recombinase under the control of the *adipocyte protein 2* (*aP2*) gene promoter. mRNA expression of the *Cre* recombinase was detected in adipocytes isolated from EFAT of *Rictor*^{aP2KO} mice **(Figure 2-2-3)**. Further, the *Cre* recombinase was highly expressed in the stromal vascular fraction (SVF) separated from EFAT, in the heart as well as in the brain regions suprachiasmatic nucleus (SCN) and cortex **(Figure 2-2-3)**. In the liver and the kidney *Cre* recombinase was not expressed.

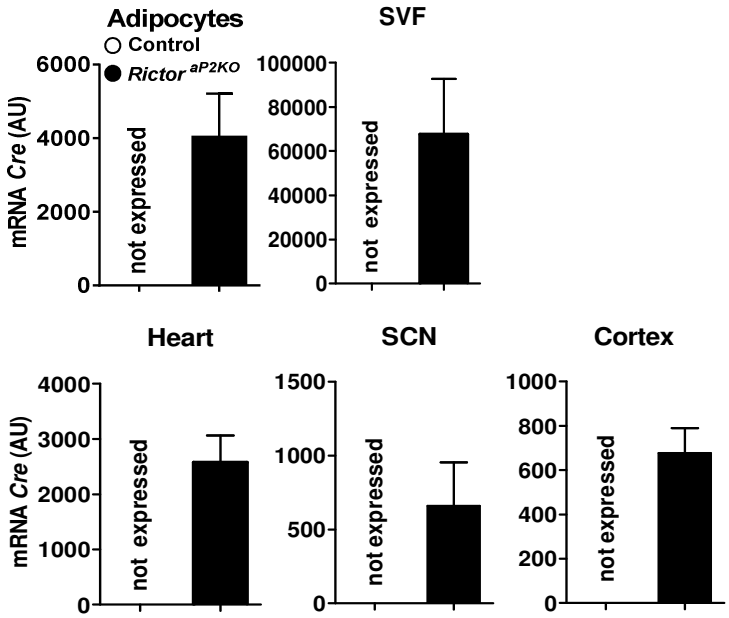

Figure 2-2-3: *Cre*-recombinase is expressed in adipocytes, but also in the stromal vascular fraction and non-adipose tissues. *Cre*-recombinase expression was analyzed in epididymal adipose tissue derived adipocytes (n=11), stromal vascular fraction (SVF; n=4), and further in heart (n=7), suprachiasmatic nuclei (SCN; n=3) and cortex (n=3) of *Rictor*^{aP2KO} and control mice. mRNA expression levels were analyzed using quantitative RT-PCR, specific mouse primers and calculated by ΔCT. Expression data were normalized to the housekeeping gene *Arbp* (adipocytes), *Gapdh* (SCN, cortex), *Cyclophelin B* (heart) and *Tbh* (SVF). Values are represented as means ± SEM. AU (arbitrary units).

2.2.3 Perivascular adipose tissue genome wide mRNA expression analysis in *Rictor*^{aP2KO} and control mice

To identify differentially expressed genes in PVAT of *Rictor*^{aP2KO} mice compared to controls, a micro array analysis of the expressed PVAT genome was performed. 68 genes were differentially expressed in PVAT of *Rictor*^{aP2KO} mice. To validate the expressional changes of the 10 most increased and the 10 most reduced genes (see results part I, table S4), steady state mRNA expression levels were analyzed using quantitative real time PCR (qRT-PCR).

Analysis of the steady state mRNA expression levels revealed a significant increase of the genes *interferon regulatory factor 4* (*Irf4,* +298 %), *neuronal pas domain protein 2* (*Npas2,* +243 %), *mast cell protease 4* (*Mcpt4,* +160 %), *sestrin 2* (*Sesn2,* +189 %) and *sprouty 4* (*Spry4,* +311 %) in PVAT of *Rictor*^{aP2KO} mice compared to controls (**Figure 2-2-4**). Deletion of *Rictor* had no effect on *triadin* (*Trdn*), *cryptochrome 1* (*Cry1*) and *nuclear factor, interleukin 3 regulated* (*Nfil3*) mRNA expression levels in PVAT of *Rictor*^{aP2KO} mice. Expression of the *cation transporter regulator like-1* (*Chac1*) was not detected in PVAT of both mouse groups.

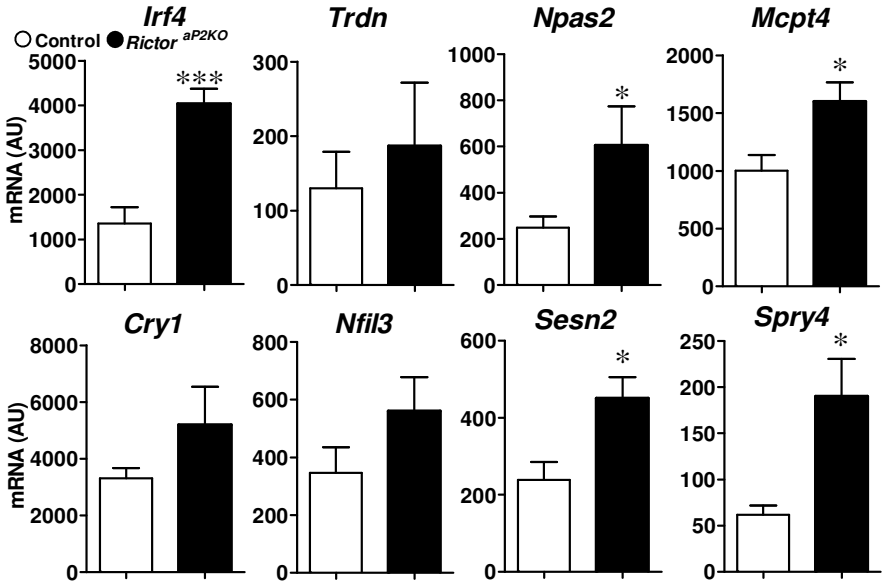

Figure 2-2-4: Validation of the 10 most increased genes identified with the micro array study revealed only mRNA expression levels of 4 genes to be sustainably changed in PVAT of *Rictor*^{aP2KO} mice. mRNA expression levels of target genes *Irf4*, *Trdn*, *Npas2*, *Mcpt4*, *Cry1, Nfil3, Sesn2* and *Spry4* were analyzed in PVAT of *Rictor*^{aP2KO} mice and control littermates. mRNA expression was analyzed using quantitative RT-PCR and calculated using ΔCT method. Gene expression was normalized to the housekeeping gene *Arbp*. Values are represented as means ± SEM. **P*<0.05 and ****P*<0.005. n=6-10. AU (arbitrary units).

In addition to the 10 most increased genes identified with genome expression analysis in PVAT of *Rictor*^{aP2KO} mice, the 10 most reduced genes were validated. Analysis of steady state mRNA expression levels revealed are significantly reduction of the genes *serine (or cysteine) peptidase*

inhibitor, clade E, member 1 (*Serpine1;* also known as *Pai-1,* -350 %) and *S100 protein, beta polypeptide, neural* (*S100b,* -229 %) in PVAT of *Rictor*^{aP2KO} mice (**Figure 2-2-5**). The genes *growth arrest and DNA-damage-inducible 45 beta (Gadd45b*), *thyroid hormone receptor alpha* (*Thra*), *nuclear receptor subfamily 1, group D, member 1* (*Nr1d1*; also known as *Rev-Erb-α*), *FBJ osteosarcoma oncogene B* (*Fosb*), *neurocan* (*Ncan*), *U2 small nuclear RNA 10* (*Rnu2*) and *gliomedin* (*Gldn*) were similar expressed in PVAT of both mouse groups. Expression of the *nuclear receptor subfamily 2, group D, member 2* (*Nr1d2*; also known as *Rev-Erb-β*) was not detected in PVAT.

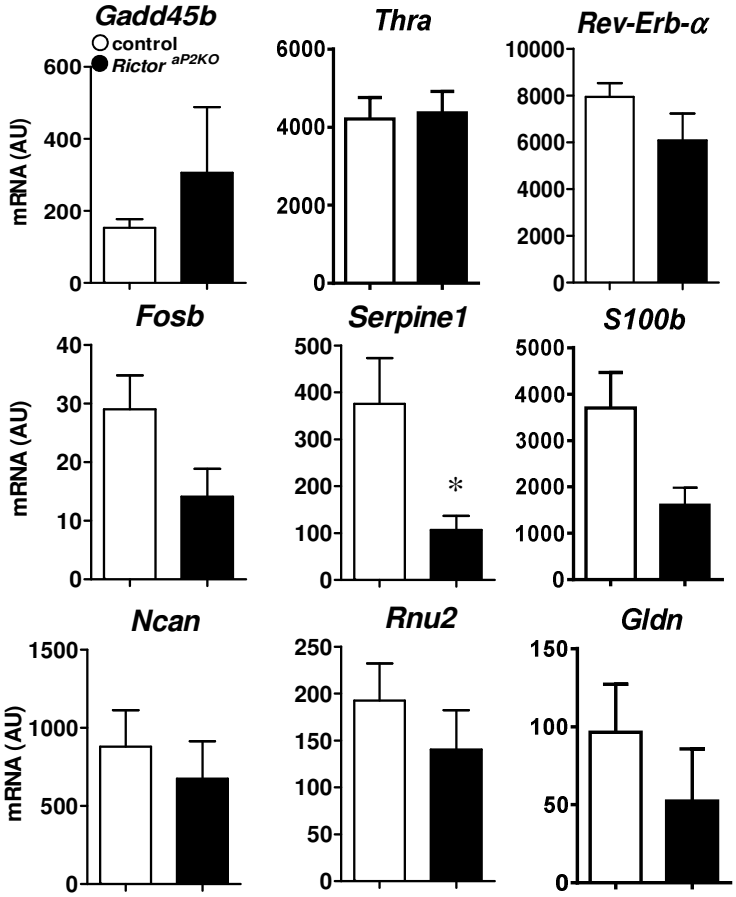

Figure 2-2-5: Validation of the 10 most reduced genes identified with the micro array study revealed only mRNA expression levels of *Serpine1* to be sustainably changed in PVAT of *Rictor*^{aP2KO} mice. mRNA expression levels of target genes *Gadd45b*, *Thra*, *Rev-Erb-α*, *Fosb*, *Serpine1, S100b, Ncan, Rnu2* and *Gldn* were analyzed in PVAT from *Rictor*^{aP2KO} mice and control littermates. mRNA expression was analyzed using quantitative RT-PCR and calculated by ΔCT. Gene expression was normalized to the housekeeping gene *Arbp*. AU (arbitrary units). Values are represented as means ± SEM. **P*<0.05. n=7-10

In addition to the 20-top ranked genes, steady state mRNA expression levels of genes associated with the cholesterol biosynthesis and/or lipid metabolism were validated (**Figure 2-2-6**). qRT-PCR analysis revealed that the mRNA expression levels of *NAD(P) dependent steroid dehydrogenase-like* (*Nsdhl*), *farnesyl diphosphate synthetase* (*Fdps*) and *cytochrome P450, family 51, subfamily A, polypeptide 1* (*Cyp51A1*) showed a non-significant downward trend in *Rictor*^{aP2KO} mice.

To accomplish this expressional analysis, mRNA expression levels of additional genes associated with the cholesterol biosynthesis and/or lipid metabolism, but not found to be differentially expressed in the micro array were analyzed. The target genes *sterol regulatory element binding transcription factor 1* (*Srebp-1c*), *fatty acid synthase* (*Fasn*), *diacylglycerol O-acyltransferase 1* (*Dgat1*) and *perilipin1* showed a similar expression profile in PVAT between the mouse groups (**Figure 2-2-6**).

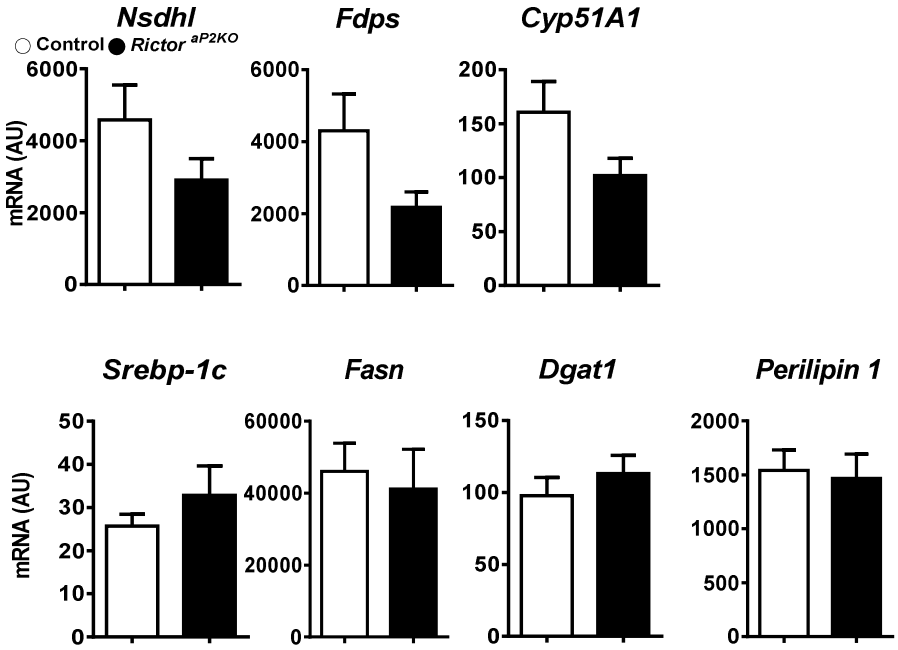

Figure 2-2-6: Deletion of *Rictor* did not affect mRNA expression levels of target genes in PVAT associated with the cholesterol biosynthesis and lipid metabolism. mRNA expression levels of indicated genes were analyzed in PVAT of *Rictor*^{aP2KO} and control mice using quantitative RT-PCR. Gene expression levels were calculated using the ΔCT method and normalized to the housekeeping gene *Arbp*. Values are expressed in arbitrary units (AU). Values are represented as means ± SEM. *Nsdhl, Fdps, Cyp*: n=8/9; *Srebp-1c, Dgat1*: n=8/10 and *Fasn, Perilipin1*: n=7

2.2.4 Fluctuating expression patterns of *Rictor* and mTORC2 downstream targets

As the micro array study identified the circadian rhythm as the most affected pathway in the *Rictor*^{aP2KO} mice, I reasoned that the *Rictor* expression during a 24 hour period might have changed. To this end, steady state mRNA expression of *Rictor* was analyzed in the different adipose tissues PVAT, brown adipose tissue (BAT) and epididymal adipose tissue (EFAT) as well as aortic tissue and the liver of control and *Rictor*^{aP2KO} mice. As expected, expression of *Rictor* was significantly reduced in adipose tissues of *Rictor*^{aP2KO} mice, but remained unchanged in aortic tissue and the liver during the light and dark period **(Figure 2-2-7)**. Surprisingly, in control mice (*Rictor*$^{fl/fl}$) time-of-day dependent fluctuations in *Rictor* mRNA expression levels were detected in PVAT and BAT (to a lesser extent in EFAT) **(Figure 2-2-7)**. Highest mRNA expression levels of *Rictor* were measured at the beginning of the light period and then gradually decreased. During the dark period, in control mice *Rictor* mRNA expression was significantly lower as compared to the light period (PVAT: -62 %, $P < 0.0001$; BAT: -45 %, $P < 0.01$). Interestingly, during the dark period mRNA expression levels of *Rictor* were similar in control and *Rictor*^{aP2KO} mice (**Figure 2-2-7).**

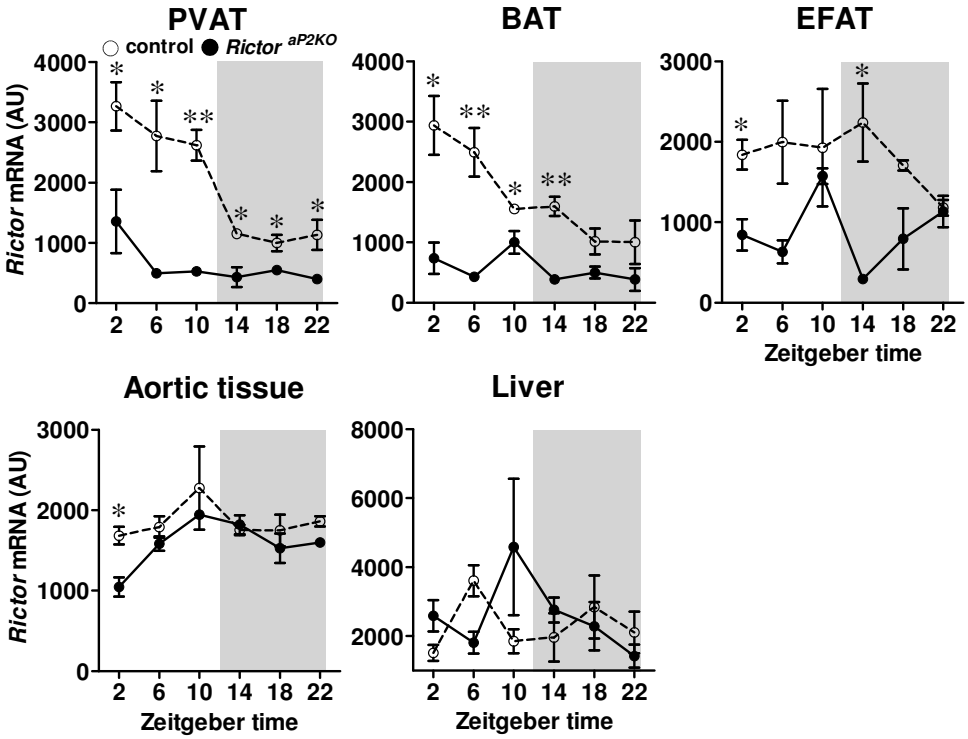

Figure 2-2-7: *Rictor* mRNA exhibit fluctuating expression in different adipose tissue depots, but not aortic tissue and liver. *Rictor* mRNA expression was determined in perivascular adipose tissue (PVAT), brown adipose tissue **(**BAT), epididymal fat (EFAT) and aortic tissue from control and *Rictor*^{aP2KO} mice at different zeitgeber times (ZT) over a period of 24 hours. Mice were kept under constant 12-hours light/ 12 hours dark period (lights on ZT 0: 7 am; light off ZT 12; 7 pm). Prior experiment, mice had access to water and food *ad libitum.* All values represent mean ± SEM, **P<0.05*, n=3 mice per group and time point. Gray shaded areas represent the 12 hour dark period.

To investigate, whether the fluctuating *Rictor* expression translates on the protein level**,** protein expression of RICTOR was analyzed in PVAT of control mice at the beginning of the light (ZT 2) and the dark period (ZT 14). Indeed, RICTOR expression was significantly lower at ZT 2 as compared to the ZT 14 **(Figure 2-2-8)**.

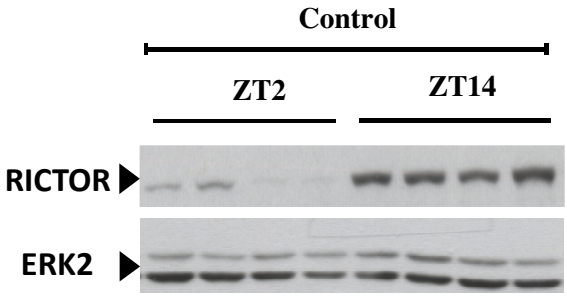

Figure 2-2-8: Time-of-day dependent protein expression of RICTOR in PVAT of control mice. Immunoblot analysis of RICTOR expression in PVAT of control mice. Total Erk2 was used as reference control for protein loading. Tissue was collected at zeitgeber times (ZT) 2 and 14. Mice were not starved before experiment.

The meter of the mTORC2 activity is its ability to phosphorylate downstream target proteins such as AKT. To examine, whether the fluctuating expression of RICTOR might affect mTORC2 activity, the phosphorylation of AKT at different residuals was investigated at ZT 2 and ZT 14 in control mice. In EFAT, basal phosphorylation of AKT at Serine 473 ($pAKT^{S473}$) was higher at ZT 2 compared to ZT 14 **(Figure 2-2-9 A)**. Stimulation with insulin (1 µmol/l) resulted in an overall increase of $pAKT^{S473}$ phosphorylation at ZT 2 and ZT 14, but the phosphorylation was still lower at ZT 14. The phosphorylation of AKT at Thr308 ($pAKT^{T308}$) followed a similar fluctuating pattern as observed for $pAKT^{S473}$. For mTOR protein expression, no time-of-day dependent differences were detected in insulin-stimulated and unstimulated conditions **(Figure 2-2-9 A).** Total AKT (tAKT) and ERK2 were used as reference controls for protein loading and showed a similar expression pattern at ZT 2 and ZT 14. Both remained unchanged upon insulin-stimulation.

In PVAT, the unstimulated and insulin-stimulated phosphorylation of $pAKT^{S473}$ was similar to EFAT **(Figure 2-2-9 B)**. However, the phosphorylation of $pAKT^{T308}$ was neither different between time points, nor unstimulated and insulin-stimulated samples. mTOR protein was equally expressed at ZT 2 and ZT 14 and did not change with stimulation of insulin. The expression of the loading controls tAKT and ERK2 was similar between times points and groups.

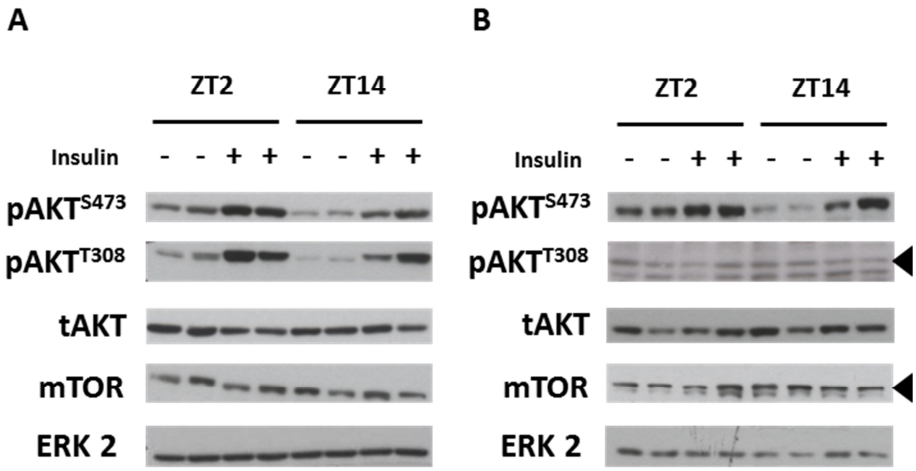

Figure 2-2-9: Immunoblot analysis of EFAT and PVAT revealed daytime dependent phosphorylation of AKT at serine 473 in control mice. Immunoblot analysis of insulin-stimulated **(A)** epididymal adipose tissue (EFAT) and **(B)** perivascular adipose tissue in control mice are shown. Total AKT and ERK 2 were used as loading control. One representative blot of 2 is shown. Protein loading: 25 µg/ lane.

Alongside the analysis of *Rictor*, 24 hour mRNA expression patterns of nutrient sensors were analyzed in PVAT. Nutrient sensors such as SIRT1 (Sirtuin1) and PGC-1α (Pparg co-activator 1 α) integrate metabolite-derived signals are believed to play a key role in the generation of daytime dependent cellular processes [225-227]. The expression of *Sirt1*, *Pgc-1α*, *RAR-related orphan receptor gamma* (*Rorc*), *nuclear factor-interleukin 3-regulated* (*Nfil3*) and *D site albumin promoter binding protein* (*Dbp*) fluctuated though the course of the day **(Figure 2-2-10)**. In *Rictor*^{aP2KO} mice, the expression of *Sirt1* and *Pgc-1α* was reduced during the light period, while during the dark period the expression was similar between groups. Fluctuating mRNA expression levels of the genes *Rorc*, *Nfil3* and *Dbp* was similar between mouse groups.

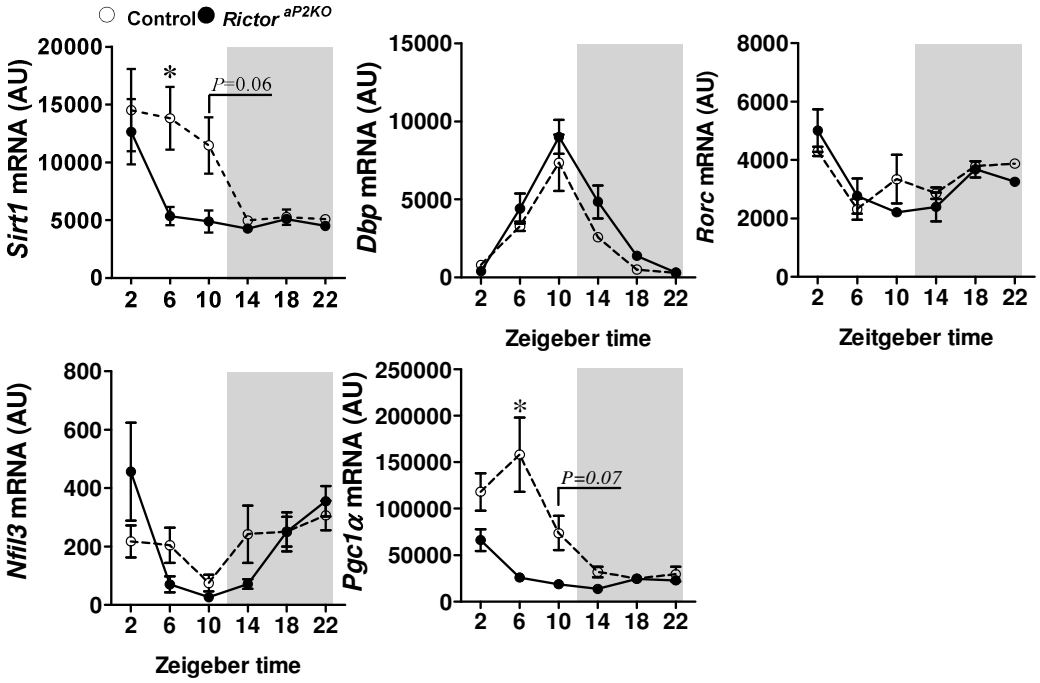

Figure 2-2-10: Fluctuating mRNA expression patterns of *Sirt1* and *Pgc1-α* are dampened in *Rictor*^{aP2KO} mice. Expression of target genes was determined in perivascular adipose tissue (PVAT) of control and *Rictor*^{aP2KO} mice at different zeitgeber times (ZT) over a period of 24 hours. Mice were kept under constant 12 hour light/ 12 hour dark cycles (lights on ZT 0: 7 am; lights off ZT 12; 7 pm). Prior experiment, mice were not starved. All values represent mean ± SEM, *$P < 0.05$, n=3 mice per group and time point. Gray shaded areas represent the 12 hour dark period.

3. Discussion

3.1 Key players in vascular reactivity

The occurrence of cardiovascular diseases including pathologies of the thoracic aorta is increasing due to prolonged life expectancy, obesity and associated comorbidities (e.g. hypertension and T2D) [228]. Traditionally, it was assumed that all physiological and pathophysiological changes of the blood vessel wall are mediated by bioactive molecules delivered by the blood stream through vascular endothelial cells ("inside-out" signaling). However, a growing body of evidence suggests that perivascular adipose tissue (PVAT) has beneficial effects on blood vessel function ("out-side-in" signaling) in healthy conditions, which are impaired in various pathologies such as hypertension [229].

To date, PVAT is widely accepted as an endocrine organ secreting vasoactive substances and affects the reactivity of the adjacent blood vessel [159]. Most studies analyzing PVAT properties and its contribution to vascular reactivity have widely focused on identifying molecules released from PVAT. Signaling pathways involved are less well understood.
To understand the contribution of the mammalian target of rapamycin complex 2 (mTORC2) to PVAT function, I aimed to analyze gene expression in thoracic PVAT and blood pressure regulation in mice lacking *Rictor* mRNA expression in adipocytes and the brain.

3.2 Perivascular adipose tissue

3.2.1 Perivascular adipose tissue function and hypertension

Anti-contractile properties of PVAT are mediated by vasoactive molecules. Their secretion was reported to be attenuated in hypertension [134]. Mechanisms contributing to changes in PVAT properties are however not well understood. In accordance with the function of PVAT, different mechanisms should be taken into consideration.
In animal models of hypertension, an increase in cell density and reduced absolute PVAT mass were reported to be strongly associated with the loss of PVAT anti-contractile properties [163-165]. In $Rictor^{aP2KO}$ mice, we observed a similar phenotype with increased cell density of the thoracic PVAT likely contributing to the attenuated vasoactive properties of PVAT. In addition to PVAT, cell density was increased in the interscapular brown adipose tissue (BAT), but not epididymal adipose tissue (EFAT) of $Rictor^{aP2KO}$ mice (data not shown). Interestingly, these morphological changes resemble the phenotype of $Rictor^{MYf5cKO}$ mice, lacking *Rictor* in brown adipocytes [230]. As PVAT has a phenotype similar to BAT [7], it would be of interest to assess PVAT vasoactive properties and vascular reactivity of the thoracic aorta in these

mice. However, at this point it remains unclear whether deletion of *Rictor* in adipocytes or the hypertensive phenotype causes the increase in perivascular cell density and warrants further investigation.

Another reason for altered PVAT vasoactive properties is inflammation. In hypertension, PVAT gets inflamed [134, 138, 173, 231] which is associated with pathophysiological changes of the blood vessel wall [232]. Pro-inflammatory molecules can be secreted either directly from perivascular adipocytes or PVAT infiltrating immune cells. In *Rictor*^{aP2KO} mice, we previously reported that increased pro-inflammatory molecule expression in PVAT added to the changes in the vascular reactivity [223]. However, the percentage of infiltrating immune cells such as leukocytes did not change in these mice [223].
In conclusion, in *Rictor*^{aP2KO} mice altered vasoactive properties of PVAT can be contributed to the increased perivascular cell density and the increased pro-inflammatory molecule expression without affecting immune cell content. It is feasible to assume that these alterations might affect PVAT properties under additional pathological inflammatory conditions. Further, a novel role of RICTOR/mTORC2 in inflammation is fostered by studies showing that the inflammatory response in mTORC2-deficient myeloid mouse cells and mouse embryonic fibroblasts as well as in dendritic cells with *Rictor* knock-down is only susceptible upon lipopolysaccharide (LPS) stimulation, but not under basal conditions [233, 234].

3.2.2 Perivascular adipose tissue, mTORC2 and clock gene expression

To connect physiological changes observed in *Rictor*^{aP2KO} mice to attenuated mTORC2 signaling, we analyzed the expressed genome in PVAT of *Rictor*^{aP2KO} mice and controls. Gene expression analysis uncovered a significant contribution of RICTOR/mTORC2 to peripheral core clock gene expression. Core clock genes form the molecular basis of the circadian clock [51] and misalignments were reported to enhance metabolic dysfunction and inflammation [80, 235]. An extended analysis of mRNA expression levels over a 24 hour cycle identified the core clock genes *Rora*, *Cry1*, *Per1*, *Per2* and *Clock* to be changed in PVAT of *Rictor*^{aP2KO} mice. Interestingly, inflammatory capability of these genes was shown for the adipose tissue [236, 237] and the cardiovascular system [238] providing evidence that misalignment of the circadian clock in these tissues contributes significantly to inflammatory processes.
Staggerer mice (*Rorα*$^{sg/sg}$), with loss-of-function of the *Rorα* gene, displayed elevated susceptibility to the development of atherosclerosis in the blood vessel wall upon high-fat diet feeding [239]. These results are in line with findings that pro-inflammatory molecule expression (e.g. *Tnfα, Il-1α*) [240] and LPS stimulated inflammatory response [241] were increased in these mice. The anti-inflammatory capability of RORα is probably mediated by the transcriptional induction of the NF-

κB (nuclear factor of kappa light polypeptide gene enhancer in B cells) negative regulator *Iκ-Bα* (*nuclear factor of kappa light polypeptide gene enhancer in B-cells inhibitor, alpha*) [242]. Controversially, pro-inflammatory capability of RORα was reported as *Rorα*$^{sg/sg}$ mice were protected against diet-induced obesity and white adipose tissue (WAT) inflammation [192, 193]. Thus, data imply that ROR*α* has anti- and pro-inflammatory capability, which might depend on the tissue analyzed and manifests in variable phenotypes.

In a nutshell, the changed peripheral core clock gene expression might explain the pro-inflammatory state of PVAT, which we previously reported in *Rictor*^{aP2KO} mice [223] and thus contribute to changes in the vascular reactivity. Given the fact that components of the molecular clock are involved in anti- and pro-inflammatory processes, a profound understanding of how the circadian clock and inflammatory processes are interconnected with each other might open new directions in the development of treatment options for common cardiovascular diseases such as hypertension.

3.3 Blood pressure regulation in *Rictor*^{aP2KO} mice

The present study uncovers an unknown contribution of RICTOR/mTORC2 to blood pressure regulation in mice. In *Rictor*^{aP2KO} mice, the mean (MAP) and the diastolic (DAP) arterial pressure as well as the heart rate (HR) were slightly elevated and resembled a pre-hypertensive phenotype in human subjects [243]. In addition, locomotor activity, specifically the time mice spent active, was increased. In general, different mechanisms on the whole body level contribute to the regulation of blood pressure. Thus, it is likely that, in addition to the functional and structural changes of PVAT, other mechanisms contribute to the elevation in blood pressure of *Rictor*^{aP2KO} mice as discussed in the following:

3.3.1 Hyperinsulinemia

In addition to the already reported hyperinsulinemic and slightly insulin resistant state [215, 244], we found insulin plasma levels to be increased in *Rictor*^{aP2KO} mice at specific time points over a 24 hour cycle.

In healthy subjects, insulin exerts protective effects on the vasculature. Postprandial, acute hyperinsulinemia increases NO and prostaglandins availability to vascular smooth muscle cells (VSMC). This promotes vasodilation [47] and small physiological changes in blood pressure [245]. In contrast, chronic hyperinsulinemia which compensates insulin resistance [246], can facilitate changes in the insulin signaling in the vasculature. This enhances the secretion of vasoconstrictors such as endothelin-1 [247]. As a consequence, the progression of vascular dysfunction and hypertension might be promoted [47].

Further evidence of the noticeable contribution of insulin, while not *per se,* to the development of hypertension is provided by studies in humans and animals. In type 2 diabetes mellitus (T2D) patients, hypertension is twice as common as in healthy subjects [248]. Genetically hypertensive rats display elevated insulin levels [249, 250], suggesting a common genetic predisposition of hyperinsulinemia and hypertension. However, a relationship between hypertension and hyperinsulinemia/insulin resistance is not always obvious. Not all T2D patients are hypertensive, and hypertensive patients are not necessarily hyperinsulinemic and/or insulin resistant [251-253]. This hypothesis is further strengthened by a missing association of hyperinsulinemia and secondary hypertension [254]. Thus, the cumulative relationship of hypertension, hyperinsulinemia and insulin resistance might have different reasons: (1) hyperinsulinemia and insulin resistance can be secondary to other pathophysiological changes observed in hypertensive subjects, or (2) hypertension, insulin resistance and hyperinsulinemia may arise from different unrelated processes.

Hyperinsulinemia can contribute by several mechanisms to the progression of vascular dysfunction and hypertension. These processes include elevated sympathetic nervous system (SNS) activity, structural and functional changes of the kidney, and a dysfunctional RAA system [255]. Long-term pathophysiological changes of these mechanisms can increase vascular resistance, cardiac output, and fluid retention in the kidney [256-258] causing elevated blood pressure. To what extend these parameters contribute to the changes in blood pressure of *Rictor*^{aP2KO} mice requires further investigations.

3.3.2 Natriuretic peptides

Chronic blood pressure elevations are associated with compensatory morphological changes of the heart and altered cardiac natriuretic peptide (NP) expression [32]. The NP family includes the mature proteins atrial NP (ANP) and B-type NP (BNP), which are predominantly secreted from cardiomyocytes, and C-type NP (CNP), found in the CNS and endothelium. NPs are hormonal regulators of vasodilation and natriuresis as well as inhibitors of the SNS and their role in blood pressure regulation is well established [259]. Transgenic mice overexpressing a non-functional ANP display a hypertensive phenotype [260]. In pre-hypertensive *Rictor*^{aP2KO} mice, cardiac *Anp* and *Bnp* mRNA expression levels were reduced. These findings are in line with human studies showing that a pre-hypertensive state is characterized by a deficiency of circulating ANP and BNP levels [261, 262]. A genetically predisposition in humans reduces circulating levels of ANP and BNP, which increases the risk of hypertension [261, 263]. Moreover, with low circulating levels, the ability of NPs to effectively inhibit SNS and RAAS activity gets lost [264]. Taken together, previous studies support a possible contribution of the reduced cardiac *Anp* and *Bnp* mRNA expression to the blood pressure elevations in *Rictor*^{aP2KO} mice.

Interestingly, NPs were reported to stimulate lipolysis in adipocytes during exercise [265] and reduced plasma levels of NPs were identified as a common predisposition for metabolic and cardiovascular disorders [32, 266]. A common initiating factor might be insulin as concentrations of circulating NPs are inversely related to plasma insulin levels [267-270]. This assumption is strengthened as transgenic mice overexpressing *Bnp* were resistant to diet-induced obesity [271]. Moreover, a “natriuretic handicap” characterized by low circulating ANP and BNP levels is common to obese subjects [269, 272]. Interestingly, in patients with T2D the release of ANP from the heart was impaired and the ability of ANP to lower blood pressure reduced [273].

3.3.3 Contribution of locomotor activity to elevation in blood pressure

Activity and rest exert profound influences on the physiology of small rodents [274] and are important parameters affecting blood pressure in mice.

In *Rictor*^{aP2KO} mice, we demonstrated an overall increase in locomotor activity parameters and its physiological decrease during the dark period was strongly reduced. The intensity of activity followed a similar fluctuating pattern as established for MAP and HR during the dark period. Thus, the increased locomotor activity observed in *Rictor*^{aP2KO} could be one important parameter responsible for the elevations in blood pressure and HR as well as the strong impairment of their physiological decline during the dark period. A similar observation has been made by Kim *et al.* showing that differences in MAP between mouse groups are no longer evident if analyzing MAP only in intervals with no activity [275]. A possible contribution of locomotor activity to blood pressure readings has further been provided by Sheward *et al.* demonstrating that episodes of activity and rest mainly account for changes in MAP and HR in vasointestinal peptide receptor 2 knockout mice [274]. These findings might further explain why the infusion of the specific iNOS inhibitor 1400W, did not result in lower blood pressure in *Rictor*^{aP2KO} mice.

3.3.4 Conclusion

To the best of our knowledge, this is the first study showing that RICTOR/mTORC2 contributes to the regulation of blood pressure and its fluctuating patterns in mice over a 24 hour light/dark cycle. Based on the findings of the present study and current literature, it is likely that several mechanisms contribute to the observed changes in blood pressure regulation in *Rictor*^{aP2KO} mice.

In my opinion, the present study and available literature suggest that the elevated locomotor activity is mainly responsible for the increase in blood pressure of *Rictor*^{aP2KO} mice, especially during the 12 hour dark period. This assumption is based on the finding that the patterns of MAP and HR are highly similar to those of the intensity of activity (see 2.1.9/ Figure S2) in these mice. Confirming data from other rodent studies, findings presented here underscore the importance of considering locomotor activity if analyzing blood pressure data in free-moving mice. To clarify the contribution of elevated locomotor activity to the blood pressure increase in *Rictor*^{aP2KO} mice, blood pressure should be recorded in immobilized *Rictor*^{aP2KO} and control mice using tail cuff method. Measurements might allow estimating the effective impact of the locomotor activity on blood pressure and to what extend other parameters might account for blood pressure elevations in *Rictor*^{aP2KO} mice. However, with the telemetric system used in this study, only horizontal movements of mice across the cage, but not specific behavioral parameters could be analyzed.

Other factors such as the hyperinsulinemic state and/or the altered NP system might contribute additionally to the blood pressure and locomotor activity elevations. However, precise mechanisms have yet to be identified. Possible explanations might be:

(1) Changes in blood pressure and locomotor activity might be secondary to the hyperinsulinemia in *Rictor*^{aP2KO} mice. This hypothesis is strengthened by studies in humans and dogs showing that hyperinsulinemia is associated with an increase in SNS activity [276] and heart rate [277]. Daily variations in MAP, HR and locomotor activity are mediated by the CNS [33, 278]. Functional changes in the CNS, particularly within regions controlling blood pressure and locomotor activity, might impact the daily regulation of these parameters. Thus, in *Rictor*^{aP2KO} mice the observed changes in blood pressure and locomotor activity might reflect an autonomic imbalance, which is initially triggered by increased insulin levels.

(2) The reduced *Anp* and *Bnp* expression in the heart might contribute to the increase in blood pressure in *Rictor*^{aP2KO} mice. Both peptides are released from the heart into the blood stream upon mechanical strain of the atria [259]. Interestingly, action of ANP was reported in the hypothalamus to influence cardiovascular homeostasis, blood pressure, and SNS activity [259]. Therefore, the deregulated NPs system might be an important contributor to cardiovascular changes of *Rictor*^{aP2KO} mice. However, additional studies are required to evaluate possible mechanisms by which *aP2* promoter-driven deletion of *Rictor* causes the alterations in the NP system.

3.4 Role of RICTOR/mTORC2 in clock gene expression in the suprachiasmatic nucleus

Rictor mRNA expression in the brain (SCN and cortex) and absolute brain mass are reduced in *Rictor*^{aP2KO} mice. These findings are in line with data published by Thomanetz *et al.* demonstrating that mTORC2 is of particular importance for brain functions [213]. Both, blood pressure and locomotor activity are also regulated through different neural mechanisms. Thus, an effect of the deletion of *Rictor* in the brain has to be considered likely facilitating blood pressure and locomotor activity changes. A key role in the regulation of daily blood pressure and locomotor activity fluctuations is achieved and coordinated by the biological master clock, the suprachiasmatic nucleus (SCN) located in the anterior hypothalamus. SCN lesions in rats [93, 94] and mutations of core clock genes in the SCN impaired the daily regulation of blood pressure and promoted the progression of hypertension [279, 280]. Consequently, it was important to analyze clock gene expression in the SCN of *Rictor*^{aP2KO} mice. Despite reduced *Rictor* expression, core clock gene expression patterns over a 24 hour period were not changed in *Rictor*^{aP2KO} mice compared to controls. Thus, data imply that physiological changes of the blood pressure and locomotor activity are likely due to alterations downstream or independent of the molecular clock mechanism in the SCN. However, in *Rictor*^{aP2KO} mice deletion of *Rictor* in the brain was not restricted to the SCN and mice exhibited reduced absolute brain mass. Accordingly, a possible impact of the *Rictor* deletion in other brain regions on the observed phenotype has to be considered. It would be of particular interest to study sympathetic and parasympathetic output of the medullary cardiovascular center, the core of blood pressure regulation driving vasculature, heart and kidney functions to regulate long-term blood pressure [1].

3.5 Gene expression profiling in perivascular adipose tissue of *Rictor*^{aP2KO} mice

Large scale gene expression profiling between different biological groups can be performed using micro arrays [281]. This technique is a powerful tool to discover new biological targets. However, sensitivity and specificity of micro arrays, variability of platforms and biological samples used are major limitations of this technique [282]. Therefore, it is required to critically validate the expression data to estimate their quality using an independent method. Usually, the method of choice is quantitative RT-PCR (qRT-PCR).

In the present study, the micro array data analysis identified 68 differentially expressed genes in PVAT of *Rictor*^{aP2KO} mice compared with controls. For the validation of micro array data, the 20 top-ranked genes (10 most increased and 10 most reduced genes) were chosen. Seven genes were validated by qRT-PCR and found to be differentially expressed in PVAT of *Rictor*^{aP2KO} mice. Validation results are in line with the statistical analysis of the micro array data, which predicted a false discovery rate (FDR) of ~ 30 % of all differentially expressed genes. The high correlation further suggests that all the different steps necessary to perform a micro array and a qRT-PCR were done accurate.

Validation of target genes showed that *Irf4*, *Npas2*, *Mcpt-4*, *Sesn2* and *Spry4* were significantly increased in PVAT of *Rictor*^{aP2KO} mice. *Serpine1* and *S100b* showed a reduction in their expression levels. Interestingly, the fold changes detected by qRT-PCR were mostly similar to those extracted from the micro array. Differential expression of the target genes *Trdn, Cry1,* and *Nfil3* in PVAT could not be confirmed using qRT-PCR. Possible reasons might be the heterogeneity of individual samples, small expression values, rather small differences between groups and/or the FDR of approx. 30 %. Interestingly, mRNA expression levels of the target genes *Rev-Erbβ* and *Chac1* were not detected in PVAT of *Rictor*^{aP2KO} and control mice. Possible explanations might be that either the genes were indeed not expressed in PVAT or non-binding primer pairs were used for the qRT-PCR.

Irf4 showed the highest increase in gene expression in PVAT of *Rictor*^{aP2KO} mice. As a member of the interferon-regulatory factor (IRF) family, IRF4 is involved in a wide range of immune functions, including lymphopoiesis, macrophage differentiation and the regulation of innate immunity, particularly as effectors of toll-like receptor (TLR) signaling [283, 284]. *Irf4* expression is restricted to immune cells and adipocytes. In adipocytes, *Irf4* expression depends on the availability of nutrients and is modulated via the insulin-FOXO1 signaling pathway [285]. A role of IRF4 has been shown during adipogenesis [286] and in mature adipocytes by the transcriptional induction of the *adipocyte triglyceride lipase* (*Atgl*) and the *hormone-sensitive lipase* (*Hsl*). [285]. However, steady

state mRNA expression levels of genes associated with the lipid metabolism and cholesterol synthesis did not change in PVAT of *Rictor*^{aP2KO} mice (see 2.2.2, figure 2-2-6).
In addition, IRF4 was associated with the regulation of the thermogenesis and mitochondrial biogenesis in brown adipocytes [287]. Interestingly, cardiac ANP and BNP were reported to induce thermogenesis in BAT [288]. Mice exposed to cold stimuli showed increased circulating NP levels. Expression of the NP receptors A and B was elevated, while the expression of the clearance receptor NPRC was significantly reduced. Taken together, data of the present study and current literature might suggest a putative impact of the increased *Irf4* expression on the lipid metabolism and thermogenic processes in PVAT of *Rictor*^{aP2KO} mice. This might involve changes in the NP system. How IRF4 and NPs are associated with each other and a possible common contribution to changes in PVAT functions needs to be shown. As genes possessing lipolytic activity (e.g. *Fdps, Nsdhl*) are also regulated post-transcriptionally on the protein level, an analysis of the abundancy of these proteins and e.g. their phosphorylation state might shed light on the impact of the increased *Irf4* expression in PVAT. In addition, an analysis of *Irf4* expression and the lipid metabolism in an adipose tissue more relevant for the rapid energy turnover would provide interesting results.

In contrast to *Irf4*, *Serpine1* showed the highest reduction in gene expression in PVAT of *Rictor*^{aP2KO} mice. SERPINE1 is a serine protease inhibitor of the tissue (tPA) and urokinase plasminogen activator (uPA), and involved in atherosclerotic and thrombotic plaque formation [289]. The transcription of *Serpine1* is mainly regulated by the transforming growth factor beta-1 (TGF-ß1) [290] and ECs are the major source of circulating SERPINE1. However, its expression was also reported in adipose tissue [291]. *In vitro*, inhibition of SERPINE1 using its specific inhibitor PAI-039 reduced the adipogenesis of human preadipocytes and led to the formation of atypical mature adipocytes [292]. Interestingly, in obese humans, circulating SERPINE1 levels positively correlated with the body mass index (BMI) [293, 294] and circulating SERPINE1 levels were reported to be elevated in *ob/ob* mice [295]. The application of PAI-039 reduced SERPINE1 levels in blood, EFAT mass and overall body weight in mice fed HFD [292]. In T2D patients an association of circulating SERPINE1 levels and the onset of diabetes was suggested [296]. Thus, data might implicate a putative impact of the reduced *Serpine1* expression on PVAT functions and morphology as well as an association with the hyperinsulinemic state in *Rictor*^{aP2KO} mice.

Mcpt-4 mRNA expression was increased in PVAT of *Rictor*^{aP2KO} mice. The MCPT-4 chymase belongs to a family of serine proteases. Similar to other family members, MCPT-4 is primarily expressed in mast cells and released upon inflammatory response and host defense [297]. In addition, MCPT-4 was shown to play a key role in the generation of the vasoactive peptides ANGII and endothelin-1

[298, 299]. Deregulation of MCPT-4 signaling pathways was suggested to contribute to the pathogenesis of hypertension and atherosclerosis [297]. Taken together, the increase in *Mcpt-4* expression in PVAT of *Rictor*^{aP2KO} mice might contribute to the altered vascular reactivity and blood pressure elevations in these mice. In this context, the formation of the ANG II in PVAT and/or aortic tissue might be involved and needs further investigations.

Sesn2, found to be increased in *Rictor*^{aP2KO} mice, encodes a member of the sestrin family and is induced by the p53 tumor suppressor protein. SESN2 is known to activate AMP-activated protein kinase (AMPK) and suppresses mTORC1-S6K activity [300, 301]. SESN2 was proposed to function mainly in the regulation of cell growth and survival in response to DNA damage and oxidative stress [302]. Lee *et al.* demonstrated that hypernutrition up-regulates SESN2 expression to maintain metabolic homeostasis in liver of obese mice [303]. Conversely, deletion of *Sesn2* in liver impaired AMPK and mTORC1-S6K and promoted glucose intolerance and insulin resistance [303]. Furthermore, double knockout of *Sesn2* and *Sestrin 3* in liver impaired hepatic mTORC1-S6K activation and promoted insulin resistance even in the absence of a nutritional overload [303]. Thus, these studies indicate that SESN2 plays a key role in the liver to control the lipid and glucose metabolism. Whether this translates to the adipose tissue metabolism and the impact of the increased *Sesn2* expression on PVAT function in *Rictor*^{aP2KO} mice remains to be shown.

To the best of my knowledge, the information about *S100b*/S100B expression in adipose tissue or its association with the mTORC2 signaling network is limited. In *Rictor*^{aP2KO} mice, *S100b* mRNA expression levels were reduced in PVAT. S100B is a low molecular weight protein characterized by two calcium binding sites and exists as a homodimer [304, 305]. S100B is primarily expressed in the CNS [306] and is associated with neurodegenerative diseases [307]. Interestingly, in humans S100B levels were elevated upon inflammatory response in the CNS and duodenal mucosa of the intestine, which stimulated iNOS synthesis and NO production in these tissues [308, 309]. Only recently, circulating S100B levels were discovered to positively correlate with blood pressure levels and found to be elevated in pre- and hypertensive patients [310]. Furthermore, circulating S100B levels were identified to correlate with the BMI in humans and might reflect adipose tissue mass [311]. Taken together, reduced *S100b* expression in PVAT might contribute to the impaired vascular reactivity of *Rictor*^{aP2KO} mice. However, a possible association of S100B to the increased iNOS expression in PVAT in these mice should be critically evaluated. In contrast to the inflammatory response in the CNS, in the present study *S100b* expression was reduced in inflamed PVAT of *Rictor*^{aP2KO} mice. Furthermore, stimulation of astrocytes with TNF-α did not potentiate NO production in a S100B-dependent manner [308]. Thus, the effect of S100B might

be tissue-specific and/or depend on acute and chronic stimuli. In regard to the pre-hypertensive phenotype in *Rictor*^{aP2KO} mice, it would be of interest to measure circulating S100B concentration.

In summary, using the micro array technology we discovered that the *aP2*-promoter/ CRE recombinase-driven deletion of *Rictor* leads to (1) at least seven differentially expressed genes and (2) the identification of the circadian rhythm as the most regulated pathway in PVAT. Literature might suggest a putative role for these genes to the functional and morphological changes in PVAT of *Rictor*^{aP2KO} mice. Whether and to what extend these genes interact with each other is not yet known. In order to examine whether the differential expression of the seven genes translates on changes in the protein level, a Western blot analysis should be performed.

3.6 Fluctuating expression of *Rictor* and mTORC2 downstream targets in adipose tissue

In addition to the master clock located in the SCN, peripheral clocks in various tissues including liver, pancreas, heart and adipose tissue have been identified [85]. Peripheral clocks dominate tissue-specific metabolism with a similar molecular clock mechanism as in the SCN. While the SCN is mainly entrained to light cues, peripheral clocks can be entrained to SCN-derived signals, feeding and temperature cues [235]. Tight daytime-dependent regulations of gene expression were found in many tissues and are necessary for a coordinated tissue-specific metabolic output. Similar, the circadian clock regulates adipose tissue metabolism [312]. This affects triglyceride storage, free fatty acid release, adipokine and cytokine secretion [190] and further manifests in 24 hour fluctuating concentrations of circulating adipokines [120, 313]. Moreover, fasting and feeding periods are important environmental cues to achieve a balanced adipose tissue metabolism and that the availability of nutrients and other metabolites contributes significantly to the generation of cellular rhythmicity [225-227].

The integration of fasting/feeding periods might involve mTOR complexes as both complexes are responsive to nutrient- and growth factor-derived signals [194, 208]. In liver, mTORC1 activity is regulated by the circadian clock [314, 315] and time of feeding affects mTORC1 signaling activity [316, 317]. Although clear evidence whether the mTORC2 signaling activity is regulated in a circadian fashion is still lacking, Zhang *et al*. showed that in hepatocytes BMAL1 maintained the protein stability of RICTOR, but not *Rictor* mRNA expression [318].

In adipose tissue, data of the present study demonstrate that *Rictor/*RICTOR expression in PVAT, BAT and EFAT dependents on the time of the day. Fluctuating *Rictor*/RICTOR expression might further translate to the mTORC2 signaling activity. In EFAT and PVAT the phosphorylation of the mTORC2 signaling target AKT at serine 473 ($pAKT^{Ser473}$) was higher at the beginning of the resting (light) period of mice. Major gaps in the understanding include how fluctuating *Rictor/*RICTOR expression and mTORC2 activity are regulated in adipose tissue. The control of *Rictor*/RICTOR expression might involve BMAL1 similar to hepatocytes [318] or can be completely independent of the circadian clock. Further, Khapre *et al*. demonstrated that *mTor* gene expression is negatively regulated by BMAL1 impairing mTORC1 signaling activity in a daytime-dependent manner [314]. This might also apply to the mTORC2 kinase activity, as mTOR is common to both complexes. However, the non-mTORC2 target side $pAKT^{Thr308}$ showed a similar phosphorylation pattern as observed for $pAKT^{Ser473}$, at least in EFAT. Thus, to what extend a possible fluctuating mTORC2 kinase activity is responsible for the daytime-dependent phosphorylation of $pAKT^{Ser473}$ needs further investigation. To obtain detailed insight on how nutrient and growth factor

availability is integrated on the cellular level to influence adipose tissue metabolism and involves mTORC2 requires further investigation.

Interestingly, patterns of fluctuating mRNA expression levels of the nutrient sensors SIRT1 (Sirtuin1) and PGC-1α (Pparg co-activator 1α) were similar to *Rictor* and impaired in *Rictor*^{aP2KO} mice. As the expression and activity of SIRT1 is regulated by the circadian clock [319, 320] findings might provide a link between the mTORC2 signaling network and molecular components of the circadian clock in adipose tissue. How deletion of *Rictor* in adipocytes and the brain cause the reduction in *Sirt1* and *Pgc-1α* mRNA expression levels has yet to be shown. As SIRT1 directly links the metabolic state with transcriptional gene regulation, SIRT1 enzymatic activity and the transcriptional regulation of SIRT1 target genes should be analyzed to obtain new insights into SIRT1 function in adipose tissues of *Rictor*^{aP2KO} mice.

3.7 Limitation of the study

3.7.1 Targeted deletion of *Rictor* in adipocytes using CRE/*loxP* system

A powerful tool to design genetically modified mouse strains is the CRE site-specific DNA recombinase of the bacteriophage P1 [321]. The CRE recombinase recognizes a 34 bp DNA fragment (*loxP*; *locus of X-over of P1*) within the bacteriophage genome and mediates DNA recombination between two *loxP* sites [321]. This technique was adapted to manipulate the mouse genome to understand the function of specific genes in cell and tissue metabolism. However, global deletion of the gene of interest was often limited due to embryonic lethality and missing tissue-specificity. Therefore, knockout mouse models expressing the CRE recombinase under the control of tissue-specific gene promoters were generated. To knockout specific genes in adipocytes, the *aP2* gene promoter was widely used. However, over the last years *aP2* was recognized to be expressed in other tissues and cell types. Moreover, expression of the *Cre*/CRE recombinase in non-adipose tissues/cells was reported in several knockout mouse models using the *aP2*/CRE/*loxP* technology [322]. In the present study, we took advantage of the *aP2*/CRE/*loxP* technology to generate a mouse model lacking *Rictor* (*Rictor*^{aP2KO}) in adipocytes. In addition to adipocytes, the *Cre* recombinase was expressed in other tissues (e.g. the brain) and *Rictor* mRNA expression levels were reduced in the brain of these mice. These findings raise the question, how specific phenotypical changes observed in *Rictor*^{aP2KO} mice can be assigned to targeted gene deletion in adipocytes. As the brain is a central regulator of various physiological processes including blood pressure and adipose tissue metabolism, results obtained should be critically scrutinized.

To overcome the disadvantages of the *aP2*/CRE/*loxP* approach, there have been different efforts to ensure CRE recombinase expression to be more stringent adipocyte-specific. One possible alternative approach might be the *adiponectin* (*Adipoq*) gene promoter [323] as expression of the transgenic *Cre* is more restricted to mature adipocytes [323]. Taking advantage of the *myogenic factor 5* (*Myf5*) gene promoter would further allow to specifically knockout the gene of interest in brown adipocytes as *Myf5* is not expressed in white mature adipocytes [230]. As PVAT characteristics are similar to the phenotype observed in BAT, it would be of interest to characterize tissue-specific *Rictor*^{Myf5} knockout mice and how possible phenotypical changes of the *Rictor*^{Myf5} mice correspond to the *Rictor*^{aP2KO} mice phenotype.

3.7.2 *Cre*-recombinase expression in adipocytes of *Rictor*^{aP2KO} mice

In addition to the tissue-specificity of the *aP2* gene promoter, other limitations of conditional gene targeting involving CRE/*loxP* evolved and might explain underlying mechanisms for the

observed reduction of only 50 - 75 % in *Rictor* gene expression in the mice used in the present study.

(1) It has been reported that the integration side of the *Cre* recombinase transgene in the mouse genome strongly influences the expression of the *Cre* recombinase [324, 325]. This might result in mosaic expression pattern of the *Cre* recombinase within a given tissue and thus varying levels of CRE-mediated *loxP* recombination.

(2) Genetically modified mice are mostly generated through random integration of the *Cre* recombinase transgene into the mouse genome [321]. As a result, unspecified genetic interactions (e.g. transactivation, silencing effects) may occur at the DNA integration side possibly affecting the efficiency and specificity of the CRE recombinase within given tissues.

(3) The breeding strategy used to maintain the mouse colony has to be considered. In the current experimental approach, we mated control mice ($Rictor^{fl/fl}$) not expressing the *Cre* recombinase transgene ($Cre^{-/-}$) with *Rictor* knockout mice ($Rictor^{aP2KO}$) expressing one *Cre* allele ($Cre^{-/+}$). Compared with other breeding strategies involving $Cre^{+/+}$ genotypes, this might result in lower CRE recombinase expression decreasing recombination events. However, maintaining $Cre^{+/+}$ genotypes fails to produce control littermates and needs an additional colony of control mice.

(4) Maintenance of the mouse colony for several generations might cause changes in the *Cre*/CRE recombinase expression and/or efficacy. As a result of chromatin inactivation or multiple recombination events expression of the *Cre* recombinase might by reduced or completely abolished.

However, a 50 - 75 % reduction of *Rictor* gene expression is in a range as observed for other transgenic mouse strains using the CRE/*loxP* system [326]. For example, *CD19-Cre* mice display recombination of 55 - 95 % [327]. Nevertheless, based on the expression data obtained from different tissues, even a 50 - 75 % reduction in *Rictor* mRNA expression strongly affected the phenotype in $Rictor^{aP2KO}$ mice.

3.7.3 Locomotor activity recordings in $Rictor^{aP2KO}$ mice

Telemetric measurements revealed elevated locomotor activity in $Rictor^{aP2KO}$ mice. However, specific behavioral parameters as putative causal factors for the elevated locomotor activity couldn't be analyzed using the telemetric system and require further experiments. One behavioral parameter might be food intake as contributing significantly to fluctuating patterns of locomotor activity over a 24 hour light/dark cycle [328]. Thus, observed elevations in locomotor activity and

the reduced decline during the 12 hour dark period might reflect changes in food intake, which was not investigated in the study presented here. Additional experiments investigating e.g. food intake over a 24 hour light/dark cycle, might ascertain the reason of the increase in locomotor activity in *Rictor*^{aP2KO} mice in more detail.

3.8 Future directions

One of the most interesting follow-up questions of the present study is which proportion of the phenotypical changes observed in *Rictor*^{aP2KO} mice can be attributed to *Rictor* deletion in (1) adipose tissues and/or (2) in the brain. Taking advantage of gene promoters allowing a more restricted expression of the CRE recombinase to adipose tissue (e.g. *Myf5* and *Adipoq*) or brain (e.g. *Nexin*) and to understand the contribution of RICTOR/mTORC2 in these tissues in regard to changes in vascular reactivity and blood pressure regulation in *Rictor*^{aP2KO} mice.

The mRNA expression of NPs and NP receptors was altered in the heart and adipose tissue of *Rictor*^{aP2KO} mice. The involvement of NPs in blood pressure regulation is well established. Moreover, evidence of an NPs association with lifestyle-related metabolic disorders (e.g. T2D and obesity) has been accumulated. Thus, the investigation of the following issues could contribute to a better understanding of how the deletion of *Rictor* add to the changes in the NP system and its signaling pathways, and the dysregulation of the NPs system to blood pressure elevations in *Rictor*^{aP2KO} mice:

(1) How does deletion of *Rictor* in adipocytes and/or the brain contribute to the reduced NP and NP receptor expression in the heart of *Rictor*^{aP2KO} mice? Are there other putative factors than the slight increase in blood pressure?
(2) Does the reduced *Anp* expression in the heart translate to the protein level and possible cause a reduction of ANP plasma levels in *Rictor*^{aP2KO} mice?
(3) ANP increases physiological renal sodium secretion and counteracts the RAA system to cause vasodilation. Although there are no morphological indications of renal dysfunction (e.g. fibrosis) in *Rictor*^{aP2KO} mice, it would be of interest to analyze whether the reduced cardiac *Anp* expression causes pathophysiological changes in the RAA system.
(4) What putative changes cause the reduction of the *Anp* and *Nprc* expression in EFAT adipocytes and PVAT? The deletion of *Rictor*, the hyperinsulinemic state and/or other yet to be identified factors?

Beside its impact on clock genes, the expression of other genes is altered by the deletion of *Rictor* in PVAT. mRNA expression of *Irf4*, *Npas2*, *Mcpt-4*, *Sesn2*, *Spry4, Serpine1* and *S100b* were significantly changed in PVAT of *Rictor*^{aP2KO} mice. It warrants further investigation to clarify a putative role of these genes in the pathophysiological changes of PVAT properties and vascular reactivity in these mice, and overall in the mTORC2 signaling network.

It would be of interest to elucidate whether *Rictor* mRNA expression in adipose tissue is modulated by molecular components of the circadian clock or follows a diurnal expression pattern. To this end, in a first step 24 hour mRNA expression patterns of *Rictor* in adipose tissues have to be analyzed in *Rictor*^{aP2KO} mice kept under constant conditions (e.g. complete darkness). Persistence of the fluctuating 24 hour mRNA expression patterns would allow assigning *Rictor* gene expression in adipose tissue as circadian. In a second step, studies to delineate mechanistically the impact of the molecular components of the circadian clock on *Rictor* expression are needed.

3.9 Conclusion

In the present dissertation, RICTOR/mTORC2 in the brain and adipose tissue was identified as a novel regulator of fluctuating physiological processes such as blood pressure and locomotor activity. This might involve the hormones natriuretic peptide and insulin, while the SCN does not seem to contribute to the pathophysiological changes of these processes in *Rictor*^{aP2KO} mice. A genome wide expression analysis in PVAT identified the clock genes, forming the molecular basis of the peripheral circadian clock, to be changed in *Rictor*^{aP2KO} mice. Changed clock gene expression might contribute to the inflamed PVAT as well as altered vascular reactivity of these mice. In addition, evidence was provided for a fluctuating mTORC2 activity in PVAT and EFAT, and a possible association with the peripheral clock and nutrient sensors in PVAT. Future studies to elucidate these complex interactions in the adipocyte-brain axis are necessary. This may contribute to a better understanding of how fluctuating physiological processes are regulated by these tissues. Our findings might lead to the identification of novel drug targets and the development of effective treatments against hypertension and dysfunctional adipose tissue metabolism.

4. Bibliography

1. Boron, W.F.B., E.L. , *Medical Physiology.* Saunders W.B, 2012. **2nd updated edition**.
2. Pugsley, M.K. and R. Tabrizchi, *The vascular system. An overview of structure and function.* J Pharmacol Toxicol Methods, 2000. **44**(2): p. 333-40.
3. Schmidt, R.F.L., F.; Heckmann, M., *Physiologie des Menschen (mit Pathophysiologie).* Springer Verlag, 2011. **31th edition**.
4. Borysenko, M., Beringer, T. , *Functional histology. . Little, Brown and Company*,, 1984. **2nd Edition**: p. 1-400.
5. Greenwald, S.E., *Ageing of the conduit arteries.* J Pathol, 2007. **211**(2): p. 157-72.
6. Majesky, M.W., et al., *The adventitia: a dynamic interface containing resident progenitor cells.* Arterioscler Thromb Vasc Biol, 2011. **31**(7): p. 1530-9.
7. Fitzgibbons, T.P., et al., *Similarity of mouse perivascular and brown adipose tissues and their resistance to diet-induced inflammation.* Am J Physiol Heart Circ Physiol, 2011. **301**(4): p. H1425-37.
8. Soltis, E.E. and L.A. Cassis, *Influence of perivascular adipose tissue on rat aortic smooth muscle responsiveness.* Clin Exp Hypertens A, 1991. **13**(2): p. 277-96.
9. Szasz, T., G.F. Bomfim, and R.C. Webb, *The influence of perivascular adipose tissue on vascular homeostasis.* Vasc Health Risk Manag, 2013. **9**: p. 105-16.
10. Cines, D.B., et al., *Endothelial cells in physiology and in the pathophysiology of vascular disorders.* Blood, 1998. **91**(10): p. 3527-61.
11. Risau, W. and I. Flamme, *Vasculogenesis.* Annu Rev Cell Dev Biol, 1995. **11**: p. 73-91.
12. Vallance, P., *Endothelial regulation of vascular tone.* Postgrad Med J, 1992. **68**(803): p. 697-701.
13. Vanhoutte, P.M., et al., *Endothelial dysfunction and vascular disease.* Acta Physiol (Oxf), 2009. **196**(2): p. 193-222.
14. Owens, G.K., M.S. Kumar, and B.R. Wamhoff, *Molecular regulation of vascular smooth muscle cell differentiation in development and disease.* Physiol Rev, 2004. **84**(3): p. 767-801.
15. Furchgott, R.F. and J.V. Zawadzki, *The obligatory role of endothelial cells in the relaxation of arterial smooth muscle by acetylcholine.* Nature, 1980. **288**(5789): p. 373-6.
16. Ignarro, L.J., et al., *Endothelium-derived relaxing factor produced and released from artery and vein is nitric oxide.* Proc Natl Acad Sci U S A, 1987. **84**(24): p. 9265-9.
17. Steinberg, H.O., et al., *Insulin-mediated skeletal muscle vasodilation is nitric oxide dependent. A novel action of insulin to increase nitric oxide release.* J Clin Invest, 1994. **94**(3): p. 1172-9.
18. Taddei, S., et al., *Effect of insulin on acetylcholine-induced vasodilation in normotensive subjects and patients with essential hypertension.* Circulation, 1995. **92**(10): p. 2911-8.
19. Chen, H., et al., *Adiponectin stimulates production of nitric oxide in vascular endothelial cells.* J Biol Chem, 2003. **278**(45): p. 45021-6.
20. Hattori, Y., et al., *Globular adiponectin upregulates nitric oxide production in vascular endothelial cells.* Diabetologia, 2003. **46**(11): p. 1543-9.
21. Spooner, P.H., et al., *Thyroid hormone analog, DITPA, improves endothelial nitric oxide and beta-adrenergic mediated vasorelaxation after myocardial infarction.* J Cardiovasc Pharmacol, 2004. **44**(4): p. 453-9.
22. Dias, R.G., C.E. Negrao, and M.H. Krieger, *Nitric oxide and the cardiovascular system: cell activation, vascular reactivity and genetic variant.* Arq Bras Cardiol, 2011. **96**(1): p. 68-75.
23. Ganz, P., *Endothelial regulation of vascular tone: From basic biology to clinical application.* Cardiology Rounds, Brigham and Womans Hospital, Boston, 2001.

24. Feletou, M. and P.M. Vanhoutte, *Endothelial dysfunction: a multifaceted disorder (The Wiggers Award Lecture).* Am J Physiol Heart Circ Physiol, 2006. **291**(3): p. H985-1002.

25. Li, H. and U. Forstermann, *Nitric oxide in the pathogenesis of vascular disease.* J Pathol, 2000. **190**(3): p. 244-54.

26. Furchgott, R.F. and P.M. Vanhoutte, *Endothelium-derived relaxing and contracting factors.* FASEB J, 1989. **3**(9): p. 2007-18.

27. Vanhoutte, P.M., M. Feletou, and S. Taddei, *Endothelium-dependent contractions in hypertension.* Br J Pharmacol, 2005. **144**(4): p. 449-58.

28. Vanhoutte, P.M., *Endothelium-dependent contractions.* Dialogues in Cardiovascular Medicine, 2002. **7**.

29. Manrique, C., G. Lastra, and J.R. Sowers, *New insights into insulin action and resistance in the vasculature.* Ann N Y Acad Sci, 2014. **1311**: p. 138-50.

30. Boydens, C., et al., *Adipose tissue as regulator of vascular tone.* Curr Hypertens Rep, 2012. **14**(3): p. 270-8.

31. Maenhaut, N. and J. Van de Voorde, *Regulation of vascular tone by adipocytes.* BMC Med, 2011. **9**: p. 25.

32. Zois, N.E., et al., *Natriuretic peptides in cardiometabolic regulation and disease.* Nat Rev Cardiol, 2014. **11**(7): p. 403-12.

33. Guyenet, P.G., *The sympathetic control of blood pressure.* Nat Rev Neurosci, 2006. **7**(5): p. 335-46.

34. *A global brief on hypertension.* World Health Organization, 2013: p. 1-40.

35. Dustan, H.P., *Etiology and pathogenesis of hypertension.* Calif Med, 1970. **112**(4): p. 86-7.

36. Go, A.S., et al., *Heart disease and stroke statistics--2014 update: a report from the American Heart Association.* Circulation, 2014. **129**(3): p. e28-e292.

37. Mancia, G.G., G.; Redon,J., *Manual of Hypertension of the European Society of Hypertension.* CRC Press, 2014. **Second Edition**.

38. Carretero, O.A. and S. Oparil, *Essential hypertension. Part I: definition and etiology.* Circulation, 2000. **101**(3): p. 329-35.

39. Calhoun, D.A., et al., *Resistant hypertension: diagnosis, evaluation, and treatment: a scientific statement from the American Heart Association Professional Education Committee of the Council for High Blood Pressure Research.* Circulation, 2008. **117**(25): p. e510-26.

40. Oparil, S., M.A. Zaman, and D.A. Calhoun, *Pathogenesis of hypertension.* Ann Intern Med, 2003. **139**(9): p. 761-76.

41. Gudmundsdottir, H., et al., *Hypertension in women: latest findings and clinical implications.* Ther Adv Chronic Dis, 2012. **3**(3): p. 137-46.

42. Garrison, R.J., et al., *Incidence and precursors of hypertension in young adults: the Framingham Offspring Study.* Prev Med, 1987. **16**(2): p. 235-51.

43. Perry, I.J., P.H. Whincup, and A.G. Shaper, *Environmental factors in the development of essential hypertension.* Br Med Bull, 1994. **50**(2): p. 246-59.

44. Ferrier, C., H. Cox, and M. Esler, *Elevated total body noradrenaline spillover in normotensive members of hypertensive families.* Clin Sci (Lond), 1993. **84**(2): p. 225-30.

45. Noll, G., et al., *Increased activation of sympathetic nervous system and endothelin by mental stress in normotensive offspring of hypertensive parents.* Circulation, 1996. **93**(5): p. 866-9.

46. Esler, M., *Sympathetic nervous system: contribution to human hypertension and related cardiovascular diseases.* J Cardiovasc Pharmacol, 1995. **26 Suppl 2**: p. S24-8.

47. Muniyappa, R., et al., *Cardiovascular actions of insulin.* Endocr Rev, 2007. **28**(5): p. 463-91.

48. Intengan, H.D. and E.L. Schiffrin, *Structure and mechanical properties of resistance arteries in hypertension: role of adhesion molecules and extracellular matrix determinants.* Hypertension, 2000. **36**(3): p. 312-8.

49. Aalkjaer, C., et al., *Evidence for increased media thickness, increased neuronal amine uptake, and depressed excitation--contraction coupling in isolated resistance vessels from essential hypertensives.* Circ Res, 1987. **61**(2): p. 181-6.

50. Renna, N.F., N. de Las Heras, and R.M. Miatello, *Pathophysiology of vascular remodeling in hypertension.* Int J Hypertens, 2013. **2013**: p. 808353.

51. Kramer, A.M., M., *Circadian clocks.* Springer Verlag, 2013: p. 3-28.

52. Kramer, A.M., M., *Circadian clocks.* Springer Verlag, 2013: p. 45-66.

53. Moore, R.Y. and V.B. Eichler, *Loss of a circadian adrenal corticosterone rhythm following suprachiasmatic lesions in the rat.* Brain Res, 1972. **42**(1): p. 201-6.

54. Stephan, F.K. and I. Zucker, *Circadian rhythms in drinking behavior and locomotor activity of rats are eliminated by hypothalamic lesions.* Proc Natl Acad Sci U S A, 1972. **69**(6): p. 1583-6.

55. Kramer, A.M., M., *Circadian clocks.* Springer Verlag, 2013: p. 67-103.

56. Maywood, E.S., et al., *A diversity of paracrine signals sustains molecular circadian cycling in suprachiasmatic nucleus circuits.* Proc Natl Acad Sci U S A. **108**(34): p. 14306-11.

57. Albus, H., et al., *A GABAergic mechanism is necessary for coupling dissociable ventral and dorsal regional oscillators within the circadian clock.* Curr Biol, 2005. **15**(10): p. 886-93.

58. Long, M.A., et al., *Electrical synapses coordinate activity in the suprachiasmatic nucleus.* Nat Neurosci, 2005. **8**(1): p. 61-6.

59. Aton, S.J., et al., *Vasoactive intestinal polypeptide mediates circadian rhythmicity and synchrony in mammalian clock neurons.* Nat Neurosci, 2005. **8**(4): p. 476-83.

60. Georg, B., J. Hannibal, and J. Fahrenkrug, *Lack of the PAC1 receptor alters the circadian expression of VIP mRNA in the suprachiasmatic nucleus of mice.* Brain Res, 2007. **1135**(1): p. 52-7.

61. Welsh, D.K., et al., *Individual neurons dissociated from rat suprachiasmatic nucleus express independently phased circadian firing rhythms.* Neuron, 1995. **14**(4): p. 697-706.

62. Nagoshi, E., et al., *Circadian gene expression in individual fibroblasts: cell-autonomous and self-sustained oscillators pass time to daughter cells.* Cell, 2004. **119**(5): p. 693-705.

63. Brown, S.A., et al., *Rhythms of mammalian body temperature can sustain peripheral circadian clocks.* Curr Biol, 2002. **12**(18): p. 1574-83.

64. Damiola, F., et al., *Restricted feeding uncouples circadian oscillators in peripheral tissues from the central pacemaker in the suprachiasmatic nucleus.* Genes Dev, 2000. **14**(23): p. 2950-61.

65. Stokkan, K.A., et al., *Entrainment of the circadian clock in the liver by feeding.* Science, 2001. **291**(5503): p. 490-3.

66. Shimba, S., et al., *Brain and muscle Arnt-like protein-1 (BMAL1), a component of the molecular clock, regulates adipogenesis.* Proc Natl Acad Sci U S A, 2005. **102**(34): p. 12071-6.

67. Paschos, G.K., et al., *Obesity in mice with adipocyte-specific deletion of clock component Arntl.* Nat Med, 2012. **18**(12): p. 1768-77.

68. Maury, E., K.M. Ramsey, and J. Bass, *Circadian rhythms and metabolic syndrome: from experimental genetics to human disease.* Circ Res, 2010. **106**(3): p. 447-62.

69. Lee, J., et al., *Bmal1 and beta-cell clock are required for adaptation to circadian disruption, and their loss of function leads to oxidative stress-induced beta-cell failure in mice.* Mol Cell Biol, 2013. **33**(11): p. 2327-38.

70. Takeda, N. and K. Maemura, *Circadian clock and cardiovascular disease.* J Cardiol, 2011. **57**(3): p. 249-56.

71. Rudic, R.D. and D.J. Fulton, *Pressed for time: the circadian clock and hypertension.* J Appl Physiol (1985), 2009. **107**(4): p. 1328-38.

72. Ko, C.H. and J.S. Takahashi, *Molecular components of the mammalian circadian clock.* Hum Mol Genet, 2006. **15 Spec No 2**: p. R271-7.

73. Lowrey, P.L., et al., *Positional syntenic cloning and functional characterization of the mammalian circadian mutation tau.* Science, 2000. **288**(5465): p. 483-92.

74. Akashi, M., et al., *Control of intracellular dynamics of mammalian period proteins by casein kinase I epsilon (CKIepsilon) and CKIdelta in cultured cells.* Mol Cell Biol, 2002. **22**(6): p. 1693-703.

75. Bellet, M.M. and P. Sassone-Corsi, *Mammalian circadian clock and metabolism - the epigenetic link.* J Cell Sci. **123**(Pt 22): p. 3837-48.

76. Guillaumond, F., et al., *Differential control of Bmal1 circadian transcription by REV-ERB and ROR nuclear receptors.* J Biol Rhythms, 2005. **20**(5): p. 391-403.

77. Preitner, N., et al., *The orphan nuclear receptor REV-ERBalpha controls circadian transcription within the positive limb of the mammalian circadian oscillator.* Cell, 2002. **110**(2): p. 251-60.

78. Triqueneaux, G., et al., *The orphan receptor Rev-erbalpha gene is a target of the circadian clock pacemaker.* J Mol Endocrinol, 2004. **33**(3): p. 585-608.

79. Kramer, A.M., M., *Circadian clocks.* Springer Verlag, 2013: p. 127-156.

80. Eckel-Mahan, K. and P. Sassone-Corsi, *Metabolism and the circadian clock converge.* Physiol Rev, 2013. **93**(1): p. 107-35.

81. Akhtar, R.A., et al., *Circadian cycling of the mouse liver transcriptome, as revealed by cDNA microarray, is driven by the suprachiasmatic nucleus.* Curr Biol, 2002. **12**(7): p. 540-50.

82. Rudic, R.D., et al., *Bioinformatic analysis of circadian gene oscillation in mouse aorta.* Circulation, 2005. **112**(17): p. 2716-24.

83. Storch, K.F., et al., *Extensive and divergent circadian gene expression in liver and heart.* Nature, 2002. **417**(6884): p. 78-83.

84. Zvonic, S., et al., *Characterization of peripheral circadian clocks in adipose tissues.* Diabetes, 2006. **55**(4): p. 962-70.

85. Huang, W., et al., *Circadian rhythms, sleep, and metabolism.* J Clin Invest, 2011. **121**(6): p. 2133-41.

86. Yoo, S.H., et al., *PERIOD2::LUCIFERASE real-time reporting of circadian dynamics reveals persistent circadian oscillations in mouse peripheral tissues.* Proc Natl Acad Sci U S A, 2004. **101**(15): p. 5339-46.

87. Karlsson, B., A. Knutsson, and B. Lindahl, *Is there an association between shift work and having a metabolic syndrome? Results from a population based study of 27,485 people.* Occup Environ Med, 2001. **58**(11): p. 747-52.

88. Ellingsen, T., A. Bener, and A.A. Gehani, *Study of shift work and risk of coronary events.* J R Soc Promot Health, 2007. **127**(6): p. 265-7.

89. Shaw, D.B., M.S. Knapp, and D.H. Davies, *Variations of bloodpressure in hypertensives during sleep.* Lancet, 1963. **1**(7285): p. 797-9.

90. Palatini, P., et al., *Clinical relevance of nighttime blood pressure and of daytime blood pressure variability.* Arch Intern Med, 1992. **152**(9): p. 1855-60.

91. Li, P., et al., *Circadian blood pressure and heart rate rhythms in mice.* Am J Physiol, 1999. **276**(2 Pt 2): p. R500-4.

92. Millar-Craig, M.W., C.N. Bishop, and E.B. Raftery, *Circadian variation of blood-pressure.* Lancet, 1978. **1**(8068): p. 795-797.

93. Witte, K., et al., *Effects of SCN lesions on circadian blood pressure rhythm in normotensive and transgenic hypertensive rats.* Chronobiol Int, 1998. **15**(2): p. 135-45.

94. Janssen, B.J., et al., *Suprachiasmatic lesions eliminate 24-h blood pressure variability in rats.* Physiol Behav, 1994. **55**(2): p. 307-11.

95. Saper, C.B., et al., *The hypothalamic integrator for circadian rhythms.* Trends Neurosci, 2005. **28**(3): p. 152-7.

96. Fontes, M.A., et al., *Descending pathways mediating cardiovascular response from dorsomedial hypothalamic nucleus.* Am J Physiol Heart Circ Physiol, 2001. **280**(6): p. H2891-901.

97. Karlsson, B.H., et al., *Metabolic disturbances in male workers with rotating three-shift work. Results of the WOLF study.* Int Arch Occup Environ Health, 2003. **76**(6): p. 424-30.

98. Knutsson, A., *Health disorders of shift workers.* Occup Med (Lond), 2003. **53**(2): p. 103-8.

99. Dominguez-Rodriguez, A., et al., *Melatonin and circadian biology in human cardiovascular disease.* J Pineal Res. **49**(1): p. 14-22.

100. Willich, S.N., et al., *Increased onset of sudden cardiac death in the first three hours after awakening.* Am J Cardiol, 1992. **70**(1): p. 65-8.

101. Muller, J.E., *Circadian variation in cardiovascular events.* Am J Hypertens, 1999. **12**(2 Pt 2): p. 35S-42S.

102. Viswambharan, H., et al., *Mutation of the circadian clock gene Per2 alters vascular endothelial function.* Circulation, 2007. **115**(16): p. 2188-95.

103. Doi, M., et al., *Salt-sensitive hypertension in circadian clock-deficient Cry-null mice involves dysregulated adrenal Hsd3b6.* Nat Med. **16**(1): p. 67-74.

104. Wang, N., et al., *Vascular PPARgamma controls circadian variation in blood pressure and heart rate through Bmal1.* Cell Metab, 2008. **8**(6): p. 482-91.

105. Czupryniak, L., et al., *Circadian blood pressure variation and antihypertensive medication adjustment in normoalbuminuric type 2 diabetes patients.* Kidney Blood Press Res, 2007. **30**(3): p. 182-6.

106. Su, W., et al., *Hypertension and disrupted blood pressure circadian rhythm in type 2 diabetic db/db mice.* Am J Physiol Heart Circ Physiol, 2008. **295**(4): p. H1634-41.

107. Bagi, Z., et al., *Type 2 diabetic mice have increased arteriolar tone and blood pressure: enhanced release of COX-2-derived constrictor prostaglandins.* Arterioscler Thromb Vasc Biol, 2005. **25**(8): p. 1610-6.

108. Didion, S.P., et al., *Impaired endothelium-dependent responses and enhanced influence of Rho-kinase in cerebral arterioles in type II diabetes.* Stroke, 2005. **36**(2): p. 342-7.

109. Kamata, K. and S. Kojima, *Characteristics of contractile responses of aorta to norepinephrine in db/db mice.* Res Commun Mol Pathol Pharmacol, 1997. **96**(3): p. 319-28.

110. Arble, D.M., et al., *Circadian timing of food intake contributes to weight gain.* Obesity (Silver Spring), 2009. **17**(11): p. 2100-2.

111. Bray, M.S., et al., *Time-of-day-dependent dietary fat consumption influences multiple cardiometabolic syndrome parameters in mice.* Int J Obes (Lond). **34**(11): p. 1589-98.

112. Gu, P. and A. Xu, *Interplay between adipose tissue and blood vessels in obesity and vascular dysfunction.* Rev Endocr Metab Disord, 2013.

113. Symonds, M.E., *Adipose tissue biology.* Springer Verlag, 2012.

114. Galic, S., J.S. Oakhill, and G.R. Steinberg, *Adipose tissue as an endocrine organ.* Mol Cell Endocrinol, 2010. **316**(2): p. 129-39.

115. Harwood, H.J., Jr., *The adipocyte as an endocrine organ in the regulation of metabolic homeostasis.* Neuropharmacology, 2012. **63**(1): p. 57-75.

116. Sethi, J.K. and A.J. Vidal-Puig, *Thematic review series: adipocyte biology. Adipose tissue function and plasticity orchestrate nutritional adaptation.* J Lipid Res, 2007. **48**(6): p. 1253-62.

117. Schulz, T.J. and Y.H. Tseng, *Brown adipose tissue: development, metabolism and beyond.* Biochem J, 2013. **453**(2): p. 167-78.

118. Fliers, E., et al., *White adipose tissue: getting nervous.* J Neuroendocrinol, 2003. **15**(11): p. 1005-10.

119. Bartness, T.J. and M. Bamshad, *Innervation of mammalian white adipose tissue: implications for the regulation of total body fat.* Am J Physiol, 1998. **275**(5 Pt 2): p. R1399-411.

120. Kalsbeek, A., et al., *The suprachiasmatic nucleus generates the diurnal changes in plasma leptin levels.* Endocrinology, 2001. **142**(6): p. 2677-85.

121. Kreier, F., et al., *Selective parasympathetic innervation of subcutaneous and intra-abdominal fat--functional implications.* J Clin Invest, 2002. **110**(9): p. 1243-50.

122. Smorlesi, A., et al., *The adipose organ: white-brown adipocyte plasticity and metabolic inflammation.* Obes Rev, 2012. **13 Suppl 2**: p. 83-96.

123. Cinti, S., *The adipose organ.* Prostaglandins Leukot Essent Fatty Acids, 2005. **73**(1): p. 9-15.

124. Cristancho, A.G. and M.A. Lazar, *Forming functional fat: a growing understanding of adipocyte differentiation.* Nat Rev Mol Cell Biol, 2011. **12**(11): p. 722-34.

125. Cinti, S., *Between brown and white: novel aspects of adipocyte differentiation.* Ann Med, 2011. **43**(2): p. 104-15.

126. Symonds, M.E., *Adipose tissue biology.* Springer Verlag, 2012: p. 71-121.

127. Frontini, A. and S. Cinti, *Distribution and development of brown adipocytes in the murine and human adipose organ.* Cell Metab. **11**(4): p. 253-6.

128. Symonds, M.E., *Adipose tissue biology.* Springer Verlag, 2012: p. 39-70.

129. Nedergaard, J., T. Bengtsson, and B. Cannon, *Unexpected evidence for active brown adipose tissue in adult humans.* Am J Physiol Endocrinol Metab, 2007. **293**(2): p. E444-52.

130. van Marken Lichtenbelt, W.D., et al., *Cold-activated brown adipose tissue in healthy men.* N Engl J Med, 2009. **360**(15): p. 1500-8.

131. Virtanen, K.A., et al., *Functional brown adipose tissue in healthy adults.* N Engl J Med, 2009. **360**(15): p. 1518-25.

132. Bjorndal, B., et al., *Different adipose depots: their role in the development of metabolic syndrome and mitochondrial response to hypolipidemic agents.* J Obes, 2011. **2011**: p. 490650.

133. Ouchi, N., et al., *Adipokines in inflammation and metabolic disease.* Nat Rev Immunol, 2011. **11**(2): p. 85-97.

134. Oriowo, M.A., *Perivascular Adipose Tissue, Vascular Reactivity and Hypertension.* Med Princ Pract, 2014.

135. Rajsheker, S., et al., *Crosstalk between perivascular adipose tissue and blood vessels.* Curr Opin Pharmacol, 2010. **10**(2): p. 191-6.

136. Police, S.B., et al., *Obesity promotes inflammation in periaortic adipose tissue and angiotensin II-induced abdominal aortic aneurysm formation.* Arterioscler Thromb Vasc Biol, 2009. **29**(10): p. 1458-64.

137. Galvez-Prieto, B., et al., *Comparative expression analysis of the renin-angiotensin system components between white and brown perivascular adipose tissue.* J Endocrinol, 2008. **197**(1): p. 55-64.

138. Chatterjee, T.K., et al., *Proinflammatory phenotype of perivascular adipocytes: influence of high-fat feeding.* Circ Res, 2009. **104**(4): p. 541-9.

139. Withers, S.B., et al., *Macrophage activation is responsible for loss of anticontractile function in inflamed perivascular fat.* Arterioscler Thromb Vasc Biol, 2011. **31**(4): p. 908-13.

140. Tilg, H. and A.R. Moschen, *Adipocytokines: mediators linking adipose tissue, inflammation and immunity.* Nat Rev Immunol, 2006. **6**(10): p. 772-83.

141. Weisberg, S.P., et al., *Obesity is associated with macrophage accumulation in adipose tissue.* J Clin Invest, 2003. **112**(12): p. 1796-808.

142. Guzik, T.J., et al., *Perivascular adipose tissue as a messenger of the brain-vessel axis: role in vascular inflammation and dysfunction.* J Physiol Pharmacol, 2007. **58**(4): p. 591-610.

143. Gollasch, M. and G. Dubrovska, *Paracrine role for periadventitial adipose tissue in the regulation of arterial tone.* Trends Pharmacol Sci, 2004. **25**(12): p. 647-53.

144. Lohn, M., et al., *Periadventitial fat releases a vascular relaxing factor.* FASEB J, 2002. **16**(9): p. 1057-63.

145. Fesus, G., et al., *Adiponectin is a novel humoral vasodilator.* Cardiovasc Res, 2007. **75**(4): p. 719-27.

146. Yamawaki, H., et al., *Visfatin causes endothelium-dependent relaxation in isolated blood vessels.* Biochem Biophys Res Commun, 2009. **383**(4): p. 503-8.

147. Lee, Y.C., et al., *Role of perivascular adipose tissue-derived methyl palmitate in vascular tone regulation and pathogenesis of hypertension.* Circulation, 2011. **124**(10): p. 1160-71.

148. Payne, G.A., et al., *Epicardial perivascular adipose-derived leptin exacerbates coronary endothelial dysfunction in metabolic syndrome via a protein kinase C-beta pathway.* Arterioscler Thromb Vasc Biol, 2010. **30**(9): p. 1711-7.

149. Thengchaisri, N. and L. Kuo, *Hydrogen peroxide induces endothelium-dependent and -independent coronary arteriolar dilation: role of cyclooxygenase and potassium channels.* Am J Physiol Heart Circ Physiol, 2003. **285**(6): p. H2255-63.

150. Lembo, G., et al., *Leptin induces direct vasodilation through distinct endothelial mechanisms.* Diabetes, 2000. **49**(2): p. 293-7.

151. Kimura, K., et al., *Involvement of nitric oxide in endothelium-dependent arterial relaxation by leptin.* Biochem Biophys Res Commun, 2000. **273**(2): p. 745-9.

152. Gil-Longo, J. and C. Gonzalez-Vazquez, *Characterization of four different effects elicited by H2O2 in rat aorta.* Vascul Pharmacol, 2005. **43**(2): p. 128-38.

153. Verlohren, S., et al., *Visceral periadventitial adipose tissue regulates arterial tone of mesenteric arteries.* Hypertension, 2004. **44**(3): p. 271-6.

154. Dubrovska, G., et al., *Mechanisms of ADRF release from rat aortic adventitial adipose tissue.* Am J Physiol Heart Circ Physiol, 2004. **286**(3): p. H1107-13.

155. Gao, Y.J., et al., *Modulation of vascular function by perivascular adipose tissue: the role of endothelium and hydrogen peroxide.* Br J Pharmacol, 2007. **151**(3): p. 323-31.

156. Galvez-Prieto, B., et al., *Anticontractile Effect of Perivascular Adipose Tissue and Leptin are Reduced in Hypertension.* Front Pharmacol, 2012. **3**: p. 103.

157. Ardanaz, N., W.H. Beierwaltes, and P.J. Pagano, *Distinct hydrogen peroxide-induced constriction in multiple mouse arteries: potential influence of vascular polarization.* Pharmacol Rep, 2008. **60**(1): p. 61-7.

158. Bulloch, J.M. and C.J. Daly, *Autonomic nerves and perivascular fat: interactive mechanisms.* Pharmacol Ther, 2014. **143**(1): p. 61-73.

159. Szasz, T. and R.C. Webb, *Perivascular adipose tissue: more than just structural support.* Clin Sci (Lond), 2012. **122**(1): p. 1-12.

160. Eringa, E.C., W. Bakker, and V.W. van Hinsbergh, *Paracrine regulation of vascular tone, inflammation and insulin sensitivity by perivascular adipose tissue.* Vascul Pharmacol, 2012. **56**(5-6): p. 204-9.

161. Ardanaz, N. and P.J. Pagano, *Hydrogen peroxide as a paracrine vascular mediator: regulation and signaling leading to dysfunction.* Exp Biol Med (Maywood), 2006. **231**(3): p. 237-51.

162. Cai, H., et al., *NAD(P)H oxidase-derived hydrogen peroxide mediates endothelial nitric oxide production in response to angiotensin II.* J Biol Chem, 2002. **277**(50): p. 48311-7.

163. Galvez-Prieto, B., et al., *A reduction in the amount and anti-contractile effect of periadventitial mesenteric adipose tissue precedes hypertension development in spontaneously hypertensive rats.* Hypertens Res, 2008. **31**(7): p. 1415-23.

164. Lee, R.M., et al., *Alteration of perivascular adipose tissue function in angiotensin II-induced hypertension.* Can J Physiol Pharmacol, 2009. **87**(11): p. 944-53.

165. Ruan, C.C., et al., *Perivascular adipose tissue-derived complement 3 is required for adventitial fibroblast functions and adventitial remodeling in deoxycorticosterone acetate-salt hypertensive rats.* Arterioscler Thromb Vasc Biol, 2010. **30**(12): p. 2568-74.

166. Li, R., et al., *Reduced anti-contractile effect of perivascular adipose tissue on mesenteric small arteries from spontaneously hypertensive rats: role of Kv7 channels.* Eur J Pharmacol, 2013. **698**(1-3): p. 310-5.

167. Bautista, L.E., et al., *Independent association between inflammatory markers (C-reactive protein, interleukin-6, and TNF-alpha) and essential hypertension.* J Hum Hypertens, 2005. **19**(2): p. 149-54.

168. Ferreri, N.R., et al., *Tumor necrosis factor-alpha-angiotensin interactions and regulation of blood pressure.* J Hypertens, 1997. **15**(12 Pt 1): p. 1481-4.

169. Giardina, J.B., et al., *TNF-alpha enhances contraction and inhibits endothelial NO-cGMP relaxation in systemic vessels of pregnant rats.* Am J Physiol Regul Integr Comp Physiol, 2002. **283**(1): p. R130-43.

170. Greenberg, S., et al., *Tumor necrosis factor-alpha inhibits endothelium-dependent relaxation.* J Appl Physiol (1985), 1993. **74**(5): p. 2394-403.

171. Arenas, I.A., et al., *Chronic tumor necrosis factor-alpha inhibition enhances NO modulation of vascular function in estrogen-deficient rats.* Hypertension, 2005. **46**(1): p. 76-81.

172. Hajri, T., et al., *Regulation of adiponectin production by insulin: interactions with tumor necrosis factor-alpha and interleukin-6.* Am J Physiol Endocrinol Metab, 2011. **300**(2): p. E350-60.

173. Greenstein, A.S., et al., *Local inflammation and hypoxia abolish the protective anticontractile properties of perivascular fat in obese patients.* Circulation, 2009. **119**(12): p. 1661-70.

174. Ma, L., et al., *Perivascular fat-mediated vascular dysfunction and remodeling through the AMPK/mTOR pathway in high-fat diet-induced obese rats.* Hypertens Res, 2010. **33**(5): p. 446-53.

175. Marchesi, C., et al., *Endothelial nitric oxide synthase uncoupling and perivascular adipose oxidative stress and inflammation contribute to vascular dysfunction in a rodent model of metabolic syndrome.* Hypertension, 2009. **54**(6): p. 1384-92.

176. Withers, S.B., et al., *Mechanisms of adiponectin-associated perivascular function in vascular disease.* Arterioscler Thromb Vasc Biol, 2014. **34**(8): p. 1637-42.

177. Ketonen, J., et al., *Periadventitial adipose tissue promotes endothelial dysfunction via oxidative stress in diet-induced obese C57Bl/6 mice.* Circ J, 2010. **74**(7): p. 1479-87.

178. Eringa, E.C., et al., *Regulation of vascular function and insulin sensitivity by adipose tissue: focus on perivascular adipose tissue.* Microcirculation, 2007. **14**(4-5): p. 389-402.

179. Grimaldi, B., et al., *PER2 controls lipid metabolism by direct regulation of PPARgamma.* Cell Metab. **12**(5): p. 509-20.

180. Wu, X., et al., *Expression profile of mRNAs encoding core circadian regulatory proteins in human subcutaneous adipose tissue: correlation with age and body mass index.* Int J Obes (Lond), 2009. **33**(9): p. 971-7.

181. Shostak, A., J. Meyer-Kovac, and H. Oster, *Circadian regulation of lipid mobilization in white adipose tissues.* Diabetes. **62**(7): p. 2195-203.

182. Gomez-Abellan, P., et al., *Circadian expression of adiponectin and its receptors in human adipose tissue.* Endocrinology. **151**(1): p. 115-22.

183. Turek, F.W., et al., *Obesity and metabolic syndrome in circadian Clock mutant mice.* Science, 2005. **308**(5724): p. 1043-5.

184. Yildiz, B.O., et al., *Alterations in the dynamics of circulating ghrelin, adiponectin, and leptin in human obesity.* Proc Natl Acad Sci U S A, 2004. **101**(28): p. 10434-9.

185. Garaulet, M., et al., *PERIOD2 variants are associated with abdominal obesity, psycho-behavioral factors, and attrition in the dietary treatment of obesity.* J Am Diet Assoc. **110**(6): p. 917-21.

186. Garaulet, M., et al., *CLOCK gene is implicated in weight reduction in obese patients participating in a dietary programme based on the Mediterranean diet.* Int J Obes (Lond). **34**(3): p. 516-23.

187. Ekmekcioglu, C. and Y. Touitou, *Chronobiological aspects of food intake and metabolism and their relevance on energy balance and weight regulation.* Obes Rev. **12**(1): p. 14-25.

188. Di Lorenzo, L., et al., *Effect of shift work on body mass index: results of a study performed in 319 glucose-tolerant men working in a Southern Italian industry.* Int J Obes Relat Metab Disord, 2003. **27**(11): p. 1353-8.

189. Kohsaka, A., et al., *High-fat diet disrupts behavioral and molecular circadian rhythms in mice.* Cell Metab, 2007. **6**(5): p. 414-21.

190. Gimble, J.M. and Z.E. Floyd, *Fat circadian biology.* J Appl Physiol (1985), 2009. **107**(5): p. 1629-37.

191. Kaneko, K., et al., *Obesity alters circadian expressions of molecular clock genes in the brainstem.* Brain Res, 2009. **1263**: p. 58-68.

192. Lau, P., et al., *Homozygous staggerer (sg/sg) mice display improved insulin sensitivity and enhanced glucose uptake in skeletal muscle.* Diabetologia, 2011. **54**(5): p. 1169-80.

193. Kang, H.S., et al., *Transcriptional profiling reveals a role for RORalpha in regulating gene expression in obesity-associated inflammation and hepatic steatosis.* Physiol Genomics, 2011. **43**(13): p. 818-28.

194. Laplante, M. and D.M. Sabatini, *mTOR signaling in growth control and disease.* Cell, 2012. **149**(2): p. 274-93.

195. Cafferkey, R., et al., *Dominant missense mutations in a novel yeast protein related to mammalian phosphatidylinositol 3-kinase and VPS34 abrogate rapamycin cytotoxicity.* Mol Cell Biol, 1993. **13**(10): p. 6012-23.

196. Kim, D.H., et al., *mTOR interacts with raptor to form a nutrient-sensitive complex that signals to the cell growth machinery.* Cell, 2002. **110**(2): p. 163-75.

197. Jacinto, E., et al., *Mammalian TOR complex 2 controls the actin cytoskeleton and is rapamycin insensitive.* Nat Cell Biol, 2004. **6**(11): p. 1122-8.

198. Jia, G., et al., *Overnutrition, mTOR signaling, and cardiovascular diseases.* Am J Physiol Regul Integr Comp Physiol, 2014. **307**(10): p. R1198-R1206.

199. Sciarretta, S., M. Volpe, and J. Sadoshima, *Mammalian target of rapamycin signaling in cardiac physiology and disease.* Circ Res, 2014. **114**(3): p. 549-64.

200. Sarbassov, D.D., et al., *Rictor, a novel binding partner of mTOR, defines a rapamycin-insensitive and raptor-independent pathway that regulates the cytoskeleton.* Curr Biol, 2004. **14**(14): p. 1296-302.

201. Frias, M.A., et al., *mSin1 is necessary for Akt/PKB phosphorylation, and its isoforms define three distinct mTORC2s.* Curr Biol, 2006. **16**(18): p. 1865-70.

202. Pearce, L.R., et al., *Identification of Protor as a novel Rictor-binding component of mTOR complex-2.* Biochem J, 2007. **405**(3): p. 513-22.

203. Yang, Z. and X.F. Ming, *mTOR signalling: the molecular interface connecting metabolic stress, aging and cardiovascular diseases.* Obes Rev, 2012. **13 Suppl 2**: p. 58-68.

204. Xie, J. and C.G. Proud, *Crosstalk between mTOR complexes.* Nat Cell Biol, 2013. **15**(11): p. 1263-5.

205. Sarbassov, D.D., et al., *Prolonged rapamycin treatment inhibits mTORC2 assembly and Akt/PKB.* Mol Cell, 2006. **22**(2): p. 159-68.

206. Cybulski, N. and M.N. Hall, *TOR complex 2: a signaling pathway of its own.* Trends Biochem Sci, 2009. **34**(12): p. 620-7.

207. Laplante, M. and D.M. Sabatini, *mTOR signaling at a glance.* J Cell Sci, 2009. **122**(Pt 20): p. 3589-94.

208. Oh, W.J. and E. Jacinto, *mTOR complex 2 signaling and functions.* Cell Cycle, 2011. **10**(14): p. 2305-16.

209. Zinzalla, V., et al., *Activation of mTORC2 by association with the ribosome.* Cell, 2011. **144**(5): p. 757-68.

210. Sarbassov, D.D., et al., *Phosphorylation and regulation of Akt/PKB by the rictor-mTOR complex.* Science, 2005. **307**(5712): p. 1098-101.

211. Garcia-Martinez, J.M. and D.R. Alessi, *mTOR complex 2 (mTORC2) controls hydrophobic motif phosphorylation and activation of serum- and glucocorticoid-induced protein kinase 1 (SGK1).* Biochem J, 2008. **416**(3): p. 375-85.

212. Gu, Y., et al., *Rictor/mTORC2 is essential for maintaining a balance between beta-cell proliferation and cell size.* Diabetes, 2011. **60**(3): p. 827-37.

213. Thomanetz, V., et al., *Ablation of the mTORC2 component rictor in brain or Purkinje cells affects size and neuron morphology.* J Cell Biol, 2013. **201**(2): p. 293-308.

214. Siuta, M.A., et al., *Dysregulation of the norepinephrine transporter sustains cortical hypodopaminergia and schizophrenia-like behaviors in neuronal rictor null mice.* PLoS Biol, 2010. **8**(6): p. e1000393.

215. Cybulski, N., et al., *mTOR complex 2 in adipose tissue negatively controls whole-body growth.* Proc Natl Acad Sci U S A, 2009. **106**(24): p. 9902-7.

216. Guertin, D.A., et al., *Ablation in mice of the mTORC components raptor, rictor, or mLST8 reveals that mTORC2 is required for signaling to Akt-FOXO and PKCalpha, but not S6K1.* Dev Cell, 2006. **11**(6): p. 859-71.

217. Shiota, C., et al., *Multiallelic disruption of the rictor gene in mice reveals that mTOR complex 2 is essential for fetal growth and viability.* Dev Cell, 2006. **11**(4): p. 583-9.

218. Zhao, X., et al., *Phosphoinositide-dependent kinase 1 and mTORC2 synergistically maintain postnatal heart growth and heart function in mice.* Mol Cell Biol, 2014. **34**(11): p. 1966-75.

219. Zhu, Y., et al., *Mechanistic target of rapamycin (Mtor) is essential for murine embryonic heart development and growth.* PLoS One, 2013. **8**(1): p. e54221.

220. Zhang, D., et al., *MTORC1 regulates cardiac function and myocyte survival through 4E-BP1 inhibition in mice.* J Clin Invest, 2010. **120**(8): p. 2805-16.

221. Yano, T., et al., *Pivotal role of mTORC2 and involvement of ribosomal protein S6 in cardioprotective signaling.* Circ Res, 2014. **114**(8): p. 1268-80.

222. Volkers, M., et al., *Mechanistic target of rapamycin complex 2 protects the heart from ischemic damage.* Circulation, 2013. **128**(19): p. 2132-44.

223. Bhattacharya, I., et al., *Rictor in perivascular adipose tissue controls vascular function by regulating inflammatory molecule expression.* Arterioscler Thromb Vasc Biol, 2013. **33**(9): p. 2105-11.

224. Harrison, D.G., et al., *Inflammation, immunity, and hypertension.* Hypertension, 2011. **57**(2): p. 132-40.

225. Nakahata, Y., et al., *Circadian control of the NAD+ salvage pathway by CLOCK-SIRT1.* Science, 2009. **324**(5927): p. 654-7.

226. Ramsey, K.M., et al., *Circadian clock feedback cycle through NAMPT-mediated NAD+ biosynthesis.* Science, 2009. **324**(5927): p. 651-4.

227. Dallmann, R., et al., *The human circadian metabolome.* Proc Natl Acad Sci U S A, 2012. **109**(7): p. 2625-9.

228. Ince, H. and C.A. Nienaber, *Etiology, pathogenesis and management of thoracic aortic aneurysm.* Nat Clin Pract Cardiovasc Med, 2007. **4**(8): p. 418-27.

229. Yudkin, J.S., E. Eringa, and C.D. Stehouwer, *"Vasocrine" signalling from perivascular fat: a mechanism linking insulin resistance to vascular disease.* Lancet, 2005. **365**(9473): p. 1817-20.

230. Hung, C.M., et al., *Rictor/mTORC2 loss in the Myf5 lineage reprograms brown fat metabolism and protects mice against obesity and metabolic disease.* Cell Rep, 2014. **8**(1): p. 256-71.

231. Lu, C., et al., *Alterations in perivascular adipose tissue structure and function in hypertension.* Eur J Pharmacol, 2011. **656**(1-3): p. 68-73.

232. Ginnan, R., et al., *Regulation of smooth muscle by inducible nitric oxide synthase and NADPH oxidase in vascular proliferative diseases.* Free Radic Biol Med, 2008. **44**(7): p. 1232-45.

233. Festuccia, W.T., et al., *Myeloid-specific Rictor deletion induces M1 macrophage polarization and potentiates in vivo pro-inflammatory response to lipopolysaccharide.* PLoS One, 2014. **9**(4): p. e95432.

234. Rosborough, B.R., et al., *Murine dendritic cell rapamycin-resistant and rictor-independent mTOR controls IL-10, B7-H1, and regulatory T-cell induction.* Blood, 2013. **121**(18): p. 3619-30.

235. Froy, O., *The circadian clock and metabolism.* Clin Sci (Lond), 2011. **120**(2): p. 65-72.

236. Yamaoka, M., et al., *Adipose hypothermia in obesity and its association with period homolog 1, insulin sensitivity, and inflammation in fat.* PLoS One, 2014. **9**(11): p. e112813.

237. Xu, H., et al., *Myeloid cell-specific disruption of Period1 and Period2 exacerbates diet-induced inflammation and insulin resistance.* J Biol Chem, 2014. **289**(23): p. 16374-88.

238. Duez, H. and B. Staels, *The nuclear receptors Rev-erbs and RORs integrate circadian rhythms and metabolism.* Diab Vasc Dis Res, 2008. **5**(2): p. 82-8.

239. Mamontova, A., et al., *Severe atherosclerosis and hypoalphalipoproteinemia in the staggerer mouse, a mutant of the nuclear receptor RORalpha.* Circulation, 1998. **98**(24): p. 2738-43.

240. Kopmels, B., et al., *Evidence for a hyperexcitability state of staggerer mutant mice macrophages.* J Neurochem, 1992. **58**(1): p. 192-9.

241. Stapleton, C.M., et al., *Enhanced susceptibility of staggerer (RORalphasg/sg) mice to lipopolysaccharide-induced lung inflammation.* Am J Physiol Lung Cell Mol Physiol, 2005. **289**(1): p. L144-52.

242. Delerive, P., et al., *The orphan nuclear receptor ROR alpha is a negative regulator of the inflammatory response.* EMBO Rep, 2001. **2**(1): p. 42-8.

243. Chobanian, A.V., et al., *The Seventh Report of the Joint National Committee on Prevention, Detection, Evaluation, and Treatment of High Blood Pressure: the JNC 7 report.* JAMA, 2003. **289**(19): p. 2560-72.

244. Kumar, A., et al., *Fat cell-specific ablation of rictor in mice impairs insulin-regulated fat cell and whole-body glucose and lipid metabolism.* Diabetes, 2010. **59**(6): p. 1397-406.

245. Scherrer, U. and C. Sartori, *Insulin as a vascular and sympathoexcitatory hormone: implications for blood pressure regulation, insulin sensitivity, and cardiovascular morbidity.* Circulation, 1997. **96**(11): p. 4104-13.

246. Younk, L.M., E.M. Lamos, and S.N. Davis, *The cardiovascular effects of insulin.* Expert Opin Drug Saf, 2014. **13**(7): p. 955-66.

247. Kuhn, M., *Molecular physiology of natriuretic peptide signalling.* Basic Res Cardiol, 2004. **99**(2): p. 76-82.

248. Haffner, S.M., et al., *Mortality from coronary heart disease in subjects with type 2 diabetes and in nondiabetic subjects with and without prior myocardial infarction.* N Engl J Med, 1998. **339**(4): p. 229-34.

249. Mondon, C.E. and G.M. Reaven, *Evidence of abnormalities of insulin metabolism in rats with spontaneous hypertension.* Metabolism, 1988. **37**(4): p. 303-5.

250. Reaven, G.M. and H. Chang, *Relationship between blood pressure, plasma insulin and triglyceride concentration, and insulin action in spontaneous hypertensive and Wistar-Kyoto rats.* Am J Hypertens, 1991. **4**(1 Pt 1): p. 34-8.

251. Cambien, F., et al., *Body mass, blood pressure, glucose, and lipids. Does plasma insulin explain their relationships?* Arteriosclerosis, 1987. **7**(2): p. 197-202.

252. Bonora, E., et al., *Relationship between blood pressure and plasma insulin in non-obese and obese non-diabetic subjects.* Diabetologia, 1987. **30**(9): p. 719-23.

253. Saad, M.F., et al., *Racial differences in the relation between blood pressure and insulin resistance.* N Engl J Med, 1991. **324**(11): p. 733-9.

254. Reaven, G.M., H. Lithell, and L. Landsberg, *Hypertension and associated metabolic abnormalities--the role of insulin resistance and the sympathoadrenal system.* N Engl J Med, 1996. **334**(6): p. 374-81.

255. El-Atat, F.A., et al., *The relationship between hyperinsulinemia, hypertension and progressive renal disease.* J Am Soc Nephrol, 2004. **15**(11): p. 2816-27.

256. Mark, A.L., *The sympathetic nervous system in hypertension: a potential long-term regulator of arterial pressure.* J Hypertens Suppl, 1996. **14**(5): p. S159-65.

257. Johnson, R.J., et al., *Pathogenesis of essential hypertension: historical paradigms and modern insights.* J Hypertens, 2008. **26**(3): p. 381-91.

258. Coffman, T.M., *Under pressure: the search for the essential mechanisms of hypertension.* Nat Med, 2011. **17**(11): p. 1402-9.

259. Gardner, D.G., et al., *Molecular biology of the natriuretic peptide system: implications for physiology and hypertension.* Hypertension, 2007. **49**(3): p. 419-26.

260. John, S.W., et al., *Blood pressure and fluid-electrolyte balance in mice with reduced or absent ANP.* Am J Physiol, 1996. **271**(1 Pt 2): p. R109-14.

261. Maimaitiming, S., et al., *Association of common variants in NPPA and NPPB with blood pressure does not translate into kidney damage in a general population study.* J Hypertens, 2010. **28**(6): p. 1230-3.

262. Macheret, F., et al., *Human hypertension is characterized by a lack of activation of the antihypertensive cardiac hormones ANP and BNP.* J Am Coll Cardiol, 2012. **60**(16): p. 1558-65.

263. Cannone, V., et al., *Atrial natriuretic peptide genetic variant rs5065 and risk for cardiovascular disease in the general community: a 9-year follow-up study.* Hypertension, 2013. **62**(5): p. 860-5.

264. El-Atat, F., et al., *Obesity and hypertension.* Endocrinol Metab Clin North Am, 2003. **32**(4): p. 823-54.

265. Sengenès, C., et al., *Natriuretic peptides: a new lipolytic pathway in human adipocytes.* FASEB J, 2000. **14**(10): p. 1345-51.

266. Gruden, G., A. Landi, and G. Bruno, *Natriuretic peptides, heart, and adipose tissue: new findings and future developments for diabetes research.* Diabetes Care, 2014. **37**(11): p. 2899-908.

267. Chang, H.R., et al., *N-terminal pro-B-type natriuretic peptide is inversely associated with metabolic syndrome in hypertensive patients.* Am J Med Sci, 2014. **348**(3): p. 210-4.

268. Olsen, M.H., et al., *N-terminal pro brain natriuretic peptide is inversely related to metabolic cardiovascular risk factors and the metabolic syndrome.* Hypertension, 2005. **46**(4): p. 660-6.

269. Wang, T.J., et al., *Association of plasma natriuretic peptide levels with metabolic risk factors in ambulatory individuals.* Circulation, 2007. **115**(11): p. 1345-53.

270. Goetze, J.P., *Plasma proANP decreases after meal intake.* Clin Chem, 2013. **59**(8): p. 1270-1.

271. Miyashita, K., et al., *Natriuretic peptides/cGMP/cGMP-dependent protein kinase cascades promote muscle mitochondrial biogenesis and prevent obesity.* Diabetes, 2009. **58**(12): p. 2880-92.

272. Wang, T.J., et al., *Impact of obesity on plasma natriuretic peptide levels.* Circulation, 2004. **109**(5): p. 594-600.

273. Nannipieri, M., et al., *Defective regulation and action of atrial natriuretic peptide in type 2 diabetes.* Horm Metab Res, 2002. **34**(5): p. 265-70.

274. Sheward, W.J., et al., *Circadian control of mouse heart rate and blood pressure by the suprachiasmatic nuclei: behavioral effects are more significant than direct outputs.* PLoS One, 2010. **5**(3): p. e9783.

275. Kim, S.M., et al., *Persistence of circadian variation in arterial blood pressure in beta1/beta2-adrenergic receptor-deficient mice.* Am J Physiol Regul Integr Comp Physiol, 2008. **294**(5): p. R1427-34.

276. Anderson, E.A., et al., *Hyperinsulinemia produces both sympathetic neural activation and vasodilation in normal humans.* J Clin Invest, 1991. **87**(6): p. 2246-52.

277. Brands, M.W., et al., *The hemodynamic response to chronic hyperinsulinemia in conscious dogs.* Am J Hypertens, 1991. **4**(2 Pt 1): p. 164-8.

278. Hughes, A.T. and H.D. Piggins, *Feedback actions of locomotor activity to the circadian clock.* Prog Brain Res, 2012. **199**: p. 305-36.

279. Sei, H., et al., *Diurnal amplitudes of arterial pressure and heart rate are dampened in Clock mutant mice and adrenalectomized mice.* Endocrinology, 2008. **149**(7): p. 3576-80.

280. Masuki, S., et al., *Reduced alpha-adrenoceptor responsiveness and enhanced baroreflex sensitivity in Cry-deficient mice lacking a biological clock.* J Physiol, 2005. **566**(Pt 1): p. 213-24.

281. Miron, M., et al., *A methodology for global validation of microarray experiments.* BMC Bioinformatics, 2006. **7**: p. 333.

282. Bryant, P.A., et al., *Technical variability is greater than biological variability in a microarray experiment but both are outweighed by changes induced by stimulation.* PLoS One, 2011. **6**(5): p. e19556.

283. Honda, K. and T. Taniguchi, *Toll-like receptor signaling and IRF transcription factors.* IUBMB Life, 2006. **58**(5-6): p. 290-5.

284. Tamura, T., et al., *The IRF family transcription factors in immunity and oncogenesis.* Annu Rev Immunol, 2008. **26**: p. 535-84.

285. Eguchi, J., et al., *Transcriptional control of adipose lipid handling by IRF4.* Cell Metab, 2011. **13**(3): p. 249-59.

286. Eguchi, J., et al., *Interferon regulatory factors are transcriptional regulators of adipogenesis.* Cell Metab, 2008. **7**(1): p. 86-94.

287. Kong, X., et al., *IRF4 is a key thermogenic transcriptional partner of PGC-1α.* Cell, 2014. **158**(1): p. 69-83.

288. Bordicchia, M., et al., *Cardiac natriuretic peptides act via p38 MAPK to induce the brown fat thermogenic program in mouse and human adipocytes.* J Clin Invest, 2012. **122**(3): p. 1022-36.

289. Binder, B.R., et al., *Plasminogen activator inhibitor 1: physiological and pathophysiological roles.* News Physiol Sci, 2002. **17**: p. 56-61.

290. Otsuka, G., et al., *Transforming growth factor beta 1 induces neointima formation through plasminogen activator inhibitor-1-dependent pathways.* Arterioscler Thromb Vasc Biol, 2006. **26**(4): p. 737-43.

291. Perez, P.M., et al., *Gene expression of adipose tissue, endothelial cells and platelets in subjects with metabolic syndrome (Review).* Mol Med Report, 2012. **5**(5): p. 1135-40.

292. Crandall, D.L., et al., *Modulation of adipose tissue development by pharmacological inhibition of PAI-1.* Arterioscler Thromb Vasc Biol, 2006. **26**(10): p. 2209-15.

293. Kockx, M., et al., *Relationship between visceral fat and PAI-1 in overweight men and women before and after weight loss.* Thromb Haemost, 1999. **82**(5): p. 1490-6.

294. Eriksson, P., et al., *Adipose tissue secretion of plasminogen activator inhibitor-1 in non-obese and obese individuals.* Diabetologia, 1998. **41**(1): p. 65-71.

295. Samad, F. and D.J. Loskutoff, *The fat mouse: a powerful genetic model to study elevated plasminogen activator inhibitor 1 in obesity/NIDDM.* Thromb Haemost, 1997. **78**(1): p. 652-5.

296. Kaur, P., et al., *SERPINE 1 Links Obesity and Diabetes: A Pilot Study.* J Proteomics Bioinform, 2010. **3**(6): p. 191-199.

297. Caughey, G.H., *Mast cell tryptases and chymases in inflammation and host defense.* Immunol Rev, 2007. **217**: p. 141-54.

298. Lundequist, A., et al., *Cooperation between mast cell carboxypeptidase A and the chymase mouse mast cell protease 4 in the formation and degradation of angiotensin II.* J Biol Chem, 2004. **279**(31): p. 32339-44.

299. Houde, M., et al., *Pivotal role of mouse mast cell protease 4 in the conversion and pressor properties of Big-endothelin-1.* J Pharmacol Exp Ther, 2013. **346**(1): p. 31-7.

300. Budanov, A.V. and M. Karin, *p53 target genes sestrin1 and sestrin2 connect genotoxic stress and mTOR signaling.* Cell, 2008. **134**(3): p. 451-60.

301. Maiuri, M.C., et al., *Stimulation of autophagy by the p53 target gene Sestrin2.* Cell Cycle, 2009. **8**(10): p. 1571-6.

302. Budanov, A.V., J.H. Lee, and M. Karin, *Stressin' Sestrins take an aging fight.* EMBO Mol Med, 2010. **2**(10): p. 388-400.

303. Lee, J.H., et al., *Maintenance of metabolic homeostasis by Sestrin2 and Sestrin3.* Cell Metab, 2012. **16**(3): p. 311-21.

304. Marenholz, I., C.W. Heizmann, and G. Fritz, *S100 proteins in mouse and man: from evolution to function and pathology (including an update of the nomenclature).* Biochem Biophys Res Commun, 2004. **322**(4): p. 1111-22.

305. Baudier, J. and D. Gerard, *Ions binding to S100 proteins: structural changes induced by calcium and zinc on S100a and S100b proteins.* Biochemistry, 1983. **22**(14): p. 3360-9.

306. Wang, D.D. and A. Bordey, *The astrocyte odyssey.* Prog Neurobiol, 2008. **86**(4): p. 342-67.

307. Steiner, J., et al., *S100B protein in neurodegenerative disorders.* Clin Chem Lab Med, 2011. **49**(3): p. 409-24.

308. Petrova, T.V., J. Hu, and L.J. Van Eldik, *Modulation of glial activation by astrocyte-derived protein S100B: differential responses of astrocyte and microglial cultures.* Brain Res, 2000. **853**(1): p. 74-80.

309. Esposito, G., et al., *Enteric glial-derived S100B protein stimulates nitric oxide production in celiac disease.* Gastroenterology, 2007. **133**(3): p. 918-25.

310. Sherstnev, V.V., et al., *Molecular markers of arterial hypertension in patients with normotony, pre-hypertension and hypertension.* Bull Exp Biol Med, 2015. **158**(5): p. 604-6.

311. Steiner, J., et al., *S100B serum levels are closely correlated with body mass index: an important caveat in neuropsychiatric research.* Psychoneuroendocrinology, 2010. **35**(2): p. 321-4.

312. Gimble, J.M., et al., *Circadian rhythms in adipose tissue: an update.* Curr Opin Clin Nutr Metab Care, 2011. **14**(6): p. 554-61.

313. Gavrila, A., et al., *Diurnal and ultradian dynamics of serum adiponectin in healthy men: comparison with leptin, circulating soluble leptin receptor, and cortisol patterns.* J Clin Endocrinol Metab, 2003. **88**(6): p. 2838-43.

314. Khapre, R.V., et al., *BMAL1-dependent regulation of the mTOR signaling pathway delays aging.* Aging (Albany NY), 2014. **6**(1): p. 48-57.

315. Cornu, M., et al., *Hepatic mTORC1 controls locomotor activity, body temperature, and lipid metabolism through FGF21.* Proc Natl Acad Sci U S A, 2014. **111**(32): p. 11592-9.

316. Hatori, M., et al., *Time-restricted feeding without reducing caloric intake prevents metabolic diseases in mice fed a high-fat diet.* Cell Metab, 2012. **15**(6): p. 848-60.

317. Vollmers, C., et al., *Time of feeding and the intrinsic circadian clock drive rhythms in hepatic gene expression.* Proc Natl Acad Sci U S A, 2009. **106**(50): p. 21453-8.

318. Zhang, D., et al., *Liver clock protein BMAL1 promotes de novo lipogenesis through insulin-mTORC2-AKT signaling.* J Biol Chem, 2014. **289**(37): p. 25925-35.

319. Asher, G., et al., *SIRT1 regulates circadian clock gene expression through PER2 deacetylation.* Cell, 2008. **134**(2): p. 317-28.

320. Nakahata, Y., et al., *The NAD+-dependent deacetylase SIRT1 modulates CLOCK-mediated chromatin remodeling and circadian control.* Cell, 2008. **134**(2): p. 329-40.

321. Sauer, B., *Inducible gene targeting in mice using the Cre/lox system.* Methods, 1998. **14**(4): p. 381-92.

322. Martens, K., A. Bottelbergs, and M. Baes, *Ectopic recombination in the central and peripheral nervous system by aP2/FABP4-Cre mice: implications for metabolism research.* FEBS Lett, 2010. **584**(5): p. 1054-8.

323. Wang, Z.V., et al., *Identification and characterization of a promoter cassette conferring adipocyte-specific gene expression.* Endocrinology, 2010. **151**(6): p. 2933-9.

324. Baker, W.K., *Position-effect variegation.* Adv Genet, 1968. **14**: p. 133-69.

325. Singh, P.B., *Molecular mechanisms of cellular determination: their relation to chromatin structure and parental imprinting.* J Cell Sci, 1994. **107 (Pt 10)**: p. 2653-68.

326. Schmidt-Supprian, M. and K. Rajewsky, *Vagaries of conditional gene targeting.* Nat Immunol, 2007. **8**(7): p. 665-8.

327. Rickert, R.C., J. Roes, and K. Rajewsky, *B lymphocyte-specific, Cre-mediated mutagenesis in mice.* Nucleic Acids Res, 1997. **25**(6): p. 1317-8.

328. van den Buuse, M. and S.C. Malpas, *24-hour recordings of blood pressure, heart rate and behavioural activity in rabbits by radio-telemetry: effects of feeding and hypertension.* Physiol Behav, 1997. **62**(1): p. 83-9.

329. Schmittgen, T.D. and K.J. Livak, *Analyzing real-time PCR data by the comparative C(T) method.* Nat Protoc, 2008. **3**(6): p. 1101-8.

Appendix

ADDITIONAL METHODS

Recording of blood pressure and locomotor activity in mice using radiofrequency transmitters - hardware set-up

Rictor^{aP2KO} mice and control littermates (n=5/6) were implanted with a radiofrequency transmitter (TA11PA-C10, Data Sciences International, St. Paul, MN, USA) via the left carotid artery. Radiofrequency transmitter used allowed recording of mean, diastolic and systolic arterial pressure, pulse pressure, heart rate, respiratory rate and locomotor activity. Each transmitter had a weight of 4 g. Hardware set-up is shown in figure A-1.

Cages with one mouse each were positioned above a receiver plate (RPC-1, Data Sciences International, St. Paul, USA). Receiver plates were connected with a data exchange matrix transmitting telemetric data. Data were collected using Dataquest A.R.T. system 4.2 (Data Sciences International, St. Paul, USA).

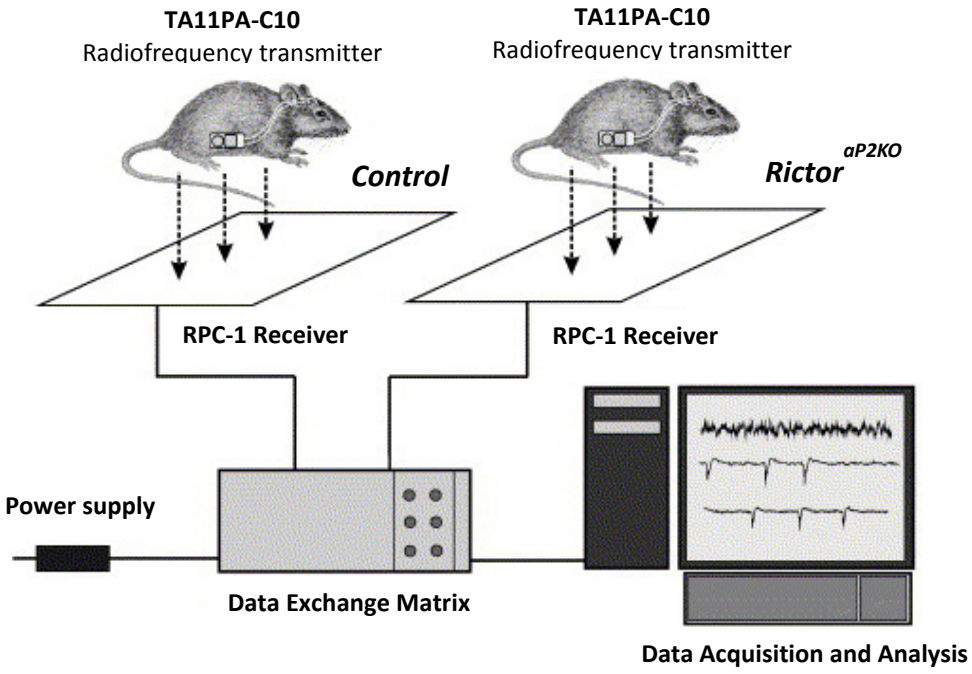

Figure A-1: Hardware set-up of blood pressure and locomotor activity recordings in *Rictor*^{aP2KO} mice and control littermates. Figure adapted from www.datasci.com

Recording of blood pressure and locomotor activity in mice using radiofrequency transmitters - timeline post-operative animal care

Mice were implanted with the radiofrequency transmitter (TA11PA-C10) at day 0. In addition to the standard chow in the food box, mice were provided with some standard chow directly inside the cage. Days zero to four after surgery, mice were single-caged at 30 °C. Temperature of the warming-cabinet was reduced to 25 °C at day five after surgery. Telemetric measurements were started at day eight after surgery.

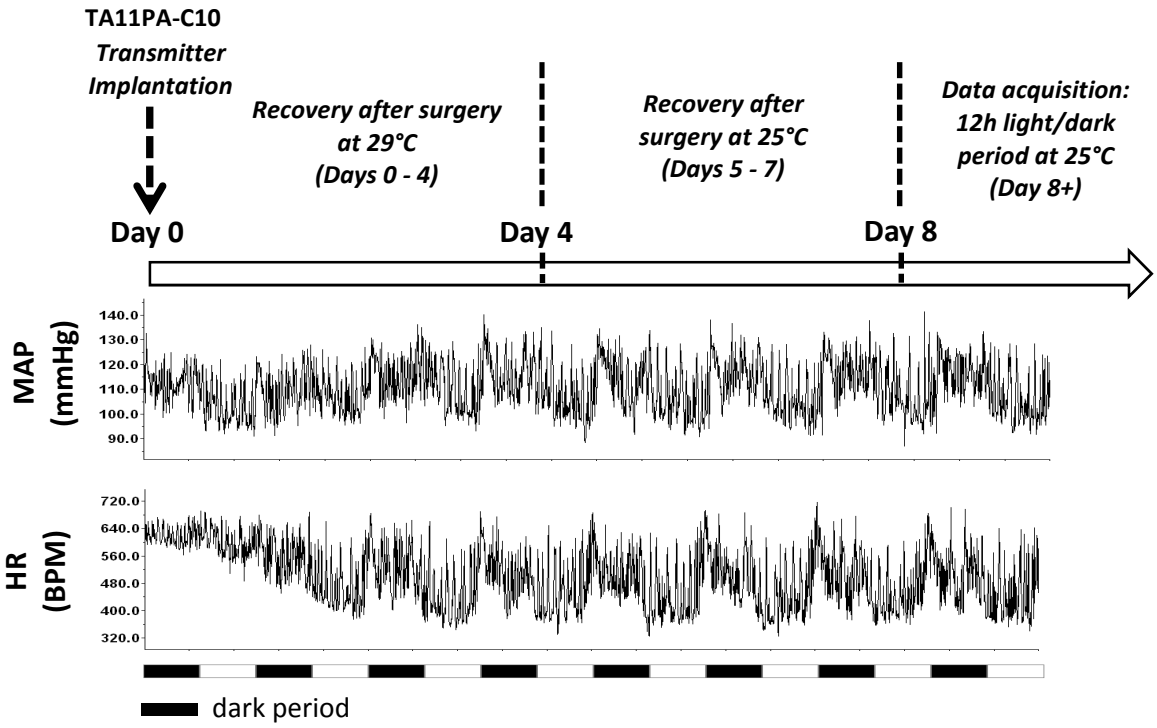

Figure A-2: Normalization of the mean arterial pressure and the heart rate after transmitter implantation. Radiofrequency transmitters (TA11PA-C10) were implanted via the left carotid artery at day zero. During the post-operative period, mice were kept at 29°C (days zero to four) and 25°C (days five to seven). For final data analysis, only telemetric data obtained from day eight on were considered. MAP (mean arterial pressure), HR (heart rate)

Implantation of osmotic mini pumps in *Rictor*^{aP2KO} mice and control littermates

For application of the iNOS-specific inhibitor 1400W (10mg/kg/day) or saline as solvent control, Alzet™ mini pumps (model 2001; DURECT Corporation, CA, USA**)** filled with either sterile 1400W or saline were implanted subcutaneously 14 days post telemetry sender implantation in *Rictor*^{aP2KO} mice. Surgery was performed under isoflurane anesthesia. Average filling volume was 220 µl and pumping rate 1µl/hour.

mRNA expressional analysis of the *Cre*-recombinase

Tissue dissection, RNA isolation, reverse transcription of RNA and qRT-PCR were performed as outlined in 2.1.10. The *Cre*-recombinase primer pair was designed alongside housekeeping genes. The sequences of the *Cre*-recombinase primers were as follows:

Forward primer: 5'-CGT ACT GAC GGT GGG AGA AT-'3
Reverse primer: 5'-CCC GGC AAA ACA GGT AGT TA-'3

Validation of the micro array data

Genes which showed expressional changes ($P < 0.05$ and fold change < 1.5) in PVAT of *Rictor*^{aP2KO} mice were ranked in descending order. The 10 most increased and 10 most reduced genes were chosen for validation with quantitative RT-PCR (qRT-PCR).
Briefly, control and *Rictor*^{aP2KO} mice were starved overnight and euthanized at 9 am (ZT 2). For tissue storage, RNA isolation and reverse transcription please refer to 2.1.10 (genome expression study). The procedure of the qRT-PCR was as followed: Gene expression was analyzed using 1x "iQ™ SYBR® Green Supermix" (Bio-Rad Laboratories GmbH, Munich, Germany), target gene specific mouse primer pairs (150 nM) and cDNA (10 ng) in a final volume of 20 µl. The qRT-PCR was performed as outlined in **table A-1** using clear 96-well plates and the CFX96® qRT-PCR system (Bio-Rad Laboratories GmbH, Munich, Germany). Specifically designed mouse primer pairs used are listed in **table A-2**. Specificity of the qRT-PCR products was confirmed by analysis of the melting curve and agarose gel electrophoresis. Gene expression was calculated using the Δ(CT)-method [329] and normalized to the housekeeping gene *acidic ribosomal phosphoprotein PO* (*Arbp*). Values are expressed as arbitrary units (AU).

Table A-1: Protocol for the quantitative RT-PCR used to validate micro array data.

	Temperature (°C)	Time (sec)	
Initial denaturation	95	180	
Denaturation	95	15	Repeat 39 x
Annealing and elongation	60*	45	
Final elongation	60	120	
Melting curve	95	60	
	65	60	
	65 - 95 (+ 0.5 °C per step)	10 (per step)	
	20	180	

* = for *Dgat1* and *Srebp-1c* 61°C and 75 nM final concentration of primers

Table A-2 Primer pairs used to validate micro array data with quantitative RT-PCR. Primer pairs were designed using «primer blast» program (NCBI, USA) and are specific to mouse cDNA.

Gene name	Forward Primer (5'-3')	Reverse Primer (5'-3')
Chac1	TAC GGC TCC CTA GTG TGG AA	CAC TCG GCC AGG CAT CTT G
Cyp51A1	GAG GCA ACT TGC TTT CCA CG	TGG TGG ACT TTT CGC TCC AG
Dgat1	AGA AGA GGA CGA GGT GCG A	GAT GGC ACC TCA GAT CCC AGT AG
Fasn	GTG ATA GCC GGT ATG TCG GG	TAG AGC CCA GCC TTC CAT CT
Fdps	TGT AGA ACT GCT CCA GGC TTT	CTT CCA GAA GCA GAG CGT CG
Fosb	GAA AAG CGA AGG GTT CGC AG	GCT GAT CAG TTT CCG CCT GA
Gadd45b	TGG TGA CGA ACC CAC ATT CA	CGG GAG ATT AAT CAC GGG CA
Glnd	GGT GCC GAT TCG AGT GAT GA	CTG ATC CAT TGT GGC CTG GT
Irf4	TGT GAA AAT GGT TGC CAG GTG	TGC TTG GCT CAA TGG GGA TT
Mcpt4	CTG GAG CTG AGG AGA TTA TTG GT	TGA ACC CTC TCT CAG TGG TG
Ncan	ATG GTG GCA CAT GAG AGT GG	CCA CAC AGC ACT GTA CCC TT
Nfil3	GAG CAG AAC CAC GAT AAC CCA T	TAC AGA CCG GAT GGA GGA GAC
Npas2	AGA GGC AGC TTG AAC CCA AA	GAG GGG CTA GGC ACA TTG TT
Nsdhl	AGC TCT AGG TGG AAA GGC AT	GTC AGA CGG GAC AGG AA
Perilipin1	CCA TTG CAA GCA CCT CTG AC	CCA CCT TCT CGA TGC TTC CC
Rnu2	CTC GGC CTT TTG GCT AAG AT	GGA GCA AGC TCC TAT TCC AA
S100b	TGC CCT CAT TGA TGT CTT CCA	TGA TTT CCT CCA GGA AGT GAG AGA G
Serpine1	TCC ACA AGT CTG ATG GCA GC	GGG GTG GTG AAC TCA GTG TA
Sesn2	CGC CAC TCA GAG AAG GTT CA	ACG GGG TAG TCA GGT CAT GT
Spry4	ACT CGG GTT CGG GGA TTT AC	CAG GCT TCT AGG GGT CTT TGA
Srebp-1c	ATC GGC GCG GAA GCT GTC GGG GTA GCG TC	ACT GTC TTG GTT GTT GAT GAG CTG GAG CAT
Thra	AAG AAT GGT GGC TTG GGT G	CGG AGC GGT CTG TTG ACA TTA
Trdn	GCC AAA CAC GCA AAC AGA AC	GGA ACT TCT GGT GCT CCC TT

Fluctuating expression of *Rictor* and mTORC2 downstream targets in adipose tissue

For tissue collection, RNA isolation, reverse transcription and qRT-PCR please refer to 2.1.10 (RNA isolation, reverse transcription and quantitative real-time PCR). Target gene specific mouse primer pairs were designed using "primer blast" (NCBI, USA) and are listed in **table A-3**. mRNA expression was analyzed over a 24 hour period.

Table A-3: Primer pairs to analyze 24 hour mRNA expression patterns of indicated target genes in PVAT with quantitative RT-PCR. The «primer blast» program (NCBI, USA) was used to design primer pair's specific to mouse cDNA.

Gene name	Forward Primer (5'-3')	Reverse Primer (5'-3')
Dbp	GGA ACT GAA GCC TCA ACC AAT C	CTC CGG CTC CAG TAC TTC TCA
Nfil3	GAG CAG AAC CAC GAT AAC CCA T	TAC AGA CCG GAT GGA GGA GAC
Pgc-1α	AGA TGA AGA GAA TGA GGC AAA C	GGC ATG GAG GAA GGA CTG
Rictor	TGC GAT ATT GGC CAT AGT GA	ACC CGG CTG CTC TTA CTT CT
Rorc	CAT CAA TGC CAA CCG TCC TG	CTT GGC TAG GAG GCC TTG TC
Sirt-1	TGA GCT GAT GGA GGG GAT CA	AGT TCC CAA TGC TGG TGG AG

The expression and phosphorylation of the indicated target proteins was analyzed in EFAT and PVAT using Western Blot as follows: After euthanized, tissues were dissection from mice and tissue samples equilibrated for 30 min in DMEM without phenol red (Sigma-Aldrich, Buchs, Switzerland) at 37 °C and stimulated for additional 10 min with insulin (1 µmol/l). Tissues were snap frozen and kept at - 80 °C until further usage. Tissues were homogenized in tissue lysis buffer using Tissue Lyser (Qiagen, Hombrechtikon, Switzerland). 6 glass beads (3 mm) were used per 2 ml safe-lock reaction tube. Tissue extracts were passed 4 times through a 20-G needle, centrifuged (10 min, 10000 x g, 4 °C) and the supernatant transferred to a new 1.5 ml reaction tube. Protein concentration was determined using Quick Start™ Bradford Protein Assay according manufactures recommendations. Protein working solutions were prepared as followed: protein lysate (2 µg/µl final concentration) and 2x sample buffer in a 50 µl volume. Samples were heated (95 °C, 5 min). Protein samples were loaded (22.5 µg protein) on a SDS-PAGE gel (**table A-4**), run (70 V for 20 min; 100 V for approx. 1 ¼ hours), transferred to a nitrocellulose membrane and analyzed using immune blot with their specific antibodies (**table A-5**). Membranes were incubated with the primary antibody overnight at 4 °C and with the secondary antibody at room temperature for 1 hour. Labelled proteins were visualized on x-ray films using a chemiluminescence reaction (SuperSignal West Pico or Femto, Life Technologies). ERK2 and total AKT were used as loading control.

(1) Tissue lysis buffer

500 mM Tris (pH 7.5), 2 mM EDTA, 2 mM EGTA, 1 % Triton X, 10 % Glycerol, proteinase/ phosphatase inhibitor (Roche, Switzerland)

(2) SDS-PAGE running buffer (1x)

25 mM Tris-Base, 192 mM Glycine, 0,1 % SDS, pH 8.1 - 8.5

(3) Transfer buffer (1x)

25 mM Tris Base, 192 mM Glycine, 10 % Ethanol (absolute)

(4) 2x SDS-PAGE sample buffer

4 % SDS, 20 % glycerol, 120 mM Tris pH 6.8 and 5 % β-mercaptoethanol

Table A-4 Composition and preparation of a SDS-PAGE gel

Separating gel	8 %
H_2O	5.4 ml
Tris-HCl (1.5 M) pH 8.8	2.5 ml
Acrylamide 29 %	2 ml
SDS 10 %	1.0 ml
APS 10 %	0.1 ml
Temed	0.01ml

Stacking Gel	3 %
H_2O	3 ml
Tris-HCl (1.0 M) pH 6.8	0.5 ml
Acrylamide 29 %	0.46 ml
SDS 10 %	0.04 ml
APS 10 %	0.04 ml
Temed	0.005 ml

Table A-5: Antibodies used in this study

Antibody	Catalog No.	Company
RICTOR	# 2140	Cell signaling
mTOR	# 2983	Cell signaling
Total AKT	# 9272	Cell signaling
phospho AKT Serine 473	# 3787	Cell signaling
phospho AKT Threonine 308	# 4056	Cell signaling
ERK 2	# sc-271451	Santa Cruz
Amersham ECL Rabbit IgG, HRP-linked whole Ab (from donkey)	# NA934-100UL	Amersham

Acknowledgment

In the first place I would like to thank Dr. Elvira Haas for supervising my PhD thesis. I am very grateful for her great support, scientific input and motivation over the last 4 years. I am indebted to her for her help in grant, manuscript and dissertation writing.

I am grateful to my doctoral father Prof. Dr. Roland Wenger for his support, being a member of my PhD committee as well as fruitful ideas and discussions in the PhD committee meetings.

I would like to thank Prof. Dr. Edouard Battegay for giving me the opportunity doing my dissertation in his lab, being a member of my PhD committee, discussions and financial support.

I would like to thank Prof. Dr. Michael Hall for being a member of the PhD committee and scientific discussions.

I am grateful to Prof. Dr. Christian Grimm for participating in my thesis defense.

I would also like to say a personal “thank you” to Dr. Indranil Bhattacharya for his scientific support and ideas over the last 4 years. Thanks for working with me in the lab day and night.

I would also like to acknowledge Ana Perez Dominguez for taking care of the mice and lab organization.

Additionally, I would like to thank all current and former members of “Edouard’s Lab” for discussions and support.

Many thanks go to the University of Zurich/ Projekt- und Personenförderung for funding my PhD project with the “Forschungskredit” (grant-No. FK-13-026).

I would also like to acknowledge Dr. Petra Seebeck for her support with blood pressure and locomotor activity recordings and nice working atmosphere. I am grateful to Petra for her help and experience in implanting telemetry devices, animal aftercare and blood pressure/ locomotor activity recordings.

Many thanks go to Prof. Steven Brown and Dr. Abdelhalim Azzi for constructive discussions, and their advice in how to analyze blood pressure and locomotor activity data, and clock gene expression. I would especially thank “Halim” for his effort in helping us to cut SCN slices from mouse brain by day and at night!

I would also like to acknowledge the effort done by Dr. Giovanni Pellegrini. I am very grateful for his expertise in analyzing cardiac hypertrophy in mice.

Special thanks to Dr. Jelena Kühn Georgijevic and Dr. Hubert Rehrauer for their effort in helping me to analyze gene expression in PVAT with micro array.

I would like to thank Dr. Ulrike Held for her comprehensive statistical analysis of blood pressure and locomotor activity data.

Many thanks to Anna Engler for reading my dissertation. I appreciate her help and critical comments.

I am deeply grateful to my family, especially my mom. Thank you so much for your support and help over the last years. Finally, I would like to thank all my friends outside the lab for sharing great moments.